Doctoral theses at NTNU, 2014:82

Martina Böhme

Spatial and temporal variability of rock slope instability in western Norway:

Implications for susceptibility and hazard assessment

Doctoral Thesis

Martina Böhme

ISBN 978-82-326-0088-5 (printed version)
ISBN 978-82-326-0089-2 (electronic version)
ISSN 1503-8181

NTNU – Trondheim
Norwegian University of
Science and Technology

Doctoral theses at NTNU, 2014:82

NTNU

NTNU
Norwegian University of Science and Technology
Thesis for the degree of Philosophiae Doctor
Faculty of Engineering Science and Technology
Department of Geology and
Mineral Resources Engineering

NTNU – Trondheim
Norwegian University of
Science and Technology

Martina Böhme

Spatial and temporal variability of rock slope instability in western Norway:

Implications for susceptibility and hazard assessment

Thesis for the degree of Philosophiae Doctor

Trondheim, March 2014

Norwegian University of Science and Technology
Faculty of Engineering Science and Technology
Department of Geology and Mineral Resources Engineering

NTNU – Trondheim
Norwegian University of
Science and Technology

NTNU
Norwegian University of Science and Technology

Thesis for the degree of Philosophiae Doctor

Faculty of Engineering Science and Technology
Department of Geology and Mineral Resources Engineering

ISBN 978-82-326-0088-5 (printed version)
ISBN 978-82-326-0089-2 (electronic version)
ISSN 1503-8181

Doctoral theses at NTNU, 2014:82

Printed by Skipnes Kommunikasjon as

Academic advisors during this study:

Michel Jaboyedoff, Center for Research on Terrestrial Environment, Faculty of Geosciences and Environment, University of Lausanne, Switzerland

Lars Harald Blikra, Åknes/Tafjord Beredskap IKS, Stranda, Norway

Bjørn Nilsen, Norwegian University of Science and Technology, Trondheim, Norway (since September 2009)

Abstract

Rock slope failures form a frequent hazard to many populated mountain regions. Especially in western Norway, the topographical and meteorological characteristics increase the vulnerability for rock slope failures. A major focus for studies in Norway is to efficiently find and investigate possible future rock slope failures in order to prevent extensive humanitarian disasters. The determination of the critical parameters involved in the development of rock slope failures is crucial in order to optimize hazard recognition. In addition, a better understanding of the spatial and temporal variability of prehistoric and historic rock slope failures as well as present day rock slope instabilities will optimize monitoring and further research on the susceptibility for future rock slope failures.

The primary aim of this study is to investigate the spatial and temporal distribution of rock slope instabilities within western Norway. It is further aimed to determine the controlling parameters on the development of rock slope instabilities within the study region. The implemented approaches range from regional scale statistical analyses towards site specific numerical modelling, while a focus is set on quantitative analyses.

Within this thesis the main controlling parameters are defined for rockfalls and rock slope instabilities on a regional scale for the entire county of Sogn & Fjordane, western Norway. It is demonstrated that always a combination of several parameters is necessary to destabilize a mountain side. Rockfalls have the strongest spatial relation to the presence of bare rock as well as landslide deposits, the degree of tectonic deformation and the geological lineament density. Large rock slope instabilities develop preferentially within relatively weak rock units, such as phyllites or weathered mafic gneisses, and at convex slope breaks. Looking more into detail, a strong structural control is confirmed by numerical modelling for the unstable rock slope at Stampa.

Susceptibility and hazard are assessed at different scales and with different measures. Quantitative rockfall susceptibility is mapped on a regional scale for the entire county of Sogn & Fjordane based on the statistical analysis of a set of controlling factors. In addition, this statistical susceptibility model is combined with a physically based model, restricting the susceptibility map to areas that are steep enough to represent a potential rockfall source. This combination allows using road inventories, with registered impact points instead of release areas, for susceptibility modelling. In contrast, relative susceptibility and also hazard are assessed locally for single parts of the unstable rock slope at Stampa based on morphology and past activity. Present day annual expectable frequencies for rock slope failures of certain volume classes are determined for the Storfjord region in western Norway based on magnitude-frequency analyses. Furthermore, a semi

quantitative hazard estimation is obtained for each potential instability based on a qualitative susceptibility assessment of each instability in this region.

This PhD thesis presents results of the first attempts of quantitative statistical analyses of different inventories covering rock slope instabilities in Norway. It is shown that susceptibility and hazard can be assessed with different measures, forming the basis for further decisions regarding risk assessment and mitigation.

Acknowledgements

First of all I thank Professor Michel Jaboyedoff for his supervision, his constructive criticism and the fruitful discussions throughout this thesis. I am very grateful for his constant help with occurring challenges even over this large distance in between Norway and Switzerland. He always contributed with new ideas and aspects, keeping me busy with new promising analyses and helping to improve the thesis and the related articles.

I thank my supervisor Dr. Lars Harald Blikra for his help and comments to improve my thesis. Equally I want to thank Professor Bjørn Nilsen for stepping in as an official supervisor in the middle of this project and for his help with many bureaucratic concerns.

I would like to address special thanks to Dr. Marc-Henri Derron and Dr. Reginald L. Hermanns for their good collaboration and many fruitful discussions throughout this thesis. You were both giving me support like a supervisor, without being it officially.

The scientific work presented in this thesis was carried out at the Geological Survey of Norway (NGU) with additional financial support from the Norwegian Water Resources and Energy Directorate (NVE). I was enrolled as a PhD student at the Department of Geology and Mineral Resources Engineering at the Norwegian University of Science and Technology (NTNU).

Thanks are also given to my colleagues at NGU and especially those of the Geohazards group. I always appreciated the good working climate here at NGU with a lot of scientific exchange but also social activities. I am especially grateful to Dr. Thierry Oppikofer and Dr. Luzia Fischer for always trying to answer my numerous questions, helping me to find good solutions and proofreading many versions of manuscripts and finally this thesis. Dr. Iain Henderson and Dr. Aline Saintot gave me the very first impressions of my future thesis topic with several weeks of fieldwork right at my start at NGU. I will never forget this first field season.

I always enjoyed my stays at former IGAR, now Centre for Research on Terrestrial Environment at the University of Lausanne. During my numerous stays I felt always welcome and there was always somebody who could help me when I needed it. The visits to Lausanne were always really fruitful for me and especially my work. Especially, I would like to thank Andrea Pedrazzini for numerous fruitful discussions and his introduction to numerical modelling with *Phase*^{2} and UDEC. Equally I would like to thank Celine Longchamp for her hospitality during my stays in Lausanne.

The realisation of this project would never have been possible without the support of my family and especially my husband Martin Panzner. It was a challenge to bring this thesis to an end with two small children, but on the other hand they were my largest motivation to finish as fast as possible. My parents have always guided and encouraged me. They, and also my "little" sister, are thanked for their numerous visits to Trondheim when we needed help.

Contents

Chapter 1

Introduction

1.1 Motivation

Rock slope failures represented a frequent hazard to populated mountain regions throughout time and still do so. This is a consequence of the topographical, geological and meteorological characteristics of mountain regions. Additionally, many mountain ranges, where high landslide hazards exist, have been affected by repeated glaciations during the Pleistocene, with the end of the Last Glacial Maximum around 20,000 years BP on the northern hemisphere (Clark et al., 2009). The landscape development in these areas is strongly influenced by glacial and postglacial processes. Glacier retreat commonly exposes a landscape that is prone to rapid changes due to a sudden unloading of glacially oversteepened slopes (Ballantyne, 2002a). Rock slope failures are common during the adaption of rock slopes to postglacial conditions. Many international studies indicate a relation between rock slope instabilities and late Pleistocene deglaciation (e.g., Agliardi et al., 2001, 2009a; Ambrosi and Crosta, 2006; Braathen et al., 2004; Eberhardt et al., 2004; Ghirotti et al., 2011).

Glacially oversteepened slopes in combination with unfavourable climatic conditions, like heavy seasonal precipitation, intense snowmelt in spring and long frost periods, increase the vulnerability for rock slope failures in western Norway (Blikra et al., 2006; Saintot et al., 2011). During the last century, Norway has suffered several natural disasters with a significant number of casualties due to rock slope failures and related tsunamis (Furseth, 2006). Several historical disasters are documented in western Norway and in total there are 659 documented fatalities during the last approximately 600 years due to rock slope failures. Owing to the present situation of global climatic change, leading to a warmer and wetter climate in Norway, factors that may trigger rock slope failures will change (Dyrrdal et al.,

2012; Flatøy et al., 2008). Whether this will lead to an increase in the frequency of rock slope failures or not is still under debate (Jaedicke et al., 2008). However, rock slope instabilities and consequent rock slope failures are related to a wide variety of environmental factors and additional parameters, besides the climate, that control their spatial distribution. The determination of the critical parameters involved in the development of rock slope failures in western Norway is crucial in order to optimize hazard recognition. In addition, a better understanding of the spatial and temporal variability of prehistoric and historic rock slope failures as well as present day rock slope instabilities will optimize monitoring and further research on the susceptibility of possible future rock slope failures. A major challenge for studies in Norway is to efficiently find and investigate possible future rock slope failures in order to prevent extensive humanitarian disasters in future.

In order to understand the spatial dependencies and controlling parameters of rock slope instabilities and failures properly, it is necessary to look at an entire region and to prevent focusing exclusively on single sites. However, up to now studies of unstable rock slopes in Norway are mainly directed towards site-specific research of large instabilities (see Chapter 3), but not towards quantitative regional scale investigations. Only few studies discuss more regional aspects of unstable rock slopes. For example Blikra et al. (2006) describe a clustering of rockslides in specific zones in Norway, but do not include the underlying reasons in this spatial approach. Saintot et al. (2011) and Henderson and Saintot (2011) describe a link between rock slope instabilities in western Norway and ductile and brittle structures, but these studies are not based on quantitative analyses. Bjerrum and Jørstad (1968) and Sandersen et al. (1996) highlight a meteorological influence on rockfalls by applying simple binary statistics of historical events. In contrast, Dunlop (2010) investigated the relation between rock slope failures and meteorological conditions as well as topography and geology quantitatively applying Weights-of-Evidence based susceptibility mapping for a region in southwestern Norway (Hordaland and Sogn & Fjordane Counties). Furthermore, Erener and Düzgün (2010) present a statistically based susceptibility map of landslides for western Norway (Møre & Romsdal County) applying different regression methods. However, their focus is strongly on the mathematical methodology, and not on the geological model. In addition, a lack of detailed knowledge about the local geological conditions as well as the used inventory is obvious.

Worldwide, systematic studies of slope failures resulting in quantitative susceptibility and hazard assessments exist numerously, but nevertheless, this topic is still a cause for ongoing debates. Catalogues of historic or prehistoric events are essential for hazard estimations. However, most inventories face temporal and spatial censoring of data to different degrees, including underreporting of data, incomplete

data, inadequate sample time intervals or protective measures in high susceptible zones (Hungr et al., 1999). Especially for large rock slope failures the inventories normally do not contain enough events given a homogeneous region in order to obtain significant results from statistical analyses. This is mainly due to the fact that historical inventories cover a too short time period in order to capture low frequency-high magnitude events adequately. Pre-historic rock slope failures need to be included to cover the entire volume spectra of potential failures. However, for those, information about the timing is sparse. All together, these limitations complicate quantitative statistical analyses of these inventories.

1.2 Primary goals of the thesis

The primary goal of this study is to quantify the spatial and temporal variability of instabilities within western Norway. It is further aimed to determine the controlling parameters on the development of rock slope instabilities within the study region. Focus is set on quantitative analyses, in order to identify controlling parameters and to assess susceptibility and hazard for rock slope instabilities. Different magnitudes of rock slope instabilities are considered and the different investigations are based on different scales, ranging from site specific investigations towards studies covering an entire county.

1.3 Organization of the thesis

This thesis consists of 7 Chapters. Following the present introduction (Chapter 1), Chapter 2 gives an overview of the scientific background on which this study is based. Chapter 3 contains an introduction to the study area in general and in more detail to rock slope failures in Norway. Chapter 4 presents an overview of the approaches used in this theses. a general discussion of the main tasks and findings is given in Chapter 5. Chapter 6 summarizes the main findings and conclusions of this thesis. Finally, Chapter 7 gives an outlook on possible future reasearch.

The full versions of the four research papers comprising the scientific work of this thesis are presented in Appendix A to E. A short overview of the research topics for each research paper is given in the following sections.

1.3.1 Paper I

Böhme, M., Derron, M.-H. and Jaboyedoff, M.: Quantitative spatial analysis of rockfalls from road inventories - a combined statistical and physical model. Submitted to Natural Hazards and Earth System Sciences (Appendix A).

In this paper, the possibility of using road inventories with registered impacts instead of release areas for susceptibility modelling is investigated. A rockfall inventory from the Norwegian Directorate of Public Roads is analysed spatially in order to investigate potential controlling parameters for the Norwegian county Sogn & Fjordane. Quantitative spatial relationships are then used to model rockfall susceptibility with the help of the probabilistic Weights-of-Evidence method. Combining the resulting statistical susceptibility model with physically determined potential rockfall source zones, restricts the susceptibility map to areas that are steep enough to represent a potential rockfall source.

1.3.2 Paper II

Böhme, M., Saintot, A., Henderson, I., Henriksen, H. and Hermanns, R.L.: Rock-slope instabilities in Sogn & Fjordane County, Norway: a detailed structural and geomorphological analysis, in: Slope Tectonics, edited by Jaboyedoff, M., Geological Society, London, Special Publications, 351, pp. 97-111, 2011 (Appendix B).

This paper gives an overview of rock slope instabilities and failures in the Norwegian county Sogn & Fjordane. A detailed structural and geomorphological analysis is presented for four selected rock slope instabilities. The main characteristics of instabilities in Sogn & Fjordane are analysed. Finally, these findings as well as the general spatial distribution of rock slope instabilities and failures in this county are compared to another Norwegian county, namely Møre & Romsdal.

1.3.3 Paper III

Böhme, M., Hermanns, R.L., Oppikofer, T., Fischer, L., Bunkholt, H.S.S., Eiken, T., Pedrazzini, A., Derron, M.-H., Jaboyedoff, M., Blikra, L.H., Nilsen, B.: Analyzing complex rock slope deformation at Stampa, western Norway, by integrating geomorphology, kinematics and numerical modeling. Engineering Geology, 154, pp. 116-130, 2013 (Appendix C).

This paper presents a detailed analysis of the unstable rock slope Stampa in Sogn & Fjordane. An analysis of yearly differential Global Navigation Satellite System surveys and detailed geomorphic and structural analyses based on field data as well as high-resolution digital elevation models were conducted. In addition, continuum and discontinuum numerical modeling were used to understand the influence of former rockslide activity as well as the deformation of the unstable

slope with respect to the failure mechanism. Two different lobes of prehistoric rock slope failures were dated with terrestrial cosmogenic nuclides in order to constrain the chronology and nature of rockslide events at Stampa and to be able to define a relative failure susceptibility for the different compartments of the instability.

1.3.4 Paper IV

Böhme, M., Hermanns, R.L., Fischer, L., Oppikofer, T., Bunkholt, H.S.S., Derron, M.-H., Carrea, D., Jaboyedoff , M., and Eiken, T.: Detailed assessment of the deep-seated gravitational deformation at Stampa above Flåm, Norway, in: Landslides and Engineered Slopes. Protecting Society through Improved Understanding: Proceedings of the 11th International & 2nd North American Symposium on Landslides, Banff, Canada, 3-8 June 2012, edited by Eberhardt, E., Froese, C., Turner, A.K. and Leroueil, S., CRC Press, pp. 647-652, 2012 (Appendix D).

This publication presents a preliminary stage of the investigations carried out at the unstable rock slope Stampa in Sogn & Fjordane. Focus is set on detailed geomorphic and structural analyses based on field data as well as high-resolution digital elevation models and the analysis of yearly differential Global Navigation Satellite System surveys. A preliminary model for the failure mechanism is developed and indications for the relative failure susceptibility are given.

1.3.5 Paper V

Böhme, M. Oppikofer, T., Longva, O., Jaboyedoff, M., Hermanns, R.L., Derron, M.-H.: Analyses of past and present rock slope instabilities in a fjord valley: Implications for hazard estimations. Manuscript, submission planned to Earth and Planetary Science Letters (Appendix E).

Within this manuscript, the temporal distributions of number and volumes of an inventory of in total 108 rock slope failure deposits within the fjords of the Storfjord region have been analysed. Terrestrial cosmogenic nuclide dating was used to validate the relative ages of three fjord deposits. Expectable present day frequencies and magnitudes of rock slope failures in the Storfjord region have been defined. Furthermore, magnitude-frequency relations have been investigated for the same deposits and additionally for a detailed inventory of ancient rockslide scars and potential instabilities for a smaller region within the study area. The magnitude-frequency relations are finally used to quantify the rockslide hazard for the study area.

Chapter 2

General scientific background

2.1 Terminology

This study focuses on landslides in massive rock slopes. Rock slope failures are within this study defined as the complete failure of a rock mass resulting in gravitational mass movements down a mountain slope. Those are today visible as a deposit on or at the foot of the slope. Rock slope instabilities are rock slopes that display signs of gravitational deformation and may form the sources of potential future rock slope failures. Both are classified after Cruden and Varnes (1996) based on the type of observed or expected slope movement and their volumes into rockfalls, rockslides and rock avalanches. Rockfalls are small rock slope failures, generally $< 10^5\,\mathrm{m}^3$, involving free falling, bouncing, rolling and sliding during down slope movement. Rockslides refer to volumes $> 10^5\,\mathrm{m}^3$ sliding along a basal failure surface. The catastrophic failure of a large rockslide might lead to a rock avalanche, characterized by a stream of rapidly moving debris originating from the disintegration of a failed rock mass and reaching long run-outs (Heim, 1932).

2.2 Controlling parameters for rock slope instabilities and failures

Rock slope instabilities and consequent rock slope failures are influenced by a wide variety of environmental factors and additional parameters controlling their spatial and temporal distribution. Jaboyedoff et al. (2005) give an overview on factors that theoretically may control rock slope instability, grouped into external and internal parameters. Internal parameters like slope morphology, geological and structural properties of the bedrock are altered over time by external factors, like climatic

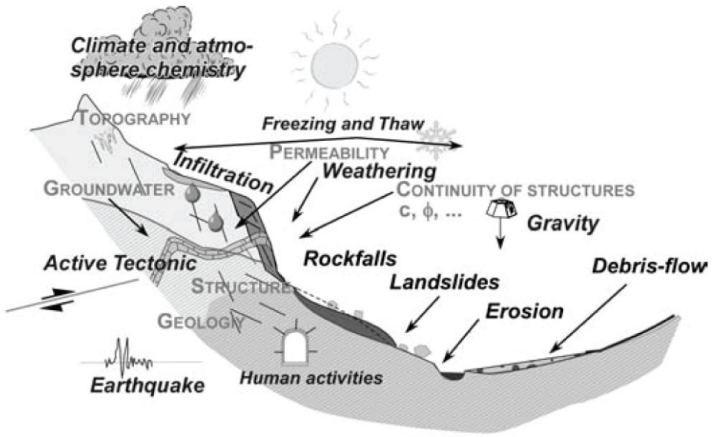

Figure 2.1: Illustration of internal and external factors that may influence rock slope instability (Source: Jaboyedoff et al. (2005), Fig. 2).

influence, gravity, active tectonics, erosion and others (Figure 2.1).

Various studies investigate rockfall locations with respect to their controlling parameters statistically (e.g., Duarte and Marquínez, 2002; Ruff and Czurda, 2008; Tanarro and Muñoz, 2012). Spatial relations between controlling parameters and rockfall locations are used to predict rockfall source areas by means of different statistical or probabilistic modelling techniques on a regional scale, resulting in susceptibility maps (e.g., Blais-Stevens et al., 2012; Frattini et al., 2008; Marquínez et al., 2003; Marzorati et al., 2002; Shirzadi et al., 2012; Zahiri et al., 2006). Major controlling parameters within these studies were lithology, slope angle, tectonic structures and morphology.

Statistical analyses of spatial controlling parameters for larger rock slope instabilities and failures are, however, rare. This is mainly due to relatively small numbers of such events in inventories, from a statistical point of view, resulting in statistically non-significant spatial relations. Therefore, existing studies mainly concentrate on descriptive statistics, comparing characteristics of rock slope instability or past failures to the characteristics of their surrounding areas. Fischer et al. (2012) analysed historic rock slope failures of different magnitudes, ranging from rockfalls to rock avalanches in the European Alps spatially. They present a higher concentration of rock slope failures in areas affected by recent deglaciation, in permafrost areas, for elevations above 2800 meter a.s.l. and on slopes with a slope gradient larger than 40°. Pedrazzini (2012) highlights a strong spatial relation in between large rock slope deformations in the Rhone valley, Switzerland and pre-existing tectonic features, orientation of main foliation, high local relief, high uplift

gradient and high seismic energy release. In contrast, Crosta et al. (2013) and Agliardi et al. (2013) succeeded with a quantitative analysis of a large inventory of deep seated gravitational slope deformations in the European Alps. They suggest that the main controlling factors for this type of rock slope instability are lithology, Last Glacial Maximum ice thickness, local relief, slope size, drainage density and river stream power.

2.3 Landslide susceptibility and hazard assessment

Landslide susceptibility is the spatial probability of occurrence of a landslide within a given area (Fell et al., 2008). It is a qualitative or quantitative measure how prone an area or a certain volume of a mountain side is to landsliding. Landslide susceptibility may include either the source or the run-out area or both. This thesis, however, focuses on the source areas only. Landslide hazard is the probability of the occurrence of a landslide of a certain magnitude within a given time period and within a specified area or at a specific location (Fell et al., 2008).

Landslide susceptibility and hazard can be assessed on different scales, ranging from site specific assessments to regional susceptibility and hazard maps. A variety of methods and models for landslide susceptibility and hazard assessment has been applied, including qualitative and quantitative methods. However, the majority of published literature assesses only landslide susceptibility and not hazard (van Westen, 2004).

Qualitative methods are based on expert knowledge about the study area and the studied phenomenon and are thus highly subjective (Hervás and Bobrowsky, 2009). They include geomorphological mapping, analysis of landslide inventories and heuristic approaches (Guzzetti et al., 1999). The latter are based on expert-weighted combinations of factors associated with landsliding in the study area.

Quantitative methods can be divided into statistically- and physically-based methods. Statistical methods are funded on the analysis of a landslide inventory in combination with several controlling parameters. The resulting spatial relations between landslides and controlling parameters form the basis for susceptibility maps. Statistically-based susceptibility maps are based on the assumption that future landslides of any type will occur under similar geological and geometrical circumstances as past landslides of the same type have occurred (Guzzetti et al., 1999). Various GIS-based statistical analysis methods for landslide susceptibility or hazard assessment have been proposed and applied in the literature. Introductions and overviews of quantitative statistical methods for landslide susceptibility or hazard assessment can be found in Brenning (2005); Chung and Fabbri (2003); Guzzetti (2005); Guzzetti et al. (1999); Hervás and Bobrowsky (2009); Soeters and

van Westen (1996); van Westen (2000). Physically-based models, also called deterministic or geotechnical models, are based on physical laws controlling slope instability. Hazard is determined with slope stability models, resulting in a factor of safety. Physically-based models are primarily applied for site specific hazard estimations due to the requirement of a large amount of geotechnical input data.

2.4 Influence of deglaciation on the stability of rock slopes

In general, three main factors that lead to the destabilization of rock slopes due to glacial processes are reported in literature and will be presented in more detail in the following sections (e.g., Ballantyne, 2002a):

1. Glacial erosion leading to oversteepened rock walls (Section 2.4.1)
2. Glacier retreat resulting in debuttressing of the valley walls (Section 2.4.2)
3. Glacial thinning causing isostatic uplift of the formerly ice-loaded area (Section 2.4.3).

Isostatic uplift acts on a regional scale and is influencing the entire formerly glaciated area. In contrast, the effect of glacial erosion and debuttressing vary on a local scale. Another effect that may influence the stability of rock slopes is erosional unloading. If glacial erosion rates are very high, this erosional unloading may cause uplift of an entire region or local rebound of valley walls and floors (MacGregor et al., 2009). However, it is generally assumed that this influence is relatively small compared to the other three factors mentioned above and is thus not described in more detail here.

Changes in temperature and moisture conditions after deglaciation may additionally have an effect on postglacial slope stability (Hewitt, 2009). Permafrost may develop in the previously ice-bound rock walls after deglaciation and can partly be responsible for the development of rock slope instabilities (Kneisel, 2003; Wegmann et al., 1998). However, only direct glacial influences, as described above, are considered here.

2.4.1 Glacial erosion and oversteepening of slopes

It is a well-known concept that glacial erosion enhances the pre-glacial topography and thus steepens rock slopes as well as deepens valleys (MacGregor, 2000). This effect is enhanced in mountainous terrain where ice flow is concentrated along glacial troughs (Ballantyne, 2002a). A typical V-shaped valley cross-section will

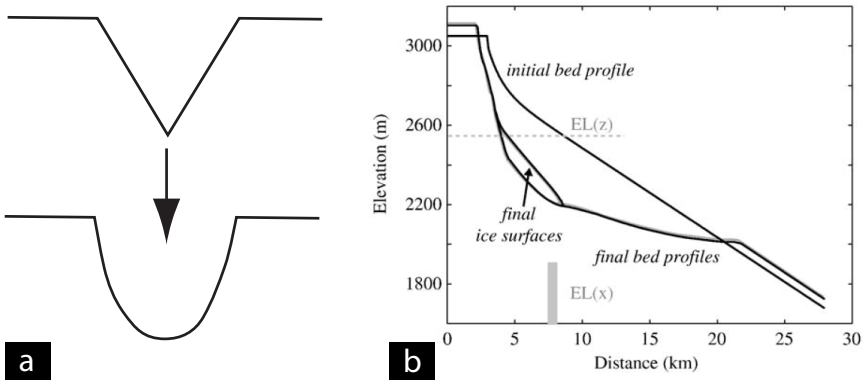

Figure 2.2: a) Originally V-shaped valley cross sections are overdeepened by glacial erosion, leaving U-shaped valleys with steeper valley walls behind. b) Initial and final bedrock profile from numerical modelling of glacial erosion (Source: MacGregor et al. (2009), Fig. 8)

develop into a U-shaped valley by glacial erosion, exhibiting steeper valley walls (Figure 2.2a; Harbor et al., 1988). MacGregor et al. (2009) modelled the valley profile development due to glacial erosion. They showed for various scenarios that valley floors flatten and the height of rock faces increases, thus the valley walls steepen (Figure 2.2b). Furthermore, they point out that the initial geological conditions, like bedrock type or pre-existing joints will strongly influence the glacial erosion and may enhance oversteepening if the geological conditions are favourable. Oversteepening of the valley walls as well as heightening of the rock faces finally leads to increased self-weight shear stresses that act within the rock mass (Figure 2.3a; e.g., Caine, 1982; Radbruch-Hall, 1978). The changed in-situ stress field will lead to failure after deglaciation if the applied stresses exceed the rock mass strength. Abele (1994) argue that glacial oversteepening of the slopes is the main causal factor for rockslides in the European Alps. Eberhardt et al. (2004) demonstrate with numerical models of the Randa rockslide in Switzerland that the stress redistribution resulting from oversteepening of the slopes intensifies the fracture propagation. Holm et al. (2004) show that recent catastrophic failures and deep-seated gravitational slope deformation in British Columbia, Canada, show a spatial correlation with slopes that were oversteepened by glacial erosion during the Little Ice Age. Glacial erosion during successive glacial phases may cause broken slope profiles. Ambrosi and Crosta (2011) presented with numerical modelling that this specific slope geometry is more prone to failure.

2.4.2 Glacial debuttressing

Glacier retreat involves the removal of the support of the glacier ice on the valley walls and thus promotes rock slope failure through the redistribution of internal rock stresses (Evans and Clague, 1994; Haeberli et al., 1997; Selby et al., 1988). Rock masses that are loaded with the weight of a thick ice sheet show much higher internal stress levels than observed only by self-weight loading (Carlsson and Olsson, 1982). If a glacier occupies a valley, the ice load is acting both on the valley floor and the valley walls. This ice-load causes a compression of the rock that leads, when applied over a long time period to a deformation which is in most rock types elastic and thus stored within the rock mass as residual strain energy (Wyrwoll, 1977). Consequently, the removal of a thick ice-sheet and thus the reduction of the confining pressure, results in unloading of the rock mass and strain energy release (Figure 2.3b; Ballantyne, 2002a). This process may alter the state of stress or even shift the orientation of the principal stress field that existed in the rock mass before deglaciation. Commonly a tensile stress region develops behind the slope (Figure 2.3a). Relaxation of these tensile stresses within the rock mass causes rebound within the valley walls (Ballantyne, 2002a). Stress release is preferentially located along pre-existing zones of weakness that are oriented in a suitable direction, otherwise by the formation of new joints. The relaxation of internal stresses after deglaciation may lead to the destabilization of the affected rock slopes, including for example local expansion of rock joints (Figure 2.3c bulging, cracking or slow movements of rock masses (Geertsema et al., 2006).

Debuttressing of formerly glaciated valley slopes is confirmed as the main reason for failure initiation in many studies by numerical modelling (e.g., Agliardi et al., 2001, 2009b; Ambrosi and Crosta, 2006, 2011; Eberhardt et al., 2004; Evans and Clague, 1994; Fischer et al., 2010; Ghirotti et al., 2011; Jaboyedoff et al., 2012). Ambrosi and Crosta (2006) indicate that deformation at the Mt. Legoncino slope in the Italian Alps was initiated directly after the start of the glacial retreat with the development of a basal shear zone. Furthermore, the thickness of the failing mass is increasing with decreasing glacier thickness during continuing deglaciation. In a similar way, Agliardi et al. (2001) suggest that postglacial unloading was the main triggering factor of deep-seated slope deformations in the Italian Alps. Their numerical models show an elastic rebound of the slope and the valley floor during glacier retreat, followed by the formation of failure surfaces and the reactivation of pre-existing fractures. Cossart et al. (2008) studied the spatial distribution of rock slope failures in the Southern Alps of France with regard to the magnitude of glacial stress release. This study showed that the failures are preferentially located where the stresses, imposed by former glacial loading, were highest. They thus conclude that glacial debuttressing and associated stress release played an important role in

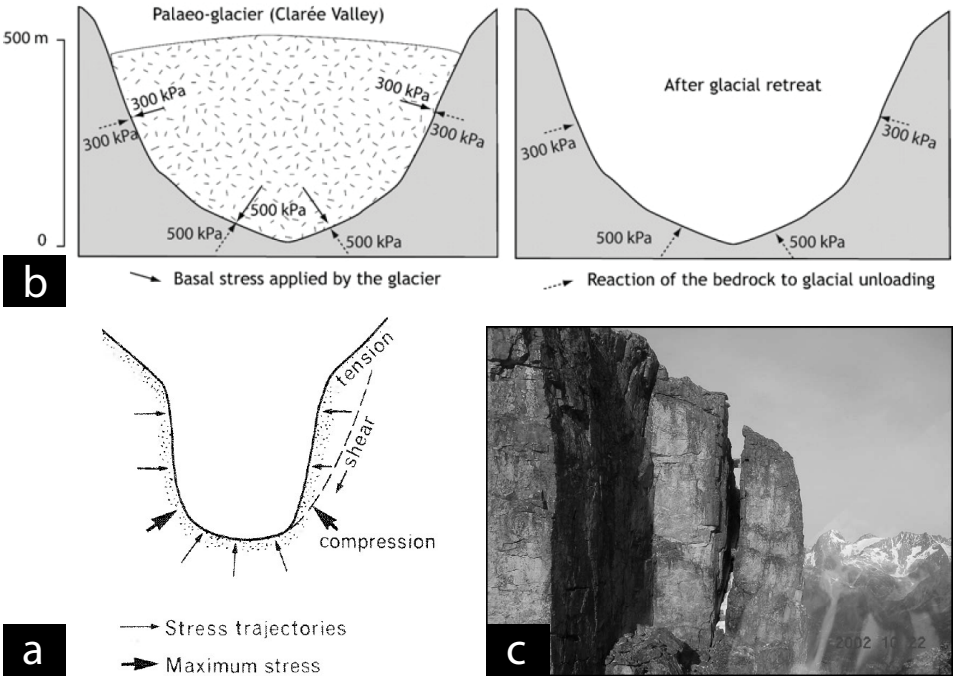

Figure 2.3: a) Many studies suggest tensile stress conditions at the top of a rock slope and compressive stresses at the base of a slope in a recently deglaciated valley (e.g., Crosta et al., 2013; Kinakin and Stead, 2005; Selby, 1993). In addition, increased shear stresses develop owing to oversteepening of the valley walls (Source: Selby (1993) Fig. 15.2). b) During glaciation, the bedrock is reacting against the glacial pressure: an equilibrium exists at the end of the glacial maximum. After deglaciation, the bedrock reaction is still sensitive, generating the deglacial stress release (Source: Cossart et al. (2008), Fig. 3B). c) Vertical joints that have opened in response to glacial debuttressing (Source: Geertsema et al. (2006), Fig. 3).

the development of the rock slope failures.

In contrast to this commonly accepted theory, McColl and Davies (2013) recently questioned that elastic strain due to glacial loading will be stored in a slope. Their studies showed that non-elastic deformation of the ice could accommodate slope deformations. Glacial retreat will after McColl and Davies (2013) only remove the confining pressure and reduce slope support for the glacially oversteepened slopes, which may lead to the development of rock slope failures.

2.4.3 Glacio-isostatic rebound

In formerly glaciated areas isostatic uplift is a consequence of the down melting of the ice sheet. Ice loading causes an elastic flexural response of the lithosphere with a wavelength of the flexure reaching the scale of a mountain range (MacGregor et al., 2009; Persaud and Pfiffner, 2004). The vertical lithospheric uplift after ice removal is a gradual return of the down-warped areas of the ice-loaded crust, back towards its original pre-ice age state. These uplift rates can reach relatively high values compared to tectonic uplift rates. In Fennoscandia, the highest measured present uplift rates are 10 mm/year in the Gulf of Bothnia (Kierulf et al., 2013) and up to 6 mm/year in Norway (Vestøl, 2006).

It has been shown that regional uplift, independent from its origins, can be the cause for an increased relief and, therefore, may negatively affect the stability of slopes (Galadini, 2006; Martino et al., 2004). A direct relation between post-glacial isostatic uplift and the development of rock slope instabilities has not been investigated so far. Henderson and Saintot (2011) present a clustering of historical gravitational slope failures as well as current instabilities at large uplift gradients within a transect through the Norwegian County Møre & Romsdal (Figure 2.4).

2.5 Temporal models of post glacial slope adjustment

Failure of previously ice-bound rock walls occurs in most published cases during or immediately after deglaciation (e.g., Agliardi et al., 2001, 2009a; Ambrosi and Crosta, 2006; Cossart et al., 2008; Hippolyte et al., 2012). However, few studies presented a delayed failure (Hippolyte et al., 2009; McColl, 2012), possibly due to time-dependent dissipation of residual stresses within the rock mass, which lead to a continuous weakening of the rock slope (McColl, 2012; Wyrwoll, 1977). In general, oversteepened slopes tend to adjust rapidly to changed stress conditions owing to glacial debuttressing. Rock slope failure on the affected slopes results in the reduction of the slope angle leading towards a strength equilibrium state

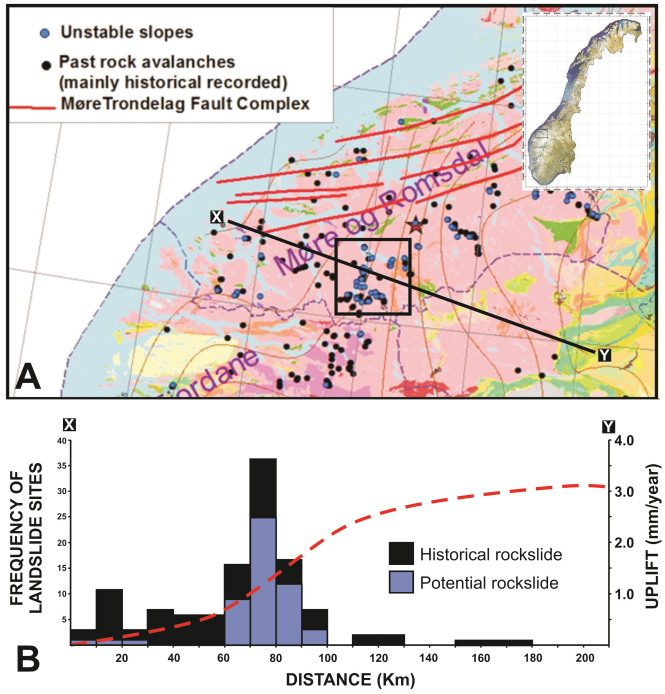

Figure 2.4: Historical rock slope failures and current instabilities cluster at large uplift gradients within a transect through the Norwegian County Møre & Romsdal. A) Overview map. B) Frequency histograms of landslide localities relative to uplift pattern. Profile X-Y includes landslides from a 60 km wide zone around each profile. (Source: Henderson and Saintot (2011), Fig. 1A & B).

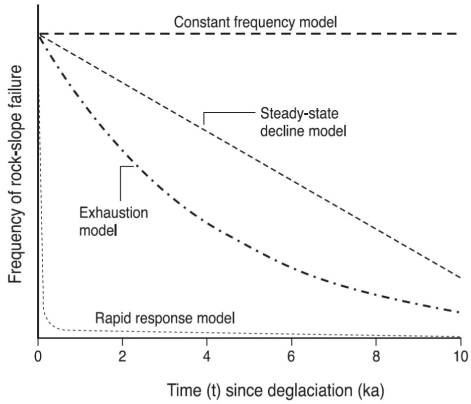

Figure 2.5: Different proposed models about how the frequency of rock slope failures may change following deglaciation (Source: Ballantyne and Stone (2013), Fig. 1)

(Ballantyne, 2002a). However, this adjustment is strongly influenced by the rock mass strength and particularly the existence of a joint network. Since the development of the latter is time-dependent, deep-seated gravitational rock slope failures may still occur long time after deglaciation (Ballantyne, 2002a; Hewitt, 2009). In many cases deep-seated gravitational rock slope deformations are formed by slow rock mass movements directly after deglaciation, producing typical landforms, like convex bulging slopes, doubled ridges, scarps, counter scarps, trenches and others (Agliardi et al., 2001; Ballantyne, 2002a; Kinakin and Stead, 2005). Even if these slope deformations may be a precursor of a catastrophic rock slope failure, many of the studied deep-seated instabilities appear to be inactive now (Agliardi et al., 2001; Ambrosi and Crosta, 2006; Ballantyne, 2002a). Others exhibit the same rate of gravitational creeping since deglaciation (Ambrosi and Crosta, 2006; Blikra et al., 2006; Hermanns et al., 2012b).

It is well accepted that rock slope failures decrease in number and size with the time elapsed since deglaciation (Ballantyne, 2002a, b; Cruden and Hu, 1993), but the exact temporal pattern has only been constructed for few inventories and is still debated (Ballantyne and Stone, 2013; Dortch et al., 2009; McColl, 2012). Different models about how the frequency of rock slope failures may change following deglaciation have been proposed in literature, namely exhaustion, steady state decline, rapid response and constant frequency model (Figure 2.5). Initially, constant frequency models were used (Cruden and Hu, 1993; Evans and Gardner, 1989), assuming that the frequency of rock slope failures in a given area does not change over time. Cruden and Hu (1993) developed an exhaustion model, based

on the observation that slopes rupture only ones. The failure frequency in a given area is thus declining exponentially with time after deglaciation, since the number of potential failure sites is continuously reduced. Ballantyne and Stone (2013) propose two additional models. First, the rapid response model, were most rock slope failures occur directly after deglaciation and only few infrequent failures happen thereafter. Second, they propose a steady-state decline model, which is characterized by a linearly decreasing frequency of rock slope failures in a given area since deglaciation.

Chapter 3

Rock slope failures in Norway

During the last century, Norway has suffered several natural disasters with large numbers of casualties due to rockslides and related tsunamis (Furseth, 2006). Several big historical disasters are documented in western Norway, among them, the Loen and Tafjord fatalities. At Loen seven big rockslides went into the adjacent lake, all of them triggering displacement waves. Two of these lake tsunamis killed together 135 people in the years 1905 and 1936 (Bjerrum and Jørstad, 1968; Grimstad, 2005). Similarly, in 1934 a tsunami wave was created by a rockslide that went into the Tafjord and killed 40 people (Furseth, 2006). Smaller magnitudes of rock slope failures are a frequent hazard in Norway, especially within the Alpine topography of the coastal fjord areas. Historical records and geological studies of western Norway show a high concentration of postglacial gravitational slope failures as well as current rock slope instabilities (Blikra et al., 2006; Saintot et al., 2011; Paper I and II). The counties Sogn & Fjordane and Møre & Romsdal, both located in western Norway, are historically most affected by rock slope failures and have the largest loss of life due to rock slope failures and related tsunamis (Figure 3.1 and 3.2). This high exposure to rock slope failures lead to several studies focusing on current rock slope instabilities in these counties and geological knowledge about rock slope instabilities in these regions was largely extended (Henderson and Saintot, 2011; Hermanns et al., 2011; Saintot et al., 2011,Paper II). Ongoing mapping activities at the Geological Survey of Norway aim to detect all rock slopes that could fail catastrophically. As a results of these studies there are presently four rock slope instabilities under continuous monitoring in Norway (Blikra and Kristensen, 2013; Blikra et al., 2013), Åknes (Blikra, 2008), Hegguraksla and Mannen (Kristensen and Blikra, 2013; Saintot et al., 2012) in western Norway and Nordnes (Nordvik et al., 2010) in northern Norway.

Previous studies of unstable rock slopes are concentrated in western Norway and

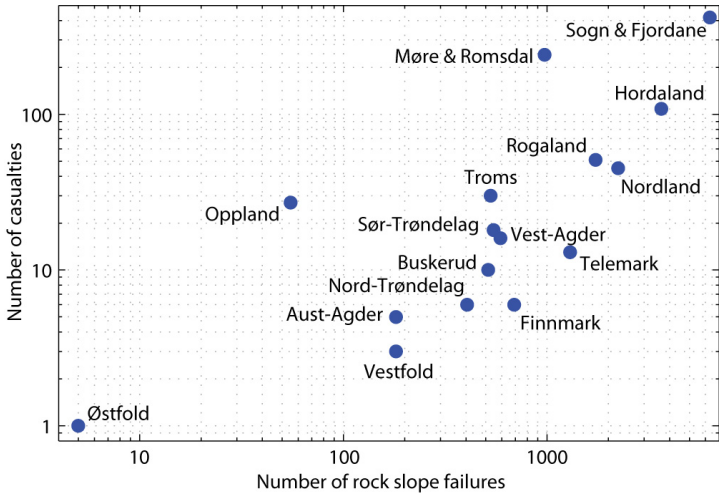

Figure 3.1: Number of rock slope failures and related casualties for each affected Norwegian county (Skrednett). Sogn & Fjordane County is historically most affected by rock slope failures and has the largest loss of life due to rock slope failures and related tsunamis.

are primarily an outcome of the Åknes/Tafjord project. The Åknes/Tafjord project was a large international research project focusing on the investigation, monitoring and early warning of the Åknes rockslide and other large unstable rock slopes in the inner Storfjord region (Figure 3.3; Blikra, 2008). Numerous site specific investigations have been conducted at the Åknes rockslide, covering geophysical investigations (e.g., Heincke et al., 2010; Roth and Blikra, 2009), numerical modelling (e.g., Grøneng et al., 2010; Kveldsvik et al., 2008, 2009a, b), the development of geological models (e.g., Ganerød et al., 2008; Jaboyedoff et al., 2011; Nordvik et al., 2009; Oppikofer et al., 2009), displacement analysis (Grøneng et al., 2011; Nordvik and Nyrnes, 2009) and hazard and risk assessments (e.g., Blikra et al., 2005; Derron et al., 2005a; Eidsvig et al., 2011; Lacasse, 2008). In addition, few studies on other unstable rock slopes in western Norway exist (Anda et al., 2002; Bhasin and Kaynia, 2004; Derron et al., 2005b; Saintot et al., 2012).

More regional investigations, including several present rock slope instabilities and discussing regional aspects of the distribution of those have been undertaken (Blikra et al., 2006; Braathen et al., 2004; Henderson and Saintot, 2011; Oppikofer, 2009; Saintot et al., 2011).

Several studies about historic rock slope failures exist in western Norway, however, they are mainly limited to three rock slope failures, namely the previously mentioned Tafjord (Bjerrum and Jørstad, 1968; Furseth, 1985, 2006; Hermanns

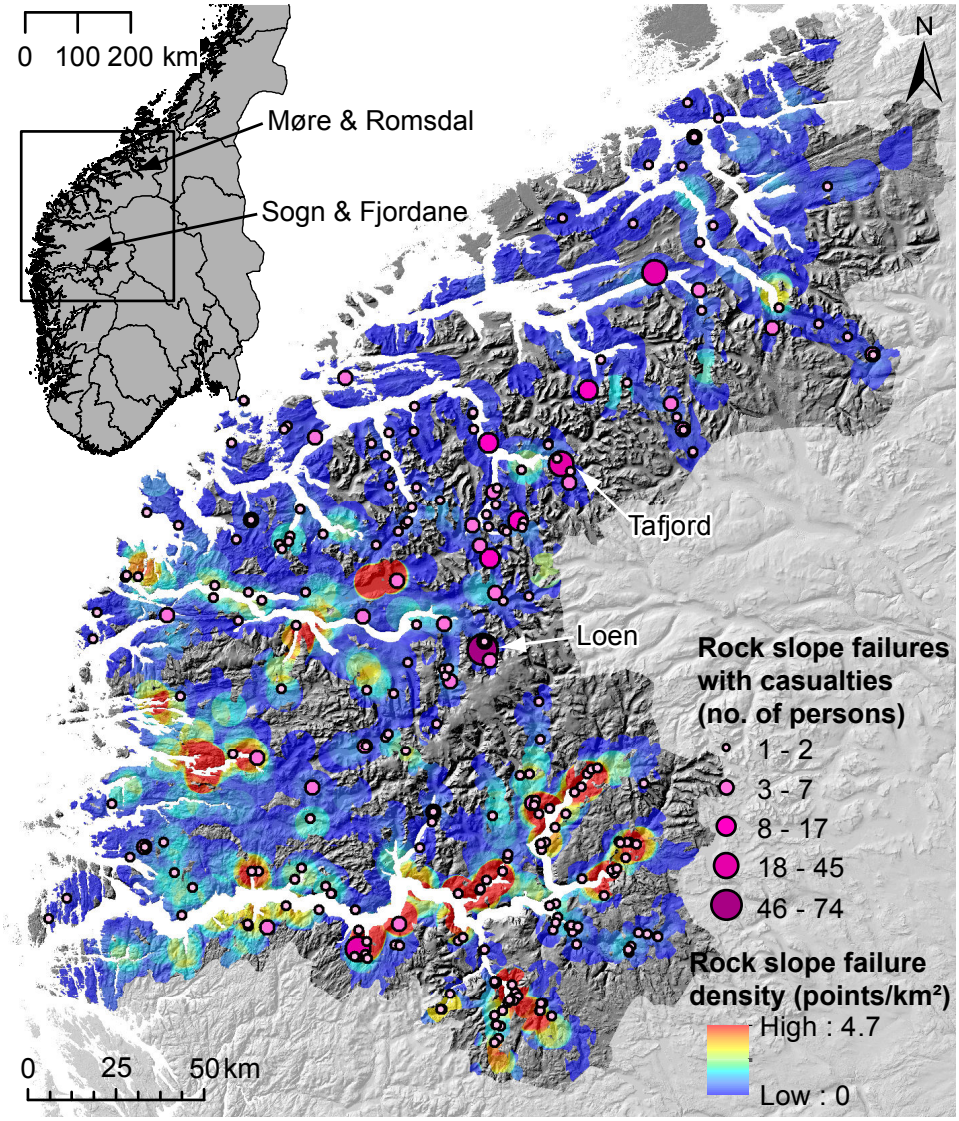

Figure 3.2: Overview of historic rock slope failures in western Norway. Rock slope failure densities are calculated based on a moving circular window with a radius of 5 km. The inset shows the location of the study area within southern Norway.

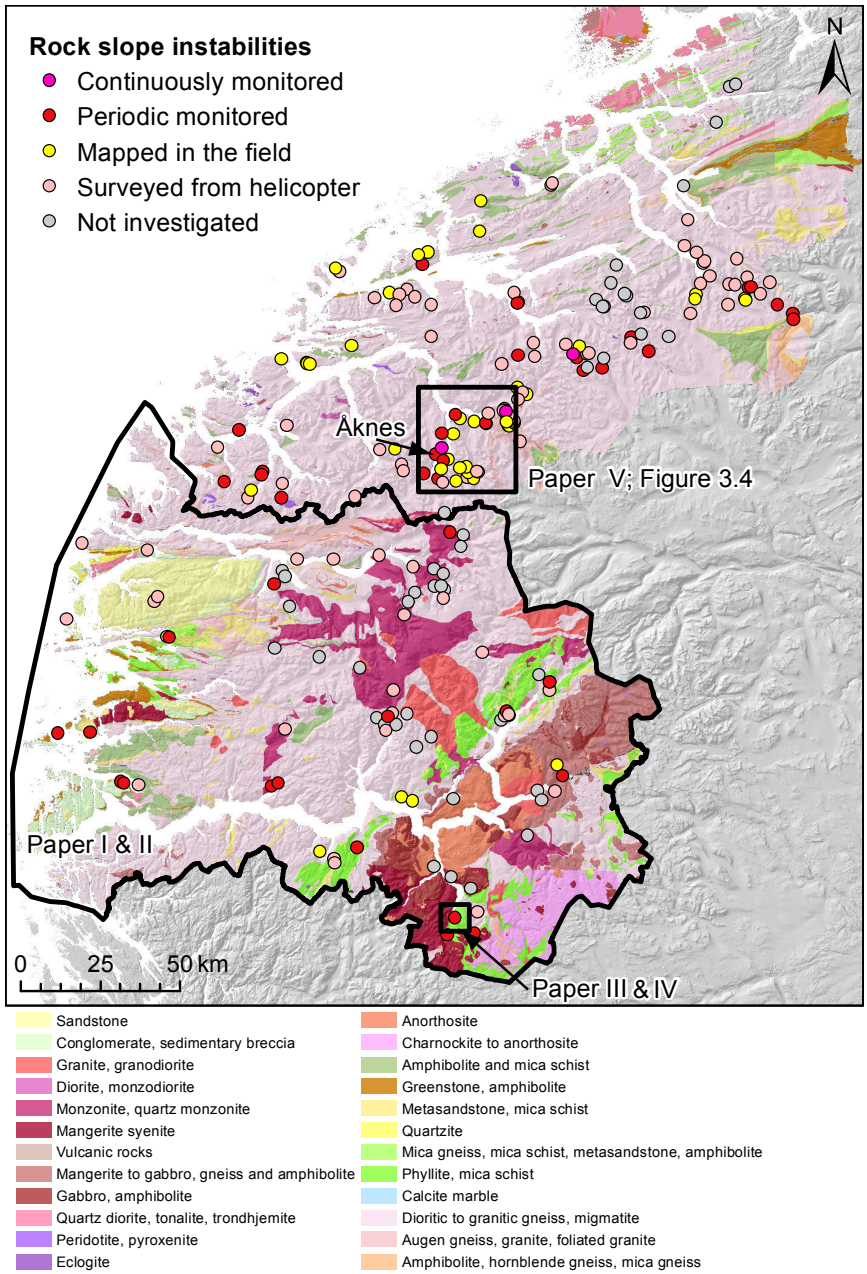

Figure 3.3: Overview of relevant rock slope instabilities in western Norway on top of the 1:250,000 bedrock map of the Geological Survey of Norway (NGU Berggrunnskart). The investigation level presents the highest level of investigation for each instability. The different study areas for each paper are marked with black outlines.

et al., 2006; Jørstad, 1968; Panthi and Nilsen, 2006; Sandersen et al., 1996) and Loen fatalities (Bjerrum and Jørstad, 1968; Furseth, 2006; Grimstad, 2005; Grimstad and Nesdal, 1990; Hermanns et al., 2006; Jørstad, 1968; Sandersen et al., 1996) and in addition a rock slope failure at Tjelle (Furseth, 2006; Jørstad, 1956, 1968; Redfield and Osmundsen, 2009). Most of these studies give only a descriptive overview of those rock slope failures, their fatalities and a general geological or geotechnical description. Besides this, Jørstad (1968) focuses on the tsunamis that have been generated by all three rock slope failures. Grimstad (2005) analysed the stability of the Loen rockslide and Panthi and Nilsen (2006) conducted a numerical analysis of the Tafjord slide. Sandersen et al. (1996) investigate the potential meteorological influence on the Loen and Tafjord rock slope failures. Redfield and Osmundsen (2009) discuss the possible triggering of the Tjelle rock slope failure by an earthquake, linking it to active tectonics.

Only few studies of pre-historic rock slope failures have been conducted in western Norway, focusing either on analysing the release areas (Oppikofer, 2009; Oppikofer et al., 2011) or on mapping and dating of the deposits (Bøe et al., 2004; Fenton et al., 2011; Longva et al., 2009).

3.1 Study area

The study area in general comprises western Norway, including the two Norwegian counties Sogn & Fjordane and Møre & Romsdal. Paper I and II cover the entire county of Sogn & Fjordane covering $18,600\,\mathrm{km}^2$ of land area. Paper III and IV focuses on the unstable rock slope Stampa in Sogn & Fjordane. Signs of postglacial deformation are visible over an area of $11\,\mathrm{km}^2$ at this unstable rock slope. Paper V concentrates on the Storfjord region in Møre & Romsdal, covering an investigated area of $400\,\mathrm{km}^2$ (Figure 3.3). Western Norway is characterized by an alpine relief. Elevations are ranging from sea level up to maximal 2400 m for the highest summit within relatively short distances.

3.1.1 Geology

The bedrock of western Norway consists mainly of Lower Palaeozoic and Precambrian metamorphic rocks. The rocks of the study area have undergone intense reworking by a general NW-SE oriented crustal shortening during the Caledonian Orogeny, resulting in a thrust sheet transport towards SE onto the Precambrian basement (Roberts and Gee, 1985). The geological setting can be divided into three units, the Precambrian basement, the Caledonian nappes and Devonian sedimentary basins including a wide range of lithologies (Figure 3.3). In addition, a significant amount of tectonic events affected the bedrock of western Norway,

including the ductile Caledonian Orogeny, the semi-ductile post-orogenic collapse and also brittle tectonics, like the Permo-Triassic and Jurassic rifting phases. This tectonic history resulted in a high density of brittle, ductile and semi-ductile structures within the study area. A clear structural control of rock slope failures as well as unstable rock slopes is visible in the field (Henderson and Saintot, 2011; Oppikofer, 2009; Oppikofer et al., 2011; Saintot et al., 2011).

3.1.2 Glacial history

Due to its high latitude, entire Norway was affected by the last glaciation, the Late Weichselian glaciation, having its maximum about 20,000 years ago. Deglaciation in western Norway took place in the period 13,000 to 11,000 calibrated ^{14}C years BP (Aarseth et al., 1997; Fareth, 1987; Larsen et al., 1991). However, the innermost fjords where not completely ice free until the glaciers re-advanced during the Younger Dryas at 11,000-10,000 calibrated ^{14}C years BP (Aarseth et al., 1997). The retreat from the Younger Dryas was rapid and the fjords were probably ice free around 10,000 calibrated ^{14}C years BP. However, in the study area exists still one large plateau glacier, the Jostedalsbreen ice cap with several outlets reaching into adjacent valleys. The outlet glaciers retreated since the Little Ice Age maximum around the year 1750 with several still stands or re-advances (Nesje, 2009). After 2000 several outlet glaciers have retreated significantly with annual frontal retreats of more than 100 m (Nesje, 2009).

The topography of western Norway is strongly influenced by the quaternary glaciations. Coastal islands, long U-shaped valleys and many deep fjords with steep slopes are dominating landforms. This steep terrain in combination with heavily fractured exposed bedrock indicates that this area is susceptible to rock slope failures. Deglaciation has in addition resulted in a sudden unloading of the glacially steepened slopes, resulting in a change of internal rock stresses and destabilization of affected rock slopes.

3.1.3 Neotectonics

For the Fennoscandian shield a maximal rebound rate of 50-500 mm/year at about 10,000 BP has been documented (Mørner, 1979). Different geodetic data exhibit a high-rated present-day uplift with rates of up to 6 mm/year within Norway and maximal 10 mm/year in the Gulf of Bothnia (Kierulf et al., 2013; Olesen et al., 2004; Vestøl, 2006). Whereas the general trend of uplift is assumed to be a result of glacial isostasy, there exists a debate about the contribution of potential neotectonic processes (Bungum et al., 2010; Fjeldskaar et al., 2000; Olesen et al., 2000). Generally, Norway has a low to intermediate seismic intensity (Fjeldskaar et al.,

2000). A concentration of earthquake activity is found west of mid-Norway, reflecting a rifted passive continental margin (Bungum et al., 2000). The postglacial tectonic activity, including isostatic rebound and large magnitude earthquakes directly after deglaciation (Fjeldskaar et al., 2000; Olesen et al., 2004), may have contributed to the high concentration of rock slope instabilities in the study area

3.1.4 Climate

The climate of western Norway displays large variations in between the coastal areas and the areas with high relief further inland. The coastal area of the study area includes the areas with the largest normal annual precipitation (3770 mm) as well as the highest normal annual temperatures (7.4°C) of entire Norway. By contrast, the mountain areas, exhibit large areas with normal annual temperatures of -4°C or less representing the lowest annual temperatures of entire Norway. The precipitation is essentially influenced by the large weather systems mainly coming from west, resulting in a zone of maximum precipitation along the coast and along the mountain front. These climatic conditions include heavy seasonal precipitation, intense snowmelt in spring and long frost periods, which increase the vulnerability for rock slope failures in western Norway (Blikra et al., 2006).

3.2 Inventories for rock slope failures and instabilities

Different inventories and databases for rock slope instabilities and failures exist in Norway. They are presented in the following.

The national database of rapid mass movements in Norway is the result of joining four independent databases into one within the GeoExtreme project (Jaedicke et al., 2008, 2009). This database differentiates between five landslide types, namely rockslides, debris slides, snow avalanches, sub-aqueous slides and icefalls. The majority of registered landslides are from the Norwegian Directorate of Public Roads including all types of events that affected a road starting registration in the year 1973. In addition, the Geological Survey of Norway (NGU), the National Rail Administration and the Norwegian Geotechnical Institute (NGI) contributed to the database. Events marked as 'rockslides' in this database represent in most instances rockfalls, however, events collected by NGU include a significant amount of larger magnitude events, like rockslides and rock avalanches and spanning a larger time period with the oldest registered event in the year 900. The combined database contains presently 7278 rockslide events for Møre & Romsdal and Sogn & Fjordane County (Figure 3.2), whereof 6574 are registered by the road authorities, 120 by the

National Rail Administration, 46 by NGI, and 538 historically documented events causing significant damage and fatalities collected at NGU (Furseth, 2006). The majority of events are registered as points where the event hit the road, railway or the location of the damaged object and not at the release area. This complicates the statistical analysis of the database with respect to the controlling factors.

A new database of potential unstable rock slopes in Norway was developed at NGU during the last years (Bunkholt et al., 2013). The rock slope instabilities included in the database are commonly $> 10^5\,m^3$. In the study area, 414 potentially unstable rock slopes have been currently identified (Figure 3.3). However, this database is until now not covering entire Norway systematically. The two counties of the study area are together with Troms County in northern Norway the most systematically mapped counties. All included sites have been investigated to different details, ranging from not mapped to continuous monitoring. In the study area, 3 unstable slopes are continuously monitored, namely Åknes, Hegguraksla and Mannen (Blikra and Kristensen, 2013; Blikra et al., 2013), 50 are periodically monitored, 55 have been mapped in the field, 204 have been surveyed from a helicopter and 102 are just identified based on the interpretation of aerial photographs, InSAR (interferometric synthetic aperture radar) data (Lauknes et al., 2010) or observations of local residents (Figure 3.3). Of all investigated potential instabilities, 188 have been classified as not relevant, either because of too small magnitudes or missing signs of gravitational deformation. A classification system in order to assign relative hazard and risk levels to all rock slope instabilities has been developed (Hermanns et al., 2012a), but is not implemented so far.

In addition, two local but more detailed inventories exist in the Storfjord region, Møre & Romsdal. Longva et al. (2009) mapped 108 prehistoric and historic rockslide and rock avalanche deposits in the inner parts of Storfjord and its tributary fjords based on a complete swath bathymetry and high-resolution reflection-seismic profiles (Figure 3.4). The inventory covers the entire time period after deglaciation and includes the areal extend, volume estimations and a relative age for each slide deposit. Oppikofer (2009) identified and analysed 17 scars of ancient rockslides, 20 potential rock slope instabilities and three deep-seated gravitational slope deformations from field observations and analysis of a high-resolution digital elevation model as well as aerial photographs at the northeastern flank of Tafjord, a tributary fjord of the Storfjord (Figure 3.4). This database includes a detailed structural description of each site, including volume estimations.

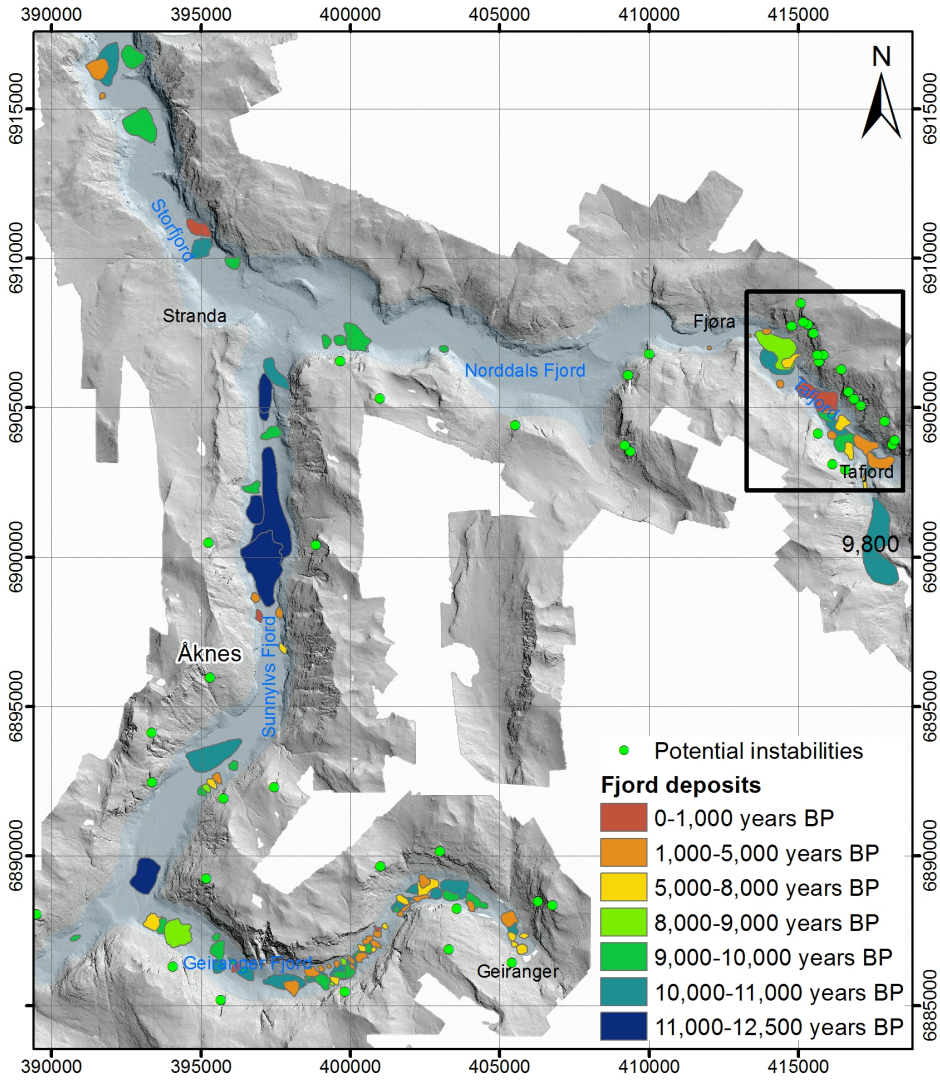

Figure 3.4: Detailed inventory of rockslide deposits in the Storfjord region (Longva et al., 2009). In addition, Oppikofer (2009) analysed Tafjord in more detail and delimited several rock slope instabilities, resulting in a higher density of potential instabilities in this area (outlined in black).

Chapter 4

Methodological approach

A wide variety of methods and techniques have been used in this study at different scales. The studied scales range from local-scale studies covering several single slope instabilities to regional-scale analyses covering the innermost part of a fjord system and up to an entire county. This chapter is giving an overview of the applied methodologies and used data. All methodologies are described in more detail in the corresponding papers.

Available base data, covering the entire study area and thus forming a base for all papers include a digital elevation model with a cell size of 25 m, a 1:250,000 bedrock map of the Geological Survey of Norway (NGU Berggrunnskart), a quaternary map of the Geological Survey of Norway (NGU Løsmassekart), mainly at a scale of 1:250,000 and 1:50,000 for the study area, aerial photographs and topographic maps. In addition, more specific and more detailed datasets were used for the different studies. For the regional-scale studies those include different inventories of rock slope failures and instabilities (Paper I, II and V), as well as neotectonic and climatic data (Paper I). On a local-scale a digital elevation model with higher resolution (Paper III and IV), field data (Paper II, III and IV), differential Global Navigation Satellite System surveys (Paper III and IV) and terrestrial cosmogenic nuclide dates (Paper III and V) have been aquired. Each specific dataset is described in more detail in the corresponding paper.

4.1 Regional-scale approaches

Mainly descriptive statistics were used for the regional-scale studies (Paper I, II and V). Within Paper I and II the locations of rock slope failures and instabilities are investigated statistically with respect to their controlling parameters. Whereas Paper I is based on quantitative GIS-based analyses using the Weights-of-Evidence

method, Paper II is comparing characteristics of different rock slope instabilities in order to define specific characteristics that are typical for the investigated instabilities. The Weights-of-Evidence method is a probabilistic method that uses known occurrences of a feature, which are rock slope instabilities within this study, to quantify spatial associations between these features and the controlling parameters that cause the features to occur (Bonham-Carter et al., 1989). In Paper V the temporal distributions of number and volumes of rockslide deposits on the fjord bottom have been analysed with descriptive statistics in order to define the expectable present day frequencies and magnitudes of rock slope failures in the Storfjord region. In a similar way magnitude-frequency relations have been investigated for the same deposits and additionally for ancient rockslide scars and potential instabilities in order to define the hazard that is due to rock slope failures in this region.

4.2 Local-scale approaches

Local-scale approaches focus on rock slope instabilities in Sogn & Fjordane (Paper II, III and IV) and are strongly based on fieldwork, including geomorphological and structural mapping, in combination with the analysis of high-resolution digital elevation models based on airborne and terrestrial laser scanning data. Volume calculations were possible based on the developed geomorphological and structural models of the instabilities. In addition, simple kinematic feasibility tests for planar sliding, wedge failure and toppling have been made based on the structural data and the criteria defined by Richards et al. (1978) and Hoek and Bray (1981).

Numerical modelling of the most critical area of the unstable rock slope at Stampa (Paper III) was used to investigate the influence of former rockslide activity and to better understand the failure mechanism. A 2D continuum model was used to analyse the stress distribution within the slope and to investigate the influence of unloading the slope due to a prehistoric rockslide using the finite element software *Phase*^{2} (Rocscience, 2012). Furthermore, the potential failure mechanism was investigated in more detail using a discontinuum model with the aim to reproduce the current slope morphology from an assumed pre-deformation topography using the distinct element code UDEC (Itasca, 2004).

Chapter 5

Discussion

In this chapter, the main achievements and particular challenges of the thesis are discussed linking together the research presented in Papers I-V. Specific discussions can be found in the corresponding sections of each paper.

5.1 Rock slope instability inventories

This thesis is primarily based on the analysis of rock slope instability inventories existing in Norway. The distribution and characteristics of registered rock slope instabilities and failures are assumed to reflect the controlling parameters of rock slope instability in the study area.

It has been questioned whether the existing slope failure inventories in Norway are suitable for statistical analysis or not, because of their strong restrictions, mainly temporal and spatial discontinuity and incompleteness (see Section 3.2). However, temporal and spatial censoring of data is a problem that most inventories face including under-reporting of data, incomplete data, inadequate sample time intervals or protective measures in high susceptible zones (Hungr et al., 1999). Especially the registration of most rockfalls within the national rock slope failure database at the place of impact instead of the release area posed a major challenge for statistical analyses.

As emphasized by Fell et al. (2008) and van Westen et al. (2005) it is necessary to analyse different types of landslides separately due to the specific parameters controlling their failure mechanisms. However, the number of statistical analyses focusing specifically on instabilities in massive rock slopes is still very limited compared those studying landslides in general. Hence, this thesis focuses on instabilities in massive rock slopes only.

The studied inventories cover a volume range from few m^3 up to almost 2×10^8 m^3.

This wide range implies that different failure mechanisms and different controlling parameters have to be kept in mind. Therefore, a separation not only into different types of landslides, but also into different volume groups is appropriate for statistical analyses. Different magnitudes of rock slope failures have been analysed on different scales within this thesis. It is expectable to detect different controlling parameters on different scale as well as for different magnitudes. However, this theory could not be investigated systematically, since it was not possible to define the controlling parameters for all magnitudes on all scales.

5.2 Assessment of controlling parameters and susceptibility

This thesis aimed to investigate the feasibility of statistic and probabilistic methods for analysing the rock slope instability inventories existing in Norway with respect to their controlling parameters and in order to assess susceptibility on different scales. The assessment of susceptibility for rock slope instability is closely related to the determination of their controlling parameters. Quantitative statistically-based regional susceptibility assessment depends always on the quantification and spatial mapping of controlling parameters. GIS-based statistical analyses allow the spatial combination of several parameters on a regional scale. Only those studies result in quantitative relations in between controlling parameters and registered events in an inventory allowing to calculate quantitative susceptibility maps.

The results of this thesis confirm that the existing inventories in Norway partially can be used to gain further knowledge about the controlling parameters for rock slope failures. Quantitative statistical analyses of all rockfall events that were registered by the Norwegian Directorate of Public Roads lead to reasonable results in spite of strong restrictions (Paper I). However, an attempt to analyse the controlling parameters for historical rockslides and rock avalanches with the Weights-of-Evidence method did not result in statistically significant results. The same problems were encountered, analysing the database of unstable rock slopes for western Norway quantitatively. This is mainly due to a low density of larger rock slope failures and instabilities. In addition, the development of larger rock slope failures in complex geological and morphological settings like in western Norway cannot be attributed to single causes, but is underlying a complex combination of several controlling parameters, of which not all can be extrapolated to larger regions. Equivalent to numerous studies worldwide (e.g., Agliardi et al., 2001; Hermanns and Strecker, 1999; Jaboyedoff et al., 2009; Sartori et al., 2003; Terzaghi, 1962), a strong structural control of large rock slope instabilities and failures in western Norway is demonstrated on a local scale (Paper II to IV, Henderson and

Saintot, 2011; Oppikofer and Jaboyedoff, 2008; Oppikofer et al., 2011; Saintot et al., 2011). However, owing to the complex structural geological setting, the orientation of specific structures, like foliation or joints, cannot be modelled over larger areas and can thus not be analysed quantitatively on a regional scale. Due to the impossibility of quantifying the relations in between controlling parameters and large rock slope instabilities, quantitative susceptibility could only be assessed for rock slope failures of small magnitudes (Paper I).

However, even if numerous studies claim to produce quantitative susceptibility maps for rock slope failures (e.g., Paper I; Blais-Stevens et al., 2012; Frattini et al., 2008; Marquínez et al., 2003; Marzorati et al., 2002; Shirzadi et al., 2012; Zahiri et al., 2006), a certain degree of subjectivity remains always, when choosing the parameters for the final susceptibility map. Spatial relations of the controlling parameters are judged based on expert knowledge whether they are geologically reasonable or not. In addition, detailed geological knowledge about the study area is always required in order to be able to produce credible susceptibility maps.

Regional scale susceptibility maps (Paper I) should primarily be used as a first-order susceptibility map in order to detect hot spot areas, where critical factor combinations occur. Furthermore, van Westen et al. (2005) recommend to concentrate only on assessing susceptibility instead of hazard or risk for medium to large investigation areas. More detailed investigations should be performed in areas that were identified as especially critical so that more precise susceptibility maps and additionally hazard maps can be prepared.

On a local scale, only relative susceptibilities are obtained for different compartments of the large rock slope instability Stampa based on geomorphological observations and current displacement patterns (Paper III and IV). Recently, Hermanns et al. (2012a) proposed a qualitative hazard classification for Norway to ensure equal and comparable assignments of relative susceptibilities to all rock slope instabilities in Norway. Hazard within this classification, corresponds to susceptibility as defined within this thesis. The proposed method results in a relative susceptibility ranking, based on qualitative evaluation of a series of geomorphological, engineering geological and structural criteria, as well as signs of activity. The outcome of the classification system is a score ranging from 0 (very low susceptibility) to 12 (very high susceptibility). Uncertainties on the susceptibility score can be evaluated using probabilities for each of the criteria (Hermanns et al., 2012a). This classification method should be applied to the unstable rock slope Stampa in order to obtain reproducible and less subjective relative susceptibilities.

As mentioned in the Introduction (Section 1.1) and more detailed in Section 2.4 glacial processes and deglaciation influence the stability of rock slopes and are thus potential controlling parameters. However, this has not been investigated in detail

within this thesis. It is demonstrated that the direct response after deglaciation lasted only a few thousand years in western Norway (Paper V). However, it is unclear in how far the last glaciation and following deglaciation still has an influence on present rock slope instability. The development of most instabilities at convex slope breaks is highlighted within this thesis (Paper II). Likewise, Holm et al. (2004) observed a concentration of rockfall along convex slope breaks. These slope breaks are assumed to be in most cases of glacial origin resulting from successive glacial phases. Ambrosi and Crosta (2011) confirmed with numerical modelling that broken slope profiles are more prone to failure than linear slope profiles. Most of the periodically monitored rock slope instabilities in western Norway exhibit very slow movement rates of $< 4\,\mathrm{mm/year}$. In addition, Hermanns et al. (2012b, 2013) present low long-term movement rates determined by cosmogenic nuclide dating of exposed sliding surfaces of two active unstable rock slopes in Norway. Their results indicate that the presently observable slow movement rates are most likely present since the end of the last glaciation without any significant acceleration. They may thus represent long-term movement rates, that are not critical for a failure in the near future assuming aseismic conditions. Those arguments indicate the need for more detailed studies on the glacial influence on rock slope stability in Norway.

Potential triggering factors for rock slope failures, like for example meteorological effects or seismicity, have not been investigated within this thesis. Indeed, the majority of investigations in Norway is assuming aseismic conditions. As described in Chapter 3.1.3, Norway has a low to intermediate seismic intensity (Fjeldskaar et al., 2000). Seismicity may represent a potential trigger of rock slope failures (e.g., Keefer, 1984; Marzorati et al., 2002) or may lead to rock mass strength reduction as a long term predisposing factor (Jaboyedoff et al., 2003). In the study area the seismicity on land is in general too low in order to trigger rock slope failures (Keefer, 1984) and it should primarily be considered as a long term predisposing factor. A clear spatial relation in between rockfalls and earthquake density could, however, not be defined within this thesis (Paper I). Nevertheless, it cannot completely be excluded that earthquakes with larger magnitudes may occur (NORSAR and NGI, 1998). Bhasin and Kaynia (2004) demonstrate with numerical modelling the partly collapse of a large unstable rock slope in Møre & Romsdal after seismic loading with a peak ground acceleration of $1\,\mathrm{m/s^2}$ for a return period of 475 years (NORSAR and NGI, 1998). This may point out the need for a larger awareness with respect to seismicity as a potential trigger of rock slope failures in Norway.

5.3 Hazard assessment

Hazard assessment of rock slope instabilities is a complex topic, and for example van Westen et al. (2005) state that it cannot be performed over large areas at a sufficient level of detail. In order to define the hazard that is posed to certain regions or specific locations by rock slope instabilities, information about timing, frequency and magnitude distribution of past events is necessary. Historical inventories normally contain only a limited number of large rock slope failures, due to the fact that they cover too short time periods to capture low frequency-high magnitude events adequately. It is thus not possible to obtain significant results from statistical analyses given a homogeneous region. Pre-historic rock slope failures need to be included in order to assess hazard for these magnitudes quantitatively. However, information about the timing for those is sparse.

In Norway, as in many other counties worldwide, there does not exist an inventory covering larger parts of the country that does allow for quantifying hazard over several magnitudes. The national database of rapid mass movements in Norway is unfortunately lacking information on the magnitude of most registered historic rockfall events. In addition, this inventory is most likely not complete and hazard assessments will thus be inaccurate. Several prehistoric rockslide or rock avalanche deposits have been dated either direct or indirect by dating corresponding sliding planes in Norway (e.g., Paper III, V, Aa et al., 2007; Blikra et al., 2006; Fenton et al., 2011; Goehring et al., 2012; Hermanns et al., 2009, 2011; Longva et al., 2009; Oppikofer et al., 2013). However, these are mainly punctual data spread over the entire county, making it difficult to access the hazard regionally nor locally for specific unstable rock slopes. An exception forms the database from Longva et al. (2009). Based on this unique complete inventory of fjord deposits in the Storfjord region (Figure 3.4), present day annual expectable frequencies for different volume classes are assessed based on magnitude-frequency relations (Paper V). In addition, semi-quantitative hazard estimations for potential instabilities in the Storfjord region are obtained (Paper V). However, this study is based on a unique data set and equivalent datasets with the same detail are not existing in Norway. It is thus necessary to investigate in how far the results can be transferred to other regions in Norway and also worldwide. Regions with a similar geology, a similar glacial history and a similar topography should show similar magnitude-frequency relations.

5.4 Temporal distribution of rock slope failures after deglaciation

The assessment of hazard requires information about the temporal distribution of slope failures. A temporal analysis of historic events is difficult due to temporal inconsistency of the national database of rapid mass movements in Norway. In general, the number of registered events increases continuously from the first registered event in the year 900 until present. It is assumed that this increase is due to extended recording activities because of increasing population density as well as enhanced economic and touristic developments in the fjord regions of western Norway, but not to a real increase of rock slope failures.

Considering longer time scales and larger magnitudes, a complete postglacial inventory of rockslide deposits in the Storfjord region exists (Longva et al., 2009). This allowed to define the temporal distribution of rock slope failures following the deglaciation for the inner part of this fjord system in western Norway (Paper V). The results are valuable for other deglaciated regions in the world, but a larger dataset with absolute dates would be necessary in order to be able to define an exact temporal model.

Changing frequencies over time within an inventory may represent temporal changes of controlling parameters. Potential changes during the last century cannot be captured with the existing inventories in Norway, due to the previously mentioned temporal inconsistency. However, for the Storfjord region a direct response with very high rock slope failure activity within 1000 to 2000 years after the deglaciation, followed by a lower but constant frequency, is presented within this thesis (Paper V). The glacier retreat is in this case representing a major change in several controlling parameters (Section 2.4).

Chapter 6

Conclusions

This PhD thesis presents results of the first attempts of quantitative statistical analyses of different inventories covering rock slope instabilities in western Norway. The main parameters controlling the development of rock slope instabilities are defined on different scales for different magnitudes. Furthermore, it is shown that susceptibility and hazard can be assessed with different measures, forming the basis for further decisions regarding risk assessment and mitigation.

Until now, only a limited number of quantitative statistical susceptibility studies focus specifically on rockfall (e.g., Blais-Stevens et al., 2012; Frattini et al., 2008; Marquínez et al., 2003; Marzorati et al., 2002; Shirzadi et al., 2012; Zahiri et al., 2006), compared to those studying landslides in general. In addition, this thesis analyses significantly more and other parameters in order to produce a quantitative statistical rockfall susceptibility map, compared to existing studies, whereas important standard slope-morphological parameters, like slope angle or curvature, are excluded due to restrictions of the inventory (Paper I). This thesis shows as one of the first studies, that a combination of statistically and physically based susceptibility models makes it possible to use road inventories, with registered rockfall impacts instead of sources, for susceptibility modelling (Paper I).

Furthermore, only few studies have analysed large rock slope instabilities spatially (e.g., Agliardi et al., 2013; Crosta et al., 2013; Fischer et al., 2012; Pedrazzini, 2012). This thesis contributes to those with a description of the general spatial distribution of rock slope instabilities in the Norwegian county Sogn & Fjordane, western Norway (Paper II).

The integration of different data sources and results from different analysis methods, including classic geological field investigations, analyses of high-resolution digital elevation models and numerical modelling, allowed to evaluate possible failure mechanisms, to improve process understanding and to assess relative failure

susceptibility and hazard for one specific unstable slope (Paper III and IV).

Owing to the existence of one of the most complete rock slope instability inventories worldwide, which is based on the unique combination of independently mapped fjord deposits (Longva et al., 2009), ancient rockslide scars and potential instabilities (Oppikofer, 2009), regional hazard values are assessed for a region larger than previously reported in literature (Paper V). Furthermore, semi-quantitative hazard values are assigned to a number of potential instabilities in the same study area, compared to previously only site specific hazard assessments.

It is well accepted that rock slope failures decrease in number and size with the time elapsed since deglaciation (e.g., Abele, 1974; Ballantyne, 2002a, b; Cruden and Hu, 1993; Hermanns and Longva, 2012; McColl, 2012), but the exact temporal pattern has only been constructed for few inventories and is still debated (Ballantyne, 2002a, b; Ballantyne and Stone, 2013; Cruden and Hu, 1993). This thesis contributes to this debate with the temporal analysis of an extensive inventory of 108 postglacial rock slope failures (Paper V). Based on the frequency and volume distribution a model composed of a rapid response directly after deglaciation followed by a constant frequency is used for hazard analysis. However, a steady state decline model cannot be excluded.

More specific major findings of this thesis are summarized in the following sections (Section 6.1 to 6.3).

6.1 Parameters controlling development of rock slope instabilities and failures

The spatial relations between rockfalls and several geological and geographical parameters are quantified for the entire county of Sogn & Fjordane (Paper I). The presence of bare rock as well as landslide deposits, the degree of tectonic deformation and the geological lineament density have the strongest spatial relationship to the occurrence of rockfalls in the county of Sogn & Fjordane.

Furthermore, the spatial characteristics of rock slope instabilities in Sogn & Fjordane are analysed (Paper II). The results reveal a preferred location within relatively weak rock units, such as phyllites and weathered mafic gneisses, and the development of most instabilities at convex slope breaks, which are evident as knick-points in the slope profile.

The geological and topographic controlling parameters are investigated on a local scale for the rock slope instability at Stampa (Paper III and IV). Kinematic analyses, displacement measurements and numerical modelling indicate that gravitational slope deformation in the study area is strongly controlled by inherited structures, like pre-existing joint sets and the metamorphic foliation of the phyl-

lites. Large open fractures or surface depressions developed along the main joint sets or a combination of two of them. Numerical modelling also supports a structurally controlled failure, where discontinuities with a low strength dominate the rock mass behaviour.

6.2 Susceptibility assessment for rock slope failures

Susceptibility assessments are addressed at different scales and with different measures (Paper I, III and IV), ranging from a quantitative susceptibility map for the entire county of Sogn & Fjordane, to qualitative measures for susceptibility on a site specific local scale.

A rockfall susceptibility map for the entire county of Sogn & Fjordane is calculated based on statistical analyses of the controlling parameters (Paper I). The model with best performance includes the controlling parameters tectono-stratigraphic position, quaternary geology, geological lineament density, relative relief and slope aspect. Combining the statistical susceptibility model with a physically based model, restricts the susceptibility map to areas that are steep enough to represent a potential rockfall source.

Relative susceptibilities are assigned for single blocks of the unstable rock slope at Stampa (Paper III and IV). Based upon geomorphological studies of prehistoric events, structural variability and monitored displacements it is interpreted that slope deformation and collapse of the slope in future will be similar to the past. It is concluded that the small frontal blocks are very prone to failure, while the free-standing blocks along the cliff with volumes $> 10^5\,\mathrm{m}^3$ are less prone to failure. A failure of a larger volume involving several million m^3 is presently considered to be of very low likelihood.

6.3 Hazard assessment for rock slope failures

Implications for the hazard that is posed by different parts of an unstable rock slope can be assessed based on geomorphological mapping and dated pre-historic events (Paper III). For the unstable rock slope Stampa, small collapses of blocks $< 10^5\,\mathrm{m}^3$ along the frontal cliff will be more frequent, because several deposits of this magnitude have been mapped on the slope. Medium-sized collapses of free-standing blocks along the cliff with volumes $> 10^5\,\mathrm{m}^3$, cannot be ruled out. At least two such events have occurred since the end of the last glaciation. Large rockslide deposits on the fjord bottom, which date back to the end of the last glaciation (Blikra et al., 2006), indicate that a collapse involving several million m^3 is of very low likelihood and most likely linked to major climatic changes like

glacial-interglacial cycles.

The detailed inventory of rockslide deposits in the inner parts of Storfjord, Møre & Romsdal (Longva et al., 2009), which includes relative ages, allowed a more detailed hazard analysis of rock slope failures in this region (Paper V). Present day annual expectable frequencies for certain volume classes have been assessed for the Storfjord region based on magnitude-frequency analyses. For example, the annual frequency for rock slope failures of $V \geq 1 \times 10^6\,\mathrm{m}^3$ in the entire Storfjord region is approximately 1/1,200. Semi quantitative hazard estimations for each potential instability have been obtained based on a qualitative susceptibility assessment of each instability. The annual failure probabilities for the individual instabilities are very low and vary from 1/10,000 to 1/48,000

Chapter 7

Recommendations for future work

This thesis is a first approach to quantitatively analyse the controlling parameters of rock slope failures and instabilities in Norway. In addition, possibilities for susceptibility and hazard assessments were investigated. The results are promising, but it is evident that some results require more testing and could be further improved.

The controlling parameters for rockfalls and the rockfall susceptibility have been analysed for the county Sogn & Fjordane only (Paper I). However, it would be interesting to extend the investigations to other regions in Norway, in order to study potential regional variations within the controlling parameters. Furthermore, the produced susceptibility map is limited to the source areas. It would be beneficial to also transfer the different likelihoods of the source zones to the propagation zones of the existing physical rockfall susceptibility map (Derron, 2010).

For analysing larger rock slope failures and instabilities it would probably be beneficial to test other statistical methods than Weights-of-Evidence in order to be able to obtain statistically significant results. Especially the important structural control of large instabilities in Norway has potential for more quantitative analyses (Paper III and IV). It should be tested to model the orientation of structures over a limited region, in order to analyse the spatial dependencies in between structures and rock slope instabilities or failures. An optimal study area for testing this, would be the Storfjord region as there exist large amounts of structural data.

So far, rock slope instabilities have been studied systematically in only three counties of Norway, which are Møre & Romsdal, Sogn & Fjordane and Troms. Knowledge about their spatial controlling parameters in those counties should be systematised and quantified in order to be applied to counties that have not yet

been studied systematically and to detect potential rock slope failures in those more efficiently. In order to define the spatial controlling parameters of rock slope instabilities, more parameters have to be involved than it has been done in Paper II, including both, parameters that favour failure on certain locations as well as parameters that are due to the development of an instability, like for example typical morphologies.

In this thesis, the controlling parameters have just been analysed spatially, but the underlying physical reasons have not been studied in detail. However, several results encourage for further investigations, as for example the preferred development of rock slope instabilities along knick-points of the slope profiles (Paper II).

In order to assess the hazard that is posed by large rock slope instabilities for larger regions than it has been done in Paper V, a systematic mapping of pre-historic rock slope failures would be necessary, preferably including absolute or relative information about the timing. Regarding the hazard due to rockfall, combined spatial and temporal analysis of rockfalls in the national database should be conducted.

As already mentioned in the introduction (Section 1.1) and more detailed in Section 2.4 glacial processes and deglaciation influence the stability of rock slopes. The alpine topography of western Norway is especially prone to rock slope failures after deglaciation (Section 3.1.2). This thesis analysed the temporal distribution of rock slope failures after deglaciation, but did not investigate in more detail the glacial processes that may have lead to destabilization. Therefore, more research on the glacial influence for rock slope stability in western Norway is necessary.

References

Aa, A. R., Sjåstad, J., Sønstegaard, E., and Blikra, L. H.: Chronology of Holocene rock-avalanche deposits based on Schmidt-hammer relative dating and dust stratigraphy in nearby bog deposits, Vora, inner Nordfjord, Norway, The Holocene, 17, 955–964, 2007.

Aarseth, I., Austbø, P., and Risnes, H.: Seismic stratigraphy of Younger Dryas ice-marginal deposits in western Norwegian fjords, Norsk Geologisk Tidsskrift, 77, 65–86, 1997.

Abele, G.: Bergstürze in den Alpen: ihre Verbreitung, Morphologie und Folgeerscheinungen, Wissenschaftliche Alpenvereinshefte, Heft 25, 230, 1974.

Abele, G.: Large rockslides: their causes and movement on internal sliding planes, Mountain Research and Development, 14, 315–320, 1994.

Agliardi, F., Crosta, G. B., and Zanchi, A.: Structural constraints on deep-seated slope deformation kinematics, Engineering Geology, 59, 83–102, 2001.

Agliardi, F., Crosta, G. B., Zanchi, A., and Ravazzi, C.: Onset and timing of deep-seated gravitational slope deformations in the eastern Alps, Italy, Geomorphology, 103, 113–129, 2009a.

Agliardi, F., Zanchi, A., and Crosta, G. B.: Tectonic vs. gravitational morphostructures in the central Eastern Alps (Italy): Constraints on the recent evolution of the mountain range, Tectonophysics, 474, 250, 2009b.

Agliardi, F., Crosta, G. B., Frattini, P., and Malusà, M. G.: Giant non-catastrophic landslides and the long-term exhumation of the European Alps, Earth and Planetary Science Letters, 365, 263–274, 2013.

Ambrosi, C. and Crosta, G. B.: Large sackung along major tectonic features in the Central Italian Alps, Engineering Geology, 83, 183–200, 2006.

Ambrosi, C. and Crosta, G. B.: Valley shape influence on deformation mechanisms of rock slopes, in: Slope Tectonics, edited by Jaboyedoff, M., pp. 215–233, Geological Society, London, Special Publications, 351, 2011.

Anda, E., Blikra, L. H., and Braathen, A.: The Berill Fault-first evidence of neotectonic faulting in southern Norway, Norsk Geologisk Tidsskrift, 82, 175–182, 2002.

Ballantyne, C. K.: Paraglacial geomorphology, Quaternary Science Reviews, 21, 1935–2017, 2002a.

Ballantyne, C. K.: A general model of paraglacial landscape response, The Holocene, 12, 371–376, 2002b.

Ballantyne, C. K. and Stone, J. O.: Timing and periodicity of paraglacial rock-slope failures in the Scottish Highlands, Geomorphology, 186, 150–161, 2013.

Bhasin, R. and Kaynia, A. M.: Static and dynamic simulation of a 700-m high rock slope in western Norway, Engineering Geology, 71, 213–226, 2004.

Bjerrum, L. and Jørstad, F. A.: Stability of rock slopes in Norway, Tech. Rep. NGI report no. 79, Norwegian Geotechnical Institute, 1968.

Blais-Stevens, A., Behnia, P., Kremer, M., Page, A., Kung, R., and Bonham-Carter, G.: Landslide susceptibility mapping of the Sea to Sky transportation corridor, British Columbia, Canada: comparison of two methods, Bulletin of Engineering Geology and the Environment, 71, 447–466, 2012.

Blikra, L., Longva, O., Harbitz, C., and Løvholt, F.: Quantification of rock-avalanche and tsunami hazard in Storfjorden, western Norway, in: Landslides and avalanches ICFL 2005 Norway, edited by Senneset K, Flaate K, L. J., pp. 57–64, Taylor & Francis Group, 2005.

Blikra, L. H.: The Åknes rockslide; monitoring, threshold values and early-warning, in: Landslides and Engineered Slopes. From the Past to the Future - Proceedings of the 10th International Symposium on Landslides and Engineered Slopes, 30 June - 4 July 2008, Xi'an, China, edited by Chen, Z., Zhang, J., Li, Z., Wu, F., and Ho, K., vol. 2, pp. 1089–1094, Taylor & Francis Group, London, 2008.

Blikra, L. H. and Kristensen, L.: Monitoring concepts and requirements for large rockslides in Norway, in: Landslide Science and Practice, pp. 193–200, Springer, 2013.

Blikra, L. H., Longva, O., Braathen, A., Anda, E., Dehls, J. F., and Stalsberg, K.: Rock slope failures in Norwegian fjord areas: Examples, spatial distribution

and temporal pattern, in: Landslides from Massive Rock Slope Failure; NATO Science Series, IV. Earth and Environmental Sciences, Vol 49, edited by Evans, S. G., Scarascia Mugnozza, G., Strom, A., and Hermanns, R. L., pp. 475–496, Springer, Dodrecht, Netherlands, 2006.

Blikra, L. H., Kristensen, L., and Lovisolo, M.: Subsurface monitoring of large rockslides in Norway: A key requirement for early warning, in: International Conference Vajont 1963-2013. Thoughts and analyses after 50 years since the catastrophic landslide, Padua, Italy - 8-10 October 2013, edited by Genevais, R. and Prestininzi, A., pp. 307–314, Sapienza Università Editrice, 2013.

Bøe, R., Longva, O., Lepland, A., Blikra, L. H., Sønstegaard, E., Hadlidason, H., Bryn, P., and Lien, R.: Postglacial mass movements and their causes in fjords and lakes in western Norway, Norwegian Journal of Geology, 84, 35–56, 2004.

Bonham-Carter, G. F., Agterberg, F. P., and Wright, D. F.: Weigths of evidence modeling: a new approach to mapping mineral potential, in: Statistical Applications in the Earth Sciences, edited by Agterberg, F. P. and Bonham-Carter, G. F., pp. 171–183, Geological Survey of Canada, Report 89-09, 1989.

Braathen, A., Blikra, L. H., Berg, S. S., and Karlsen, F.: Rock-slope failure in Norway; type, geometry, deformation mechanisms and stability, Norwegian Journal of Geology, 84, 67–88, 2004.

Brenning, A.: Spatial prediction models for landslide hazards: review, comparison and evaluation, Natural Hazards and Earth System Science, 5, 853–862, 2005.

Bungum, H., Lindholm, C. D., Dahle, A., Woo, G., Nadim, F., Holme, J. K., Gudmestad, O. T., Hagberg, T., and Karthigeyan, K.: New seismic zoning maps for Norway, the North Sea, and the United Kingdom, Seismological Research Letters, 71, 687–697, 2000.

Bungum, H., Olesen, O., Pascal, C., Gibbons, S., Lindholm, C., and Vestøl, O.: To what extent is the present seismicity of Norway driven by post-glacial rebound?, Journal of the Geological Society, 167, 373–384, 2010.

Bunkholt, H. S. S., Nordahl, B., Hermanns, R. L., Oppikofer, T., Fischer, L., Blikra, L. H., Anda, E., Dahle, H., and Sætre, S.: Database of unstable rock slopes of Norway, in: Landslide Science and Practice, pp. 423–428, Springer, 2013.

Caine, N.: Toppling failures from alpine cliffs on Ben Lomond, Tasmania, Earth Surface Processes and Landforms, 7, 133–152, 1982.

Carlsson, A. and Olsson, T.: High rock stresses as a consequence of glaciation, Nature, 298, 739–742, 1982.

Chung, C.-J. F. and Fabbri, A. G.: Validation of spatial prediction models for landslide hazard mapping, Natural Hazards, 30, 451–472, 2003.

Clark, P. U., Dyke, A. S., Shakun, J. D., Carlson, A. E., Clark, J., Wohlfarth, B., Mitrovica, J. X., Hostetler, S. W., and McCabe, A. M.: The last glacial maximum, Science, 325, 710–714, 2009.

Cossart, E., Braucher, R., Fort, M., Bourles, D. L., and Carcaillet, J.: Slope instability in relation to glacial debuttressing in alpine areas (Upper Durance catchment, southeastern France): Evidence from field data and ^{10}Be cosmic ray exposure ages, Geomorphology, 95, 3–26, 2008.

Crosta, G. B., Frattini, P., and Agliardi, F.: Deep seated gravitational slope deformations in the European Alps, Tectonophysics, 605, 13–33, 2013.

Cruden, D. and Hu, X.: Exhaustion and steady state models for predicting landslide hazards in the Canadian Rocky Mountains, Geomorphology, 8, 279–285, 1993.

Cruden, D. M. and Varnes, D. J.: Landslide types and process, in: Landslides Investigation and Mitigation, edited by Turner, A. K. and Schuster, R. L., vol. Special Report 247, pp. 36–75, Transportation Research Board, National Research Council, National Academy Press, Washington, DC, 1996.

Derron, M.-H.: Method for the susceptibility mapping of rock falls in Norway - Technical report, Tech. rep., Geological Survey of Norway, 2010.

Derron, M.-H., Blikra, L. H., and Jaboyedoff, M.: High resolution digital elevation model analysis for landslide hazard assessment (Åkerneset, Norway), in: Landslides and Avalanches: ICFL 2005 Norway, edited by Senneset, K., Flaate, K., and Larsen, J. O., pp. 101–106, Taylor & Francis Group, London, 2005a.

Derron, M.-H., Jaboyedoff, M., and Blikra, L. H.: Preliminary assessment of rockslide and rockfall hazards using a DEM (Oppstadhornet, Norway), Natural Hazards and Earth System Sciences, 5, 285–292, 2005b.

Dortch, J. M., Owen, L. A., Haneberg, W. C., Caffee, M. W., Dietsch, C., and Kamp, U.: Nature and timing of large landslides in the Himalaya and Transhimalaya of northern India, Quaternary Science Reviews, 28, 1037–1054, 2009.

Duarte, R. M. and Marquínez, J.: The influence of environmental and lithologic factors on rockfall at a regional scale: an evaluation using GIS, Geomorphology, 43, 117–136, 2002.

Dunlop, S.: Rockslides in a changing climate: Establishing relationships between meteorological conditions and rockslides in southwestern Norway for the Purposes of Developing a Hazard Forecast System, Master's thesis, Queen' s University Kingston, Ontario, Canada, 2010.

Dyrrdal, A. V., Isaksen, K., Hygen, H. O., and Meyer, N. K.: Changes in meteorological variables that can trigger natural hazards in Norway, Clim Res, 55, 153–165, 2012.

Eberhardt, E., Stead, D., and Coggan, J. S.: Numerical analysis of initiation and progressive failure in natural rock slopes - the 1991 Randa rockslide, International Journal of Rock Mechanics & Mining Sciences, 41, 69–87, 2004.

Eidsvig, U. M., Medina-Cetina, Z., Kveldsvik, V., Glimsdal, S., Harbitz, C. B., and Sandersen, F.: Risk assessment of a tsunamigenic rockslide at Åknes, Natural Hazards, 56, 529–545, 2011.

Erener, A. and Düzgün, H. S. B.: Improvement of statistical landslide susceptibility mapping by using spatial and global regression methods in the case of Møre and Romsdal (Norway), Landslides, 7, 55–68, 2010.

Evans, S. G. and Clague, J. J.: Recent climatic change and catastrophic geomorphic processes in mountain environments, Geomorphology, 10, 107–128, 1994.

Evans, S. G. and Gardner, J. S.: Geological hazards in the Canadian Cordillera, in: Quaternary Geology of Canada and Greenland. Geology of North America. Vol. K-1., edited by Fulton, R. J., chap. 1, pp. 702–713, Geological Society of America, Boulder, CO, 1989.

Fareth, O. W.: Glacial geology of middle and inner Nordfjord, western Norway, Tech. Rep. 408, Norwegian geological survey, 1987.

Fell, R., Corominas, J., Bonnard, C., Cascini, L., Leroi, E., and Savage, W. Z.: Guidelines for landslide susceptibility, hazard and risk zoning for land use planning, Engineering Geology, 102, 85–98, 2008.

Fenton, C. R., Hermanns, R. L., Blikra, L. H., Kubik, P. W., Bryant, C., Niedermann, S., Meixner, A., and Goethals, M. M.: Regional ^{10}Be production rate calibration for the past 12ka deduced from the radiocarbon-dated Grøtlandsura and Russenes rock avalanches at 69°N, Norway, Quaternary Geochronology, 6, 437–452, 2011.

Fischer, L., Amann, F., Moore, J. R., and Huggel, C.: Assessment of periglacial slope stability for the 1988 Tschierva rock avalanche (Piz Morteratsch, Switzerland), Engineering Geology, 116, 32–43, 2010.

Fischer, L., Purves, R., Huggel, C., Noetzli, J., and Haeberli, W.: On the influence of topographic, geological and cryospheric factors on rock avalanches and rockfalls in high-mountain areas, Natural Hazards and Earth System Sciences, 12, 241–254, 2012.

Fjeldskaar, W., Lindholm, C., Dehls, J. F., and Fjeldskaar, I.: Postglacial uplift, neotectonics and seismicity in Fennoscandia, Quaternary Science Reviews, 19, 1413–1422, 2000.

Flatøy, F., Barstad, I., and Sorteberg, A.: The GeoExtreme project, Module B: Description of the current climate and investigation of future climate scenarios, in: 33rd International Geological Congress (33IGC), Oslo, Norway - General proceedings, pp. 6–14, IUGS, Oslo, Norway, 2008.

Frattini, P., Crosta, G. B., Carrara, A., and Agliardi, F.: Assessment of rockfall susceptibility by integrating statistical and physically-based approaches, Geomorphology, 94, 419–437, 2008.

Furseth, A.: Dommedagsfjellet - Tafjord 1934, Gyldendal Norsk Ferlag A/S, 1985.

Furseth, A.: Skredulykker i Norge, Tun Forlag, Oslo, Norway, 2006.

Galadini, F.: Quaternary tectonics and large-scale gravitational deformations with evidence of rock-slide displacements in the Central Apennines (central Italy), Geomorphology, 82, 201–228, 2006.

Ganerød, G. V., Grøneng, G., Rønning, J. S., Dalsegg, E., Elvebakk, H., Tønnesen, J. F., Kveldsvik, V., Eiken, T., Blikra, L. H., and Braathen, A.: Geological model of the Åknes rockslide, western Norway, Engineering Geology, 102, 1–18, 2008.

Geertsema, M., Clague, J. J., Schwab, J. W., and Evans, S. G.: An overview of recent large catastrophic landslides in northern British Columbia, Canada, Engineering Geology, 83, 120–143, 2006.

Ghirotti, M., Martin, S., and Genevois, R.: The Celentino deep-seated gravitational slope deformation (DSGSD): structural and geomechanical analyses (Peio Valley, NE Italy), in: Slope Tectonics, edited by Jaboyedoff, M., pp. 235–251, Geological Society, London, Special Publications, 351, 2011.

Goehring, B. M., Lohne, Ø. S., Mangerud, J., Svendsen, J. I., Gyllencreutz, R., Schaefer, J., and Finkel, R.: Late glacial and holocene ^{10}Be production rates for western Norway, Journal of Quaternary Science, 27, 89–96, 2012.

Grimstad, E.: The Loen rock slide - an analysis of the stability, in: Landslides and Avalanches: ICFL 2005 Norway, edited by Senneset, K., Flaate, K., and Larsen, J. O., pp. 129–135, Taylor & Francis Group, London, 2005.

Grimstad, E. and Nesdal, S.: The Loen rockslides - A historical review, in: Rock joints: Proceedings of the International Symposium on Rock Joints, Loen, Norway, 4-6 June, 1990, edited by Barton, N. and Stephansson, O., pp. 3–8, A.A. Balkema, Rotterdam, 1990.

Grøneng, G., Lu, M., Nilsen, B., and Jenssen, A. K.: Modelling of time-dependent behavior of the basal sliding surface of the Åknes rockslide area in western Norway, Engineering Geology, 114, 414–422, 2010.

Grøneng, G., Christiansen, H. H., Nilsen, B., and Blikra, L. H.: Meteorological effects on seasonal displacements of the Åknes rockslide, western Norway, Landslides, 8, 1–15, 2011.

Guzzetti, F.: Landslide Hazard and Risk Assessment, Ph.D. thesis, Rheinische Friedrich-Wilhelms-Universität Bonn, Germany, 2005.

Guzzetti, F., Carrara, A., Cardinali, M., and Reichenbach, P.: Landslide hazard evaluation: a review of current techniques and their application in a multi-scale study, Central Italy, Geomorphology, 31, 181–216, 1999.

Haeberli, W., Wegmann, M., and der Muhll, D. V.: Slope stability problems related to glacier shrinkage and permafrost degradation in the Alps, Eclogae Geologicae Helvetiae, 90, 407–414, 1997.

Harbor, J. M., Hallet, B., and Raymond, C. F.: A numerical model of landform development by glacial erosion, Nature, 333, 347–349, 1988.

Heim, A.: Bergsturz und Menschenleben, Vierteljahrsschrift der Naturforschenden Gesellschaft in ZÃ¼rich, 77, 1–214, 1932.

Heincke, B., Günther, T., Dalsegg, E., Rønning, J. S., Ganerød, G. V., and Elvebakk, H.: Combined three-dimensional electric and seismic tomography study on the Åknes rockslide in western Norway, Journal of Applied Geophysics, 70, 292–306, 2010.

Henderson, I. H. C. and Saintot, A.: Regional spatial variations in rockslide distribution from structural geology ranking: an example from Storfjord, western Norway, in: Slope Tectonics, edited by Jaboyedoff, M., pp. 79–95, Geological Society, London, Special Publications, 351, 2011.

Hermanns, R. L. and Longva, O.: Rapid rock-slope failures, in: Landslides: Types, Mechanisms and Modeling, edited by Clague, J. J. and Stead, D., pp. 59–70, Cambridge University Press, Cambridge, UK, 2012.

Hermanns, R. L. and Strecker, M. R.: Structural and lithological controls on large Quaternary rock avalanches (sturzstroms) in arid northwestern Argentina, Geological Society of America Bulletin, 111, 934–948, 1999.

Hermanns, R. L., Blikra, L. H., Naumann, M., Nilsen, B., Panthi, K. K., Stromeyer, D., and Longva, O.: Examples of multiple rock-slope collapses from Köfels (Ötz valley, Austria) and western Norway, Engineering Geology, 83, 94–108, 2006.

Hermanns, R. L., Blikra, L. H., and Longva, O.: Relation between rockslide dam and valley morphology and its impact on rockslide dam longevity and control on potential breach development based on examples from Norway and the Andes, in: Proceedings of the 2nd International Conference on Long Term Behavior of Dams, 12th-13th October 2009, Graz, Austria, edited by Bauer, E., Semprich, S., and Zenz, G., pp. 789–794, Gray Universitz of Technology, Graz, Austria, 2009.

Hermanns, R. L., Fischer, L., Oppikofer, T., Böhme, M., Dehls, J. F., Henriksen, H., Booth, A., Eilertsen, R., Longva, O., and Eiken, T.: Mapping of unstable and potentially unstable slopes in Sogn og Fjordane (work report 2008-2010), Tech. Rep. 2011.055, Geological Survey of Norway, 2011.

Hermanns, R. L., Oppikofer, T., Anda, E., Blikra, L. H., Böhme, M., Bunkholt, H., Crosta, G. B., Dahle, H., Devoli, G., Fischer, L., Jaboyedoff, M., Loew, S., Sætre, S., and Molina, F. Y.: Recommended hazard and risk classification system for large unstable rock slopes in Norway, Tech. Rep. 2012.029, Geological Survey of Norway, 2012a.

Hermanns, R. L., Redfield, T. F., Bunkholt, H., Fischer, L., Oppikofer, T., Gosse, J., and Eiken, T.: Cosmogenic nuclide dating of slow moving rockslides in Norway in order to assess long-term slide velocities, in: Landslides and Engineered Slopes. Protecting Society through Improved Understanding: Proceedings of the 11th International & 2nd North American Symposium on Landslides, Banff, Canada, 3-8 June 2012, edited by Eberhardt, E., Froese, C., Turner, A. K., and Leroueil, S., CRC Press, 2012b.

Hermanns, R. L., Oppikofer, T., Dahle, H., Eiken, T., Ivy-Ochs, S., and Blikra, L. H.: Understanding long-term slope deformation for stability assessment of rock slopes: the case of the Oppstadhornet rockslide, Norway, in: International Conference Vajont 1963-2013. Thoughts and analyses after 50 years since the

catastrophic landslide, Padua, Italy - 8-10 October 2013, edited by Genevais, R. and Prestininzi, A., pp. 255–264, Sapienza Università Editrice, 2013.

Hervás, J. and Bobrowsky, P.: Mapping: inventories, susceptibility, hazard and risk, in: Landslides - Disaster Risk Reduction, edited by Sassa, K. and Canuti, P., pp. 321–349, Springer, Berlin, 2009.

Hewitt, K.: Glacially conditioned rock-slope failures and disturbance-regime landscapes, Upper Indus Basin, northern Pakistan, Geological Society, London, Special Publications, 320, 235–255, 2009.

Hippolyte, J.-C., Bourlès, D., Braucher, R., Carcaillet, J., Léanni, L., Arnold, M., and Aumaitre, G.: Cosmogenic ^{10}Be dating of a sackung and its faulted rock glaciers, in the Alps of Savoy (France), Geomorphology, 108, 312–320, 2009.

Hippolyte, J.-C., Bourlès, D., Lèanni, L., Braucher, R., Chauvet, F., and Lebatard, A. E.: ^{10}Be ages reveal >12ka of gravitational movement in a major sackung of the Western Alps (France), Geomorphology, 171, 139–153, 2012.

Hoek, E. and Bray, J.: Rock Slope Engineering, E & FN Spon, London, 3rd edn., 1981.

Holm, K., Bovis, M., and Jakob, M.: The landslide response of alpine basins to post-Little Ice Age glacial thinning and retreat in southwestern British Columbia, Geomorphology, 57, 201–216, 2004.

Hungr, O., Evans, S., and Hazzard, J.: Magnitude and frequency of rock falls and rock slides along the main transportation corridors of southwestern British Columbia, Canadian Geotechnical Journal, 36, 224–238, 1999.

Itasca: UDEC-Universal Distinct Element Code v4.0: Numerical modeling code for advanced geotechnical analysis of soil, rock, and structural support in two dimensions, Tech. rep., Itasca Consulting Group, 2004.

Jaboyedoff, M., Baillifard, F., and Derron, M.-H.: Preliminary note on uplift rates gradient, seismic activity and possible implications for brittle tectonics and rockslide prone areas: The example of western Switzerland, Bulletin de Géologie de l'Université de Lausanne, 88, 401–420, 2003.

Jaboyedoff, M., Baillifard, F., Derron, M.-H., Couture, R., Locat, J., and Locat, P.: Modular and evolving rock slope hazard assessment methods, in: Landslides and Avalanches: ICFL 2005 Norway, edited by Senneset, K., Flaate, K., and Larsen, J. O., pp. 187–194, Taylor & Francis Group, London, 2005.

Jaboyedoff, M., Couture, R., and Locat, P.: Structural analysis of Turtle Mountain (Alberta) using digital elevation model: Toward a progressive failure, Geomorphology, 103, 5–16, 2009.

Jaboyedoff, M., Oppikofer, T., Derron, M.-H., Blikra, L. H., Böhme, M., and Saintot, A.: Complex landslide behaviour and structural control: a three-dimensional conceptual model of Åknes rockslide, Norway, in: Slope tectonics, edited by Jaboyedoff, M., pp. 147–161, Geological Society, London, Special Publications, 351, 2011.

Jaboyedoff, M., Derron, M.-H., Jakubowski, J., Oppikofer, T., and Pedrazzini, A.: Mt. Eiger, European Alps, in: Landslides: Types, Mechanisms and Modeling, edited by Clague, J. J. and Stead, D., Cambridge University Press, Cambridge, UK, 2012.

Jaedicke, C., Solheim, A., Blikra, L. H., Stalsberg, K., Sorteberg, A., Aaheim, A., Kronholm, K., Vikhamar-Schuler, D., Isaksen, K., Sletten, K., Kristensen, K., Barstad, I., Melchiorre, C., Høydal, O. A., and Mestl, H.: Spatial and temporal variations of Norwegian geohazards in a changing climate, the GeoExtreme Project, Natural Hazards and Earth System Sciences, 8, 893–904, 2008.

Jaedicke, C., Lied, K., and Kronholm, K.: Integrated database for rapid mass movements in Norway, Natural Hazards and Earth System Sciences, 9, 469–479, 2009.

Jørstad, F. A.: Fjellskredet ved Tjelle. Et 200-års minne, Naturen, 80, 1956.

Jørstad, F. A.: Waves generated by landslides in Norwegian fjords and lakes, Tech. Rep. NGI report no. 79, Norwegian Geotechnical Institute, 1968.

Keefer, D. K.: Landslides caused by earthquakes, Geological Society of America Bulletin, 95, 406–421, 1984.

Kierulf, H. P., Ouassou, M., Simpson, M. J. R., and Vestøl, O.: A continuous velocity field for Norway, Journal of Geodesy, 87, 337–349, 2013.

Kinakin, D. and Stead, D.: Analysis of the distributions of stress in natural ridge forms: implications for the deformation mechanisms of rock slopes and the formation of sackung, Geomorphology, 65, 85–100, 2005.

Kneisel, C.: Permafrost in recently deglaciated glacier forefields-measurements and observations in the eastern Swiss Alps and northern Sweden, Zeitschrift für Geomorphologie, NF, 47, 289–305, 2003.

Kristensen, L. and Blikra, L. H.: Monitoring displacement on the Mannen rockslide in western Norway, in: Landslide Science and Practice, pp. 251–256, Springer, 2013.

Kveldsvik, V., Nilsen, B., Einstein, H., and Nadim, F.: Alternative approaches for analyses of a $100,000\,m^3$ rock slide based on Barton-Bandis shear strength criterion, Landslides, 5, 161–176, 2008.

Kveldsvik, V., Einstein, H. H., Nilsen, B., and Blikra, L. H.: Numerical analysis of the $650,000\,m^2$ Åknes rock slope based on measured displacements and geotechnical data, Rock Mechanics and Rock Engineering, 42, 689–728, 2009a.

Kveldsvik, V., Kaynia, A. M., Nadim, F., Bhasin, R., Nilsen, B., and Einstein, H. H.: Dynamic distinct-element analysis of the 800m high Åknes rock slope, International Journal of Rock Mechanics and Mining Sciences, 46, 686–698, 2009b.

Lacasse, S.: Event tree analysis of Åknes rock slide hazard, in: 4th Canadian Conference on Geohazards : From Causes to Management, pp. 551–558, Quebec, Canada, 2008.

Larsen, E., Longva, O., and Follestad, B. A.: Formation of De Geer moraines and implications for deglaciation dynamics, Journal of Quaternary Science, 6, 263–277, 1991.

Lauknes, T. R., Shanker, A. P., Dehls, J. F., Zebker, H. A., Henderson, I. H. C., and Larsen, Y.: Detailed rockslide mapping in northern Norway with small baseline and persistent scatterer interferometric SAR time series methods, Remote Sensing of Environment, 114, 2097–2109, 2010.

Longva, O., Blikra, L. H., and Dehls, J.: Rock avalanches - distribution and frequencies in the inner part of Storfjorden, Møre og Romsdal County, Norway, Tech. Rep. 2009.002, Geological Survey of Norway, 2009.

MacGregor, K. R.: Numerical simulations of glacial-valley longitudinal profile evolution, Geology, 28, 1031–1034, 2000.

MacGregor, K. R., Anderson, R. S., and Waddington, E. D.: Numerical modeling of glacial erosion and headwall processes in alpine valleys, Geomorphology, 103, 189–204, 2009.

Marquínez, J., Duarte, R. M., Farias, P., and Sánchez, M. J.: Predictive GIS-based model of rockfall activity in mountain cliffs, Natural Hazards, 30, 341–360, 2003.

Martino, S., Moscatelli, M., and Mugnozza, G. S.: Quaternary mass movements controlled by a structurally complex setting in the central Apennines (Italy), Engineering Geology, 72, 33–55, 2004.

Marzorati, S., Luzi, L., and Amicis, M. D.: Rock falls induced by earthquakes: a statistical approach, Soil Dynamics and Earthquake Engineering, 22, 565–577, 2002.

McColl, S. T.: Paraglacial rock-slope stability, Geomorphology, 153-154, 1–16, 2012.

McColl, S. T. and Davies, T. R. H.: Large ice-contact slope movements: glacial buttressing, deformation and erosion, Earth Surface Processes and Landforms, 38, 1102–1115, 2013.

Mørner, N.-A.: The Fennoscandian uplift and Late Cenozoic geodynamics: geological evidence, GeoJournal, 3, 287–318, 1979.

Nesje, A.: Latest Pleistocene and Holocene alpine glacier fluctuations in Scandinavia, Quaternary Science Reviews, 28, 2119, 2009.

NGU Berggrunnskart: NGU Berggrunn - Nasjonal berggrunnsdatabase `http://geo.ngu.no/kart/berggrunn/`, 2013.

NGU Løsmassekart: NGU Løsmasser - Nasjonal løsmassedatabase `http://geo.ngu.no/kart/losmasse/`, 2013.

Nordvik, T. and Nyrnes, E.: Statistical analysis of surface displacements - an example from the Åknes rockslide, western Norway, Natural Hazards and Earth System Sciences, 9, 713–724, 2009.

Nordvik, T., Grøneng, G., Ganerød, G. V., Nilsen, B., Harding, C., and Blikra, L. H.: Geovisualization, geometric modelling and volume estimation of the Åknes rockslide, Western Norway, Bulletin of Engineering Geology and the Environment, 68, 245–256, 2009.

Nordvik, T., Blikra, L. H., Nyrnes, E., and Derron, M.-H.: Statistical analysis of seasonal displacements at the Nordnes rockslide, northern Norway, Engineering Geology, 114, 228–237, 2010.

NORSAR and NGI: Development of a seismic zonation for Norway, Report for Norwegian Council for Building Standardization, Tech. rep., 1998.

Olesen, O., Dehls, J., Bungum, H., Riis, F., Hicks, E., Lindholm, C., Blikra, L. H., Fjeldskaar, W., Olsen, L., and Longva, O.: Neotectonics in Norway, Final Report, Tech. Rep. 2000.002, Geological Survey of Norway, 2000.

Olesen, O., Blikra, L. H., Braathen, A., Dehls, J. F., Olsen, L., Rise, L., Roberts, D., Riis, F., Faleide, J. I., and Anda, E.: Neotectonic deformation in Norway and its implications: a review, Norsk Geologisk Tidsskrift, 84, 3–34, 2004.

Oppikofer, T.: Detection, analysis and monitoring of slope movements by high-resolution digital elevation models, Ph.D. thesis, University of Lausanne, Switzerland, 2009.

Oppikofer, T. and Jaboyedoff, M.: Åknes/Tafjord project: Analysis of ancient rockslide scars and potential instabilities in the Tafjord area & Laser scanner monitoring of instabilities at Hegguraksla, Tech. Rep. IGAR-TO-009, Institute of Geomatics and Analysis of Risk, University of Lausanne, 2008.

Oppikofer, T., Jaboyedoff, M., Blikra, L. H., and Derron, M.-H.: Characterization and monitoring of the Åknes rockslide using terrestrial laser scanning, Natural Hazards and Earth System Sciences, 9, 1003–1019, 2009.

Oppikofer, T., Jaboyedoff, M., Pedrazzini, A., Derron, M.-H., and Blikra, L. H.: Detailed DEM analysis of a rockslide scar to improve the basal failure surface model of active rockslides, Journal of Geophysical Research, 116, F02 016, 2011.

Oppikofer, T., Saintot, A., Otterå, S., Hermanns, R. L., Anda, E., Dahle, H., and Eiken, T.: Investigations on unstable or potential unstable rock slopes in Møre og Romsdal - status and plans after field surveys in 2012, Tech. Rep. 2013.014, Geological Survey of Norway, 2013.

Panthi, K. and Nilsen, B.: Numerical analysis of stresses and displacements for the Tafjord slide, Norway, Bulletin of Engineering Geology and the Environment, 65, 57–63, 2006.

Pedrazzini, A.: Characterization of gravitational rock slope deformations at different spatial scales based on field, remote sensing and numerical approaches, Ph.D. thesis, University of Lausanne, Switzerland, 2012.

Persaud, M. and Pfiffner, O. A.: Active deformation in the eastern Swiss Alps: post-glacial faults, seismicity and surface uplift, Tectonophysics, 385, 59–84, 2004.

Radbruch-Hall, D.: Gravitational creep of rock masses on slopes, Rockslides and avalanches, 1, 607–657, 1978.

Redfield, T. F. and Osmundsen, P. T.: The Tjellefonna fault system of Western Norway: Linking late-Caledonian extension, post-Caledonian normal faulting, and Tertiary rock column uplift with the landslide-generated tsunami event of 1756, Tectonophysics, 474, 106, 2009.

Richards, L. R., Leg, G. M. M., and Whittle, R. A.: Appraisal of stability conditions in rock slopes, in: Foundation Engineering in Difficult Ground, edited by Bell, F. G., pp. 449–512, Newnes-Butterworth, London, UK, 1978.

Roberts, D. and Gee, D. G.: An introduction to the structure of the Scandinavian Caledonides, in: The Caledonide orogen-Scandinavia and related areas, edited by Gee, D. G. and Sturt, B. A., vol. 1, pp. 55–68, John Wiley & Sons, 1985.

Rocscience: Phase2 v8.0: Finite Element Analysis for Excavations and Slopes, Tech. rep., Rocscience Inc., Canada, 2012.

Roth, M. and Blikra, L. H.: Seismic monitoring of the unstable rock slope at Åknes, Norway, Geophysical Research Abstracts, 11, 3680, 2009.

Ruff, M. and Czurda, K.: Landslide susceptibility analysis with a heuristic approach in the Eastern Alps (Vorarlberg, Austria), Geomorphology, 94, 314–324, 2008.

Saintot, A., Henderson, I., and Derron, M.-H.: Inheritance of ductile and brittle structures in the development of large rock slope instabilities: examples from western Norway, in: Slope tectonics, edited by Jaboyedoff, M., pp. 27–78, Geological Society, London, Special Publications, 351, 2011.

Saintot, A., Oppikofer, T., and Derron, M.-H.: Large gravitational rock slope deformation in Romsdalen valley (Western Norway), Revista de la Asociación Geológica Argentina, 69, 354–371, 2012.

Sandersen, F., Bakkehøi, S., Hestnes, E., and Lied, K.: The influence of meteorological factors on the initiation of debris flows, rockfalls, rockslides and rockmass stability, in: Proceedings of the 7th International Symposium on Landslides, Trondheim, edited by Senneset, K., pp. 97–114, Balkema, Rotterdam, 1996.

Sartori, M., Baillifard, F., Jaboyedoff, M., and Rouiller, J.-D.: Kinematics of the 1991 Randa rockslides (Valais, Switzerland), Natural Hazards and Earth System Sciences, 3, 423–433, 2003.

Selby, M. J.: Hillslope Materials and Processes, Oxford University Press, New York, 2nd edition edn., 1993.

Selby, M. J., Augustinus, P., Moon, V. G., and Stevenson, R. J.: Slopes on strong rock masses: modelling and influences of stress distributions and geomechanical properties, Modelling Geomorphological Systems, edited by MG Anderson, pp. 341–374, 1988.

Shirzadi, A., Saro, L., Joo, O. H., and Chapi, K.: A GIS-based logistic regression model in rock-fall susceptibility mapping along a mountainous road: Salavat Abad case study, Kurdistan, Iran, Natural Hazards, 64, 1639–1656, 2012.

Skrednett: `http://www.skrednett.no`, 2013.

Soeters, R. and van Westen, C. J.: Slope stability: recognition, analysis and zonation, in: Landslides Investigation and Mitigation, edited by Turner, A. K. and Schuster, R. L., vol. Special Report 247, pp. 129–177, Transportation Research Board, National Research Council, National Academy Press, Washington, DC, 1996.

Tanarro, L. M. and Muñoz, J.: Rockfalls in the Duratón canyon, central Spain: Inventory and statistical analysis, Geomorphology, 169-170, 17–29, 2012.

Terzaghi, K.: Stability of steep slopes on hard unweathered rock, Geotechnique, 12, 251–263, 1962.

van Westen, C. J.: The modelling of landslide hazards using GIS, Surveys in Geophysics, 21, 241–255, 2000.

van Westen, C. J.: Geo-information tools for landslide risk assessment : an overview of recent developments, in: 9th International symposium on landslides, pp. 39–56, London: Balkema, Rio de Janeiro, Brasil, 2004.

van Westen, C. J., van Asch, T. W. J., and Soeters, R.: Landslide hazard and risk zonation - why is it still so difficult?, Bulletin of Engineering Geology and the Environment, 65, 167–184, 2005.

Vestøl, O.: Determination of postglacial land uplift in Fennoscandia from leveling, tide-gauges and continuous GPS stations using least squares collocation, Journal of Geodesy, 80, 248–258, 2006.

Wegmann, M., Gudmundsson, G. H., and Haeberli, W.: Permafrost changes in rock walls and the retreat of Alpine glaciers: a thermal modelling approach, Permafrost and Periglacial Processes, 9, 23–33, 1998.

Wyrwoll, K.-H.: Causes of rock-slope failure in a cold area: Labrador-Ungava, Geological Society of America Reviews in Engineering Geology, 3, 59–67, 1977.

Zahiri, H., Palamara, D., Flentje, P., Brassington, G., and Baafi, E.: A GIS-based weights-of-evidence model for mapping cliff instabilities associated with mine subsidence, Environmental Geology, 51, 377–386, 2006.

Appendix A

Paper I

Reference to the paper

Böhme, M., Derron, M.-H. and Jaboyedoff, M.: Quantitative spatial analysis of rockfalls from road inventories - a combined statistical and physical model. Submitted to Natural Hazards and Earth System Sciences.

Note on contributions

The candidate wrote this paper and carried out all analyses. Ideas and the final manuscript were discussed with Marc-Henry Derron and Michel Jaboyedoff.

Manuscript prepared for Nat. Hazards Earth Syst. Sci.
with version 5.0 of the LaTeX class copernicus.cls.
Date: 28 November 2013

Quantitative spatial analysis of rockfalls from road inventories: a combined statistical and physical susceptibility model

M. Böhme[1,2], M.-H. Derron[3], and M. Jaboyedoff[3]

[1]Geological Survey of Norway, Trondheim, Norway
[2]Norwegian University of Science and Technology, Trondheim, Norway
[3]Center for Research on Terrestrial Environment, University of Lausanne, Lausanne, Switzerland

Correspondence to: M. Böhme
(martina.bohme@ngu.no)

Abstract. Quantitative spatial analyses and statistical susceptibility assessments based on road inventories are often complicated due to the registration of impacts instead of source areas. A rockfall inventory from the Norwegian Directorate of Public Roads is analysed spatially in order to investigate potential controlling parameters in the Norwegian county Sogn & Fjordane. Quantitative spatial relationships are then used to model rockfall susceptibility with the help of the Weights-of-Evidence method. The controlling parameters tectono-stratigraphic position, quaternary geology, geological lineament density, relative relief and slope aspect resulted in the best performing model and thus yielded the basis for the statistical susceptibility map for the entire county of Sogn & Fjordane. Due to registered impacts instead of sources, the important parameter slope angle could not be included in the statistical models. Combining the statistical susceptibility model with a physically based model, restricts the susceptibility map to areas that are steep enough to represent a potential rockfall source. This combination makes it possible to use road inventories, with registered impacts instead of sources, for susceptibility modelling.

1 Introduction

Landslide inventories compiled by road authorities contain often the most comprehensive records, but are in many cases limited to registered impacts on the roads, lacking information about the source areas. This complicates quantitative spatial analyses of these inventories with respect to their controlling parameters depending on the resolution of the latter. Especially parameters originating from a digital elevation model (DEM), like slope angle, curvature, roughness or elevation itself, often have a resolution that is smaller than the distance between source and deposition area of landslides. Analysing the slope angle distribution for registered events of a road inventory, will in many cases yield too low slope angles. However, many studies indicate that a steep slope is the principal pre-disposing factor for landslide processes especially rock slope failures (e.g., Aleotti and Chowdhury, 1999; Blais-Stevens et al., 2012; Erener and Düzgün, 2010; Kayastha et al., 2012b; Marzorati et al., 2002; Neuhäuser et al., 2012; Shirzadi et al., 2012). Quantitative spatial analyses result thus often in a susceptibility map reproducing a slope-angle map. On the other hand, a steep slope angle is a physical requirement for the presence of rock slope failures and using physically based approaches to define a relation between slope angle and the occurrence of landslides is thus much more appropriate. Hence, we propose an approach using a physical model to determine possible rockfall source areas and to update these source zones with relative susceptibilities obtained from a statistical model. This integration of statistically and physically based rockfall susceptibility models makes it possible to use road inventories with registered data points at deposits for the calculation of susceptibility maps.

The data basis of this study forms a rockfall inventory from the Norwegian Directorate of Public Roads. Rockfalls are a frequent hazard in Norway, especially within the Alpine topography of the coastal fjord areas. Steep slopes in combination with unfavourable climatic conditions, like heavy seasonal precipitation, intense snowmelt in spring and long frost periods, increase the vulnerability for rock slope failures in these regions (Blikra et al., 2006; Saintot et al., 2011). However, these might not be the single parameters controlling the spatial distribution of rockfalls. Jaboyedoff et al. (2005)

give an overview on factors influencing rock slope instability, grouped into external and internal parameters. Various studies investigate rockfall locations with respect to their controlling parameters statistically (e.g., Duarte and Marquínez, 2002; Ruff and Czurda, 2008; Tanarro and Muñoz, 2012), or try to predict rockfall source areas by the means of different statistical or probabilistic modelling techniques on a regional scale, resulting in susceptibility maps (e.g., Blais-Stevens et al., 2012; Frattini et al., 2008; Marquínez et al., 2003; Marzorati et al., 2002; Shirzadi et al., 2012; Zahiri et al., 2006). However, the number of quantitative statistical susceptibility studies focusing specifically on rockfall is still very limited in comparison to those studying other landslide types or landslides in general, which has become very popular using GIS. Also Fell et al. (2008) and van Westen et al. (2005) emphasize that it is necessary to study the susceptibility of different types of landslides separately due to the specific parameters controlling their failure mechanism.

Up to now studies of unstable rock slopes in Norway are mainly directed towards site-specific research of large instabilities (e.g., Böhme et al., 2011; Braathen et al., 2004), but not towards quantitative regional scale investigations. Only few studies discuss some more regional aspects of unstable rock slopes. For example, Blikra et al. (2006) describe a clustering of rockslides in specific zones of Norway, but do not include the underlying reasons in this spatial approach. Saintot et al. (2011) and Henderson and Saintot (2011) describe a link between rock slope instabilities in western Norway and ductile and brittle structures, but these studies are not based on quantitative analyses. Bjerrum and Jørstad (1968) and Sandersen et al. (1996) highlight a meteorological influence on rockfalls by applying simple binary statistics of historical events. In contrast, Dunlop (2010) investigated the relation between rock slope failures and meteorological conditions as well as topography and geology quantitatively applying Weights-of-Evidence based susceptibility mapping for a region in southwestern Norway (Hordaland and Sogn & Fjordane Counties). Furthermore, Erener and Düzgün (2010) present a statistically based susceptibility map of landslides for western Norway (Møre & Romsdal County) applying different regression methods. However, their focus is strongly on the mathematical methodology, and not on the input data and geological model. In addition, a lack of detailed knowledge about the local geological conditions as well as the used inventory is obvious.

The primary objective of this study is to determine the controlling parameters involved in the development of rockfalls in western Norway with the help of a quantitative spatial analysis. Furthermore, the possibility to use a road inventory with clear limitations for quantitative spatial analyses is investigated. Therefore the Weights-of-Evidence method is here first used as an explanatory tool, helping to quantify the relation between rockfalls and certain controlling parameters and second to produce a statistically based rockfall susceptibility map. The results provide a better understanding of the spatial distribution of rockfalls in western Norway and the underlying reasons for their development. At last, the statistical susceptibility map is intersected with physically determined potential rockfall source zones (Derron, 2010) in order to obtain the final rockfall susceptibility map.

2 Study area

The study area comprises the entire county of Sogn & Fjordane, covering $18,607\,\mathrm{km}^2$ of land area (Figure 1). Historical data and geological studies show a high concentration of post-glacial gravitational slope failures as well as current rock slope instabilities in the Norwegian county Sogn & Fjordane, situated in western Norway (Blikra et al., 2006; Böhme et al., 2011; Saintot et al., 2011). This lead to several studies focusing on current rock slope instabilities in this county and geological knowledge about rock slope instabilities in these regions was largely extended (Böhme et al., 2011; Hermanns et al., 2011; Saintot et al., 2011).

The restriction to a county instead of using natural borders, the latter probably being more appropriate for modelling a natural process, was chosen due to the division of the Norwegian Directorate of Public Roads on a county base. In order to obtain the best possible homogeneity in the data, it is reasonable to use the limits of a county as the limits of the study area. Nevertheless, it is impossible to reach perfect homogeneity because of the subjective registration of rockfall events by different individuals.

3 Susceptibility assessment

Assuming that future landslides of any type will occur under similar geological and geometrical circumstances as past landslides of the same type have occurred, it is possible to study a landslide inventory in combination with several influencing factors and to analyse their spatial relation in order to prepare susceptibility maps (Guzzetti et al., 1999). Various GIS-based statistical analysis methods as well as quantitative prediction models for landslide susceptibility or hazard have been proposed and applied in the literature. Introductions and overviews of quantitative statistical methods for landslide susceptibility or hazard assessment can be found in Brenning (2005), Chung and Fabbri (2003), Guzzetti et al. (1999), Guzzetti (2005), Hervás and Bobrowsky (2009), Soeters and van Westen (1996) and van Westen (2000). New methods or modifications of existing ones are consistently developed or applied (e.g., Erener and Düzgün, 2010; Hasekioğulları and Ercanoglu, 2012; Kayastha et al., 2012a; Sezer et al., 2011). However, there is the tendency to more and more complicated mathematical models, that are certainly powerful, but their physical significance is difficult to understand and those models tend to be black boxes for the standard user which makes it difficult to control the model (Leroi, 1996). With respect to quantitative statistical rockfall susceptibility pre-

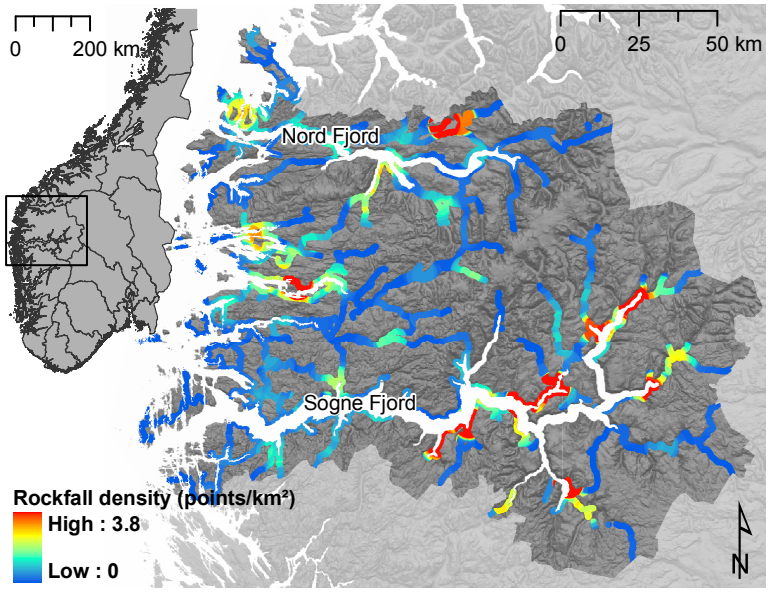

Fig. 1. Overview of the study area, Sogn & Fjordane County, displaying the rockfall density within a road buffer of 1 km. This road buffer forms the limit of the training area used for statistical analyses. The inset shows the location of the study area within Norway.

diction, namely discriminant analysis (Frattini et al., 2008), logistic regression (Marquínez et al., 2003; Marzorati et al., 2002; Shirzadi et al., 2012), Weights-of-Evidence (Zahiri et al., 2006) and fuzzi logic (Blais-Stevens et al., 2012) have been applied. In this study the Weights-of-Evidence method is used to quantify the spatial relation between rockfalls and their controlling parameters in order to finally compute a susceptibility map for rockfalls in the county Sogn & Fjordane. Our focus is hereby not on the mathematical methodology and explains thus the usage of a mathematical relatively simple model.

3.1 Weights-of-Evidence method

The Weights-of-Evidence method was first applied to spatial geoscientific questions by Bonham-Carter et al. (1989). They combined spatial evidences for mineral deposits and produced predictive mineral potential maps. The Weights-of-Evidence method is a probabilistic method that uses known occurrences of a feature, termed as inventory within this study, to quantify spatial associations between these features and the controlling parameters that cause the features to occur (Bonham-Carter et al., 1989). Originally, the Weights-of-Evidence method was developed as a binary approach, but in this study the extended Weights-of-Evidence method as introduced by Porwal et al. (2001) using multi-class controlling parameters was applied. The primary aim of the Weights-of-Evidence method is to weight and finally combine several controlling parameters, in order to get a prediction for the occurrence of a considered feature. However, in this study it is primarily used as an explanatory tool in order to investigate the spatial relations between rockfalls and their controlling parameters. The Weights-of-Evidence method has been widely applied for landslide studies (e.g., Armaş, 2012; Kayastha et al., 2012b; Lee et al., 2002; Neuhäuser et al., 2012; van Westen et al., 2003), but only limited for rockfalls explicitly (Zahiri et al., 2006).

Agterberg et al. (1990), Bonham-Carter et al. (1989) and Bonham-Carter (1994) give comprehensive descriptions of the mathematical formulation of the Weights-of-Evidence method. This method is well-known, and therefore only a basic introduction is given here.

In general, the Weights-of-Evidence method uses the theory of conditional probability, namely the rule of Bayes. It is based on the fact that the probability of an event, in this case a rockfall, will depend upon several circumstances. Weights are calculated for each controlling parameter class in order to quantify their strength of spatial influence on rockfall susceptibility, considering both the absence and presence of each controlling parameter class. Assuming that all rockfalls are known, probabilities can be estimated as simple volume proportions. The working formulas for calculating the weights are consequently the following:

$$W^+ = ln\left(\frac{N\{R\cap X_i\}/N\{R\}}{N\{\overline{R}\cap X_i\}/N\{\overline{R}\}}\right) \quad (1)$$

$$W^- = ln\left(\frac{N\{R\cap \overline{X_i}\}/N\{R\}}{N\{\overline{R}\cap \overline{X_i}\}/N\{\overline{R}\}}\right) \quad (2)$$

where $N\{R\cap X_i\}$ denotes the number of cells containing a rockfall event R and belonging to parameter class X_i. $\overline{R}$ and $\overline{X_i}$ indicate the absence of a rockfall or parameter class, respectively.

The calculated weights $W^{+/-}$ provide a measure of spatial association between the inventory and each controlling parameter class. A positive W^+ predicts that there are more rockfalls on that controlling parameter class than would occur pure randomly; conversely a negative W^+ predicts that fewer rockfalls occur than expected. The absolute value of the weights expresses how strong the spatial association between inventory and controlling parameter class is. The larger the absolute value, the stronger is the spatial association. A value of zero, or very close to zero, predicts that the rockfalls are distributed randomly with respect to that controlling parameter class.

In addition, the studentised contrast $stud(C)$ serves as a measure about the statistical significance of the spatial association between the inventory and each controlling parameter:

$$stud(C) = \frac{C}{\sigma(C)} \quad (3)$$

where the contrast $C = W^+ - W^-$ and $\sigma(C)$ is an approximation of the standard deviation of C, (see Agterberg et al., 1990 and Bonham-Carter et al., 1989 for its estimation). It is recommended that the modulus of the studentised contrast $stud(C)$ should be larger than 2 for a significant spatial association (Bonham-Carter, 1994). Weights and studentised contrasts are calculated for each controlling parameter class based on the Weights-of-Evidence method with the help of the Esri ArcGIS toolbox "Spatial Data Modeller" (Sawatzky et al., 2009) and used to quantify the spatial relationship. The controlling parameters that have a significant spatial relation to the occurrence of rockfalls are selected and reclassified according to the analysis results in order to produce a susceptibility map. This reduction of classes is necessary in order to increase the statistical robustness of the weights (Bonham-Carter, 1994). The different controlling parameters can finally be combined based on the calculated weights assuming conditional independence in between the parameters by updating the prior logit $logit\{R\}$ to the posterior logit:

$$logit\{R/X_1\cap X_2\cap \ldots X_n\} = logit\{R\} + \sum_{j=1}^{n} X_j^{+/-} \quad (4)$$

for $j = 1$ to n, where n is the total number of considered controlling parameters. "Logit" is defined as the natural logarithm of the ratio of the probability with that an event will occur to the probability that it will not occur. The posterior probability $P\{R/X_1\cap X_2\cap \ldots X_n\}$ or susceptibility can finally be obtained by back-transformation of the posterior logits into real probability values:

$$P\{R/X_1\cap X_2\cap \ldots X_n\} = \frac{e^{logit\{R/X_1\cap X_2\cap \ldots X_n\}}}{1+e^{logit\{R/X_1\cap X_2\cap \ldots X_n\}}} \quad (5)$$

3.2 Validation of susceptibility maps and test of conditional independence

Success rate and prediction rate curves were used to evaluate the predictive power of the susceptibility map based on the time partition method as proposed by Chung and Fabbri (2003). In addition, the comparison of success rate curves from different susceptibility maps, based on different parameter combinations, has been used in order to select the best performing model. Success rate curves display how many of the analysed rockfalls are successfully detected by the susceptibility map. The steeper the curve, the better is the model efficiency.

The overall conditional independence was tested by comparing the number of observed rockfalls $N\{R\}$ to the number of predicted rockfalls $N\{R_p\}$. Given conditional independence, the number of both should be equal. Bonham-Carter (1994) suggests that the ratio $N\{R\}/N\{R_p\}$ should be > 0.85.

3.3 Combined statistical-physical susceptibility map

A rockfall susceptibility map has been previously produced for entire Norway separating between potential source areas and propagation zones (Derron, 2010). This map is based on a slope analysis method as proposed by Loye et al. (2009), resulting in slope angle thresholds which are potentially unstable and could lead to rockfall. These thresholds depend on the slope angle, DEM cell size, type of bedrock and outcropping conditions. The main limitation of this rockfall susceptibility map is the limited resolution of the used DEM with a $25\,\mathrm{m}$ cell size. Small-sized rock cliffs can thus be missed during the detection of source cells. Furthermore, these maps are just displaying potential source areas without any associated probability of rockfall release. The obtained probabilistic susceptibility map was thus used to update the rockfall source areas with a relative probability. At the same time, the probabilistic susceptibility map is with this step restricted to the potential source areas and includes thereafter only areas that are actually steep enough to cause rockfalls.

4 Inventory

The national database of rapid mass movements in Norway is the result of joining four independent databases into one within the GeoExtreme project (Jaedicke et al., 2008, 2009). This database differentiates between five landslide types, namely rockslides, debris slides, snow avalanches, sub-aqueous slides and icefalls. The majority of registered landslides are from the Norwegian Directorate of Public Roads including all types of events that affected a road. For this study only events registered from the Norwegian Directorate of Public Roads within the category "ROCKSLIDE" and with a "RELEASE AREA" equal to "OPEN SLOPE" or "UNKNOWN" were extracted. Events in the category "ROCKSLIDE" represent almost exclusively rockfalls. In addition, points that are located within tunnels have been eliminated. This results in an inventory containing 3259 rockfall events spanning a time period from 1973 until 2012 for the county of Sogn & Fjordane. This dataset was divided into two subsets for validating the susceptibility map. The breakpoint was set to the end of the year 2002, because there was a reorganisation of the Norwegian Directorate of Public Roads incorporating changes in the division and potential changes in registration routines starting from 2003. Events older than this date were used as training data and events that occurred after the breakpoint are used as validation data.

There are several limitations applying for this database. It is a matter of course that all registered events are limited to public roads, but there is also no uniform registration of events along the public roads. The quality and completeness of data is strongly influenced by the internal division into road districts and personal abilities of the local observers. There exist no mandatory guidelines for the registration of events and whether an event will be registered or not depends basically on individuals. This results in a partially incomplete and biased database, both with respect to the area covered and to the time period investigated. In addition, registered locations are points where the rockfalls hit the road, but there exist no spatial information about the source area. In some cases, the registered points may even only be midpoints of a certain road section. However, it was not possible to obtain more detailed information about this conflict.

This study investigates rockfalls only spatially and temporal inconsistencies are thus not important. However, the severe spatial restrictions have been dealt with the following approaches. The first limitation, that the registrations are limited to public roads, has been solved by restricting the study area for the spatial analysis to a 1-km buffer around the road network, called training area in the following. The analysis results have then been used to predict rockfall susceptibility of the entire study area covering the complete county, assuming that the smaller training area is representative for the variability of the entire study area (Aleotti and Chowdhury, 1999; Dunlop, 2010; van Westen, 2000). The training area is covering $4,290\,\mathrm{km}^2$, corresponding to 3058 road km and the study area covers $18,607\,\mathrm{km}^2$. On average there is 1 rockfall event per road km and 0.5 events per km^2 of the training area (Table 1).

Table 1. Statistics about the rockfall events along the roads and within the training area.

Number of rockfall events	per road km	per km^2 of the training area
Minimum	0	0
Maximum	166	201
Average	1.05	0.54
Standard deviation	5.02	3.43

The second limitation, the registered impacts on the road instead of the source areas will not have an effect for most geological information, since their resolution is lower than the distance between source and impact of a rockfall. For example the used geological maps have a scale of $1:250,000$. This would mean that $1\,\mathrm{mm}$ on the map is equivalent to $250\,\mathrm{m}$ in the field. Dunlop (2010) defined the source areas of 98 rockslides recorded in the same database in a test area in Sogn & Fjordane. His results demonstrate that the average distance between source zone and impact on the road is $77\,\mathrm{m}$, which is less than the resolution of most data used. However, major problems are expected analysing the DEM with a $25\,\mathrm{m}$ resolution and corresponding derivatives of it in the statistical analysis.

5 Parameters

A large set of potential controlling parameters has been spatially analysed with the help of the Weights-of-Evidence method. However, only the parameters that have most influence have been used for mapping the final susceptibility.

5.1 Bedrock geology

The bedrock of western Norway consists mainly of Lower Palaeozoic and Precambrian metamorphic rocks. The rocks of the study area have undergone intense reworking by a general NW-SE oriented crustal shortening during the Caledonian Orogeny, resulting in a thrust sheet transport towards SE onto the Precambrian basement (Roberts and Gee, 1985). The geological setting can be divided into three units, the Precambrian basement, the Caledonian nappes and Devonian sedimentary basins including a wide range of lithologies.

The basis for the geological parameters formed the $1:250,000$ bedrock map of the Geological Survey of Norway (NGU Berggrunnskart). The original vector map was converted to a raster with 25 m cell size. Three different reclassifications were completed based on (1) the rock type, (2) the tectono-stratigraphic position and (3) the metamor-

phic grade. The first reclassification is based on the relative competence of each rock type in the study area based on experience from fieldwork and is resulting in seven classes:

(1) Granular sedimentary rocks, plutonic rocks, felsic foliated rocks, mafic and ultramafic rocks, metamorphic rocks with low mechanical strength (like amphibolites, schists and micaschists), quartzite and marble (Figure 2a)

The second reclassification is founded on the fact that tectonic deformation, thus the tectonic weakening is higher in the nappes than in the basement. This classification is not completely definite, since there exist different opinions about the affiliation of rock units to the different positions (Kildal, 1970; Ragnhildstveit and Helliksen, 1997; Sigmond, 1999; Solli and Nordgulen, 2008; Tveten et al., 1998). Therefore, different classifications have been analysed here and finally the classification displaying highest significance and largest weights has been used. The following tectono-stratigraphic positions are represented in the study area:

(2) Autochthon, lower allochthon, middle allochthon, upper allochthon, uppermost allochthon and Devonian sediments (Figure 2b)

The third reclassification with respect to the metamorphic grade is based on the geological map of the Fennoscandian Shield at a scale of $1:2$ million (Koistinen et al., 2001), resulting in four classes:

(3) No, low, medium and high metamorphic grade (Figure 2c)

5.2 Quaternary geology

In this study, the spatial relation in between the occurrence of rockfalls and landslide deposits as well as bare rock outcrops have been analysed (Figure 2d). These features were extracted from the quaternary map of the Geological Survey of Norway (NGU Løsmassekart), which is a mosaic of various scales, but mainly on a scale of $1:250{,}000$ and $1:50{,}000$ for the study area. The original vector map was used as a raster with $25\,\mathrm{m}$ cell size.

5.3 Tectonic structures

A significant amount of tectonic events affected the bedrock of western Norway, including the ductile Caledonian Orogeny, the semi-ductile post-orogenic collapse and also brittle tectonics, like the Permo-Triassic and Jurassic rifting phases; all together resulting in a high density of brittle, ductile and semi-ductile structures.

Two different sources of lineament maps have been available for this study:

- Geological lineaments from the bedrock map, mainly including thrusts and major faults at a scale of $1:250{,}000$ (Figure 2e and f; NGU Berggrunnskart).
- Geomorphological lineaments from Gabrielsen et al. (2002) based on satellite image (Landsat 7) interpretation at a scale of $1:750{,}000$ (Figure 2g and h).

All lineament maps were used in form of a density grid as well as a distance-to-closest-lineament grid, both with $25\,\mathrm{m}$ cell size.

5.4 Neotectonics

5.4.1 Present day uplift

Different geodetic data exhibit a high-rated present-day uplift in western Norway (Fjeldskaar et al., 2000; Kierulf et al., 2013; Olesen et al., 2000; Vestøl, 2006). Whereas the general trend of uplift is assumed to be a result of glacial isostasy, there exists a debate about the contribution of potential neotectonic processes (Bungum et al., 2010; Fjeldskaar et al., 2000; Olesen et al., 2000). Uplift and uplift gradient maps from Kierulf et al. (2013) have been used for statistical analysis (Figure 2i and k).

5.4.2 Seismicity

Norway has a low to intermediate seismic intensity (Fjeldskaar et al., 2000). A concentration of earthquake activity is found west of mid-Norway, reflecting a rifted passive continental margin (Bungum et al., 2000). The used earthquake catalogue, produced by NORSAR (Norwegian Seismic Array), is covering the time span from 1750 until 2007 (Dehls et al., 2000; Olesen et al., 2000). It contains 566 registered events with a magnitude $M_S \geq 2$ for western Norway and adjacent areas, whereof 6 events have a magnitude $M_S \geq 5$. In order to investigate the potential relation between earthquakes and rockfalls, earthquake density maps were calculated applying a search radius of $50\,\mathrm{km}$ and weighting each event with respect to its energy. Seismic energies E have been derived from magnitudes M_S based on the equation proposed by Gutenberg and Richter (2010):

$$\log E = 1.5 M_S + 11.8 \tag{6}$$

The earthquake density raster is mainly influenced by the earthquakes with $M_S \geq 4$ (Figure 2l).

5.5 Topography and derived parameters

The topography of western Norway is strongly influenced by the quaternary glaciations. Coastal islands, long U-shaped valleys and many deep fjords with steep slopes are dominating landforms. This steep terrain in combination with heavily fractured exposed bedrock indicates that this area is susceptible to rockfall.

A digital elevation model with a cell size of $25\,\mathrm{m}$ forms the basis for different topographic parameters like slope angle, slope aspect, planar and profile curvature, roughness

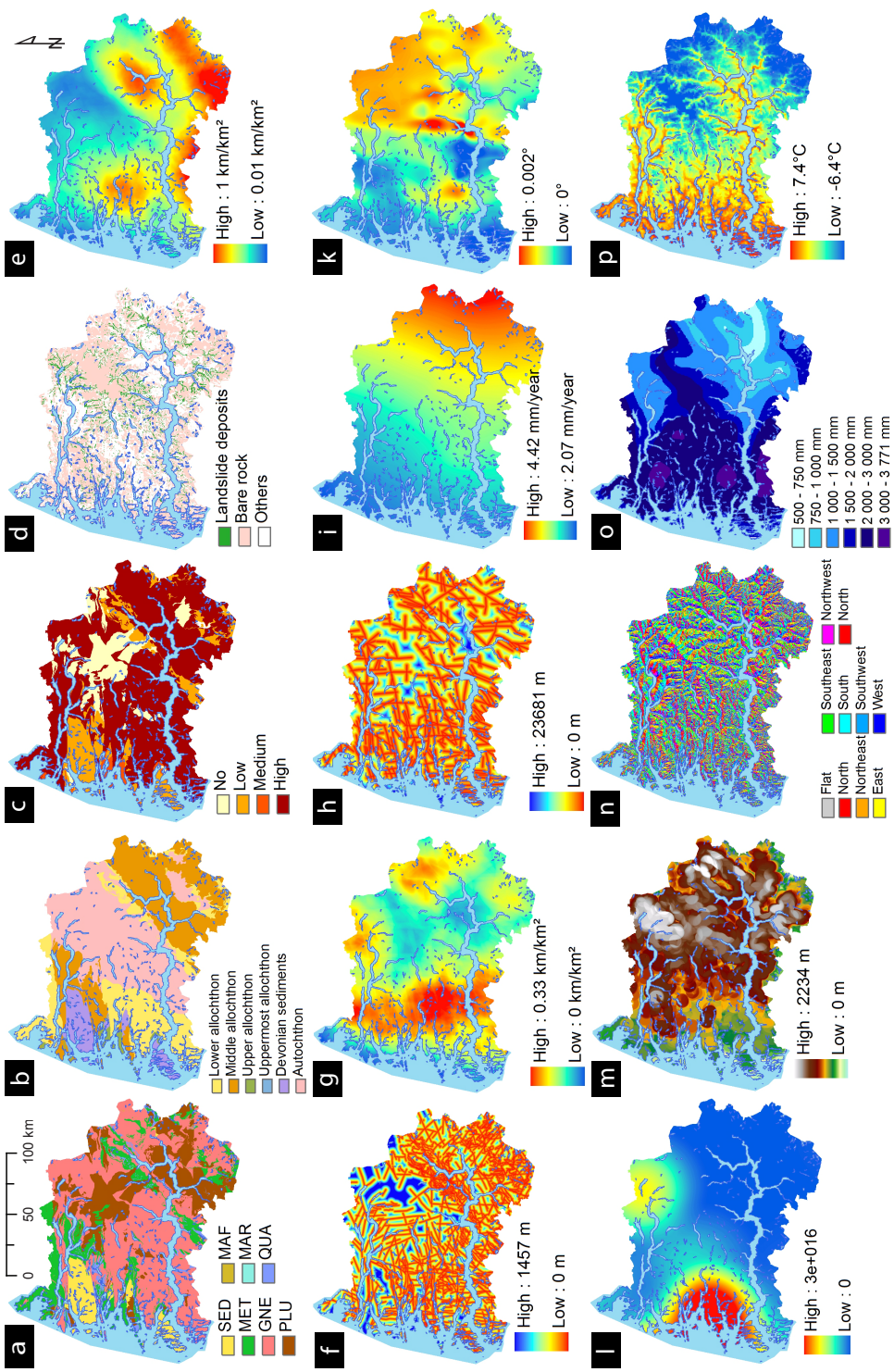

Fig. 2. Overview of analysed parameters. a) Rock type (SED: granular sedimentary rocks, MET: metamorphic rocks with low mechanical strength, GNE: felsic foliated rocks, PLU: plutonic rocks, MAF: mafic and ultramafic rocks, MAR: marble, QUA: quartzite); b) tectono-stratigraphic position; c) metamorphic grade; d) quaternary geology; e) geological lineament density; f) distance to geological lineaments; g) geomorphological lineament density; h) distance to geomorphological lineaments; i) uplift; k) uplift gradient; l) earthquake density; m) relative relief; n) slope aspect; o) normal annual total precipitation for the period 1961-1990; p) normal annual mean temperature for the period 1961-1990.

and relative relief (e.g. Figure 2m and n). Slope angle, slope aspect and curvature are calculated with standard Esri ArcGIS procedures by fitting a plane to the elevation values of a 3x3 cell neighbourhood around the corresponding cell (Horn's method). The slope angle for this plane is calculated with the average maximum technique and the aspect is the direction the plane faces (Burrough and McDonnell, 1998). The curvature is the second derivative of the fitted plane. Local roughness has been assessed with the local standard deviation of the elevation values within a 9x9 moving window. The relative relief has been calculated by determining the difference between minimum and maximum elevation within a moving circular window of $5\,\mathrm{km}$ radius.

5.6 Climate

The climate of western Norway displays large variations in between the coastal areas and the areas with high relief further inland. The coastal area of the study area includes the areas with the largest normal annual precipitation ($3770\,\mathrm{mm}$) as well as the highest normal annual temperatures ($7.47\,^{\circ}\mathrm{C}$) of entire Norway. By contrast, the mountain areas, exhibit large areas with annual temperatures of $-4\,^{\circ}\mathrm{C}$ or less representing the lowest annual temperatures. The precipitation is essentially influenced by the large weather systems mainly coming from west, resulting in a zone of maximum precipitation along the coast and the mountain front.

Climatic normals of annual mean temperature and annual total precipitation for the period 1961-1990 were obtained from the Norwegian Meteorological Institute (Figure 2o and p; Tveito et al., 2000).

6 Results of the spatial analysis

Ordered continuous parameters where classified in 40 equal classes for the spatial analysis. Weights (W^+ and W^-) and studentised contrasts $stud(C)$ were calculated for all controlling parameters class-wise and for some parameters additionally cumulatively from lowest to highest class (ascending) and highest to lowest class (descending) (Figure 3). These cumulative calculations allow defining a value where the parameters have no influence on rockfall anymore. The cumulative ascending weight calculation has been used for controlling parameters where low threshold values are expected to have a spatial influence on rockfalls, like the distance to lineaments. Cumulative descending weight calculation has been used for controlling parameters where high threshold values are expected, like seismicity, uplift, lineament density and precipitation. All spatial analyses were done within the training area, thus within a road buffer of $1\,\mathrm{km}$.

6.1 Bedrock geology

Analyses results of the bedrock geology indicate that only felsic foliated rocks have an increased susceptibility for rockfalls, whereas sedimentary rocks, metamorphic rocks with low mechanical strength, plutonic rocks and quartzite are significantly decreasing the susceptibility for rockfall (Table 2). However, the positive relations have only low weights in contrast to the negative relations, where a W^+ of -1.19 for sedimentary rocks is displaying one of the largest absolute values of the calculated weights for all parameters. Mafic and ultramafic rocks as well as marble have no significant relation to the occurrence of rockfalls. This is in contrast to Saintot et al. (2011), who claimed that metamorphic rocks with low mechanical strength as well as mafic and ultramafic rocks are particularly prone to rock slope failures. They observed that mafic and ultramafic rocks in western Norway are strongly weathered and highly fractured, yielding to larger numbers of rock slope instabilities. The positive relation of rockfalls to felsic foliated rocks may instead highlight that the structural control is larger than any lithological control on the development of rockfalls.

The analysis results of the tectono-stratigraphic positions indicate that only the middle allochthon has a significant positive relation with the occurrence of rockfalls (Table 2). The other units have all significant negative relations to the occurrence of rockfalls, except the uppermost allochthon. These results do not confirm the original assumption that the tectonic weakening, which is higher in the nappes than in the basement, may be a cause for higher rockfall activity.

Analysing the influence of the metamorphic grade on the occurrence of rockfalls yields a small positive relation to a high metamorphic grade and a negative relation to no, low and medium metamorphic grade (Table 2).

6.2 Quaternary geology

The spatial analysis of landslide deposits and bare rock outcrops with respect to the occurrence of rockfalls, exhibits a strong positive correlation of landslide deposits to rockfalls and a medium positive correlation of bare rock outcrops to rockfalls (Table 2). These results highlight the strong influence of the registered impacts on the road instead of the source areas. For registered source areas a larger positive correlation to bare rock than landslide deposits would be expected. However, present landslide deposits may highlight active rock cliffs and are thus yielding valuable information in order to define rockfall susceptibility.

6.3 Tectonic structures

Geologic lineament density indicates a positive spatial relation to the occurrence of rockfalls for high densities and a negative relation for low densities (Figure 3a). In addition, the analysis exhibits less rockfalls in the vicinity of tectonic

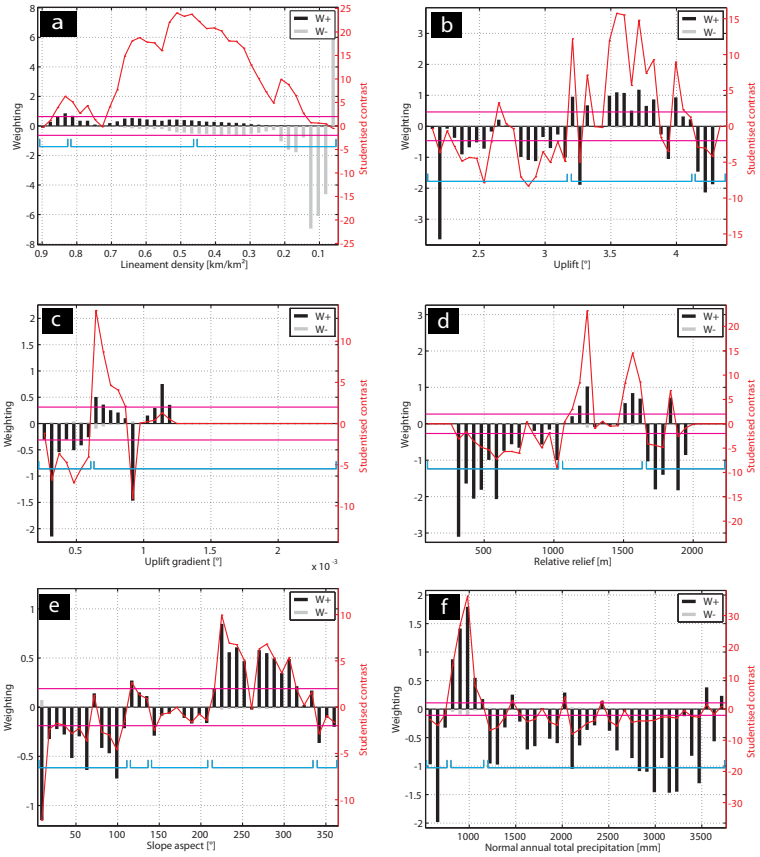

Fig. 3. Examples for results of the spatial analysis with the Weights-of-Evidence method. All continuous parameters have been reclassified into 40 classes each. Weights (W^+ and W^-) and studentised contrast $stud(C)$ have been calculated for each class seperately (b-f) or with cumulative descending (a) or ascending classes in order to obtain the spatial relation of each class to the occurrence of rockfalls. Horizontal pink lines mark $|stud(C)| = 2$, thus all studentised contrast values above or below have a significant spatial relation. The final classifications are indicated by blue brackets. a) Geological lineament density (cumulative descending classes). Local maxima of $stud(C)$ are used as breakpoints for the final reclassification. All classes right of the maximal $stud(C)$ have a negative association to the occurrence of rockfalls, resulting in decreasing W^+ and $stud(C)$. b) Uplift. No clear peaks, but in general a positive relation for medium to high uplift. c) Uplift gradient. One distinct positive peak at low uplift gradient is displayed. d) Relative relief. Weights exhibit two major positive peaks. e) Slope aspect. A clear positive relation for slopes facing SW-NW can be observed. f) Normal annual total precipitation. One major positive peak for low precipitation values can be observed.

lineaments. Rockfalls occur preferentially within a distance of 1400 to 3800 m from a geological lineament. However, it is questionable if the lineaments can theoretically still have an influence on rock slope stability at those large distances. Theoretically an increasing lineament density or a closer distance to lineaments are assumed to cause a higher amount of fractures and subsequent an increased weathering, both reducing the rock strength (Ambrosi and Crosta, 2006; Brideau et al., 2005). The geomorphic lineament map displays no clear relation in between lineament density nor distance to lineaments and the occurrence of rockfalls.

6.4 Neotectonics

6.4.1 Present day uplift

The analyses of the uplift grid indicates a positive spatial relation to the occurrence of rockfalls for medium to high uplift values, but negative relations for low and very high up-

Table 2. Overview of classified controlling parameters used to calculate the susceptibility maps and their spatial association with the occurrence of rockfalls. In italics: parameter classes that are statistically not significant. In bold: controlling parameters that are included in the best performing susceptibility model.

Parameter	Parameter class	Area $[km^2]$	Number of rockfalls	W^+	$\sigma(W^+)$	W^-	$\sigma(W^-)$	C	$\sigma(C)$	$stud(C)$
Rock type	Granular sedimentary rocks	257	50	-1.36	0.14	0.05	0.02	-1.41	0.14	-9.89
	Metamorphic rocks with low mechanical strength	905	533	-0.25	0.04	0.06	0.02	-0.31	0.05	-6.61
	Felsic foliated rocks	2296	2179	0.22	0.02	-0.34	0.03	0.56	0.04	15.08
	Plutonic rocks	657	426	-0.16	0.05	0.03	0.02	-0.18	0.05	-3.56
	Mafic and ultramafic rocks	*8*	*7*	*0.10*	*0.38*	*0.00*	*0.02*	*0.10*	*0.38*	*0.26*
	Marble	*1*	*0*	*0.00*	*0.00*	*0.00*	*0.00*	*0.00*	*0.00*	*0.00*
	Quartzite	165	64	-0.67	0.13	0.02	0.02	-0.69	0.13	-5.49
Tectono-stratigraphic position	Lower allochton	1463	704	-0.46	0.04	0.17	0.02	-0.63	0.04	-14.81
	Middle allochton	1028	1450	0.62	0.03	-0.31	0.02	0.93	0.04	26.50
	Upper allochton	155	87	-0.30	0.11	0.01	0.02	-0.31	0.11	-2.85
	Uppermost allochton	*15*	*8*	*-0.36*	*0.35*	*0.00*	*0.02*	*-0.36*	*0.35*	*-1.01*
	Devonian sediments	254	46	-1.43	0.15	0.05	0.02	-1.48	0.15	-9.97
	Autochthon	1376	964	-0.08	0.03	0.04	0.02	-0.12	0.04	-3.05
Metamorphic grade	No	425	197	-0.49	0.07	0.04	0.02	-0.54	0.07	-7.28
	Low	572	204	-0.76	0.07	0.08	0.02	-0.83	0.07	-11.54
	Medium	155	87	-0.30	0.11	0.01	0.02	-0.31	0.11	-2.85
	High	3134	2771	0.15	0.02	-0.59	0.05	0.74	0.05	15.08
Quaternary geology	Landslide deposits	489	905	0.89	0.03	-0.20	0.02	1.10	0.04	27.99
	Bare rock	1709	1618	0.22	0.02	-0.18	0.02	0.40	0.04	11.37
	Others	2092	736	-0.77	0.04	0.41	0.02	-1.18	0.04	-28.24
Geological lineament density	$0.039 - 0.447\,\mathrm{km/km^2}$	2269	1023	-0.52	0.03	0.38	0.02	-0.90	0.04	-23.78
	$0.447 - 0.812\,\mathrm{km/km^2}$	1991	2182	0.37	0.02	-0.48	0.03	0.85	0.04	22.82
	$0.812 - 0.898\,\mathrm{km/km^2}$	30	54	0.86	0.14	-0.01	0.02	0.87	0.14	6.30
Uplift	$2.09 - 3.15\,\mathrm{mm/year}$	3034	1534	-0.41	0.03	0.60	0.02	-1.01	0.04	-28.77
	$3.15 - 4.11\,\mathrm{mm/year}$	1129	1714	0.69	0.02	-0.44	0.03	1.13	0.04	32.33
	$4.11 - 4.33\,\mathrm{mm/year}$	118	11	-2.10	0.30	0.02	0.02	-2.13	0.30	-7.04
Uplift gradient	0.0002-0.0006°	1406	654	-0.49	0.04	0.17	0.02	-0.66	0.04	-15.17
	0.0006-0.0024°	2885	2605	0.17	0.02	-0.49	0.04	0.66	0.04	15.17
Relative relief	$45 - 1020\,\mathrm{m}$	2125	901	-0.58	0.03	0.36	0.02	-0.94	0.04	-24.08
	$1020 - 1620\,\mathrm{m}$	1911	2229	0.43	0.02	-0.56	0.03	0.99	0.04	26.31
	$1620 - 2217\,\mathrm{m}$	255	129	-0.41	0.09	0.02	0.02	-0.43	0.09	-4.75
Slope aspect	0-107°	1404	636	-0.52	0.04	0.18	0.02	-0.70	0.04	-15.75
	107-134°	263	240	0.19	0.06	-0.01	0.02	0.20	0.07	2.96
	134-206°	950	640	-0.12	0.04	0.03	0.02	-0.15	0.04	-3.43
	206-332°	1348	1545	0.41	0.03	-0.27	0.02	0.68	0.04	19.29
	332-359°	326	198	-0.22	0.07	0.02	0.02	-0.24	0.07	-3.26
Normal annual total precipitation	$500 - 741\,\mathrm{mm/year}$	157	46	-0.95	0.15	0.02	0.02	-0.98	0.15	-6.58
	$741 - 1143\,\mathrm{mm/year}$	624	1337	1.04	0.03	-0.37	0.02	1.41	0.04	39.46
	$1143 - 3713\,\mathrm{mm/year}$	3500	1876	-0.35	0.02	0.84	0.03	-1.20	0.04	-33.73

lift values (Table 2, Figure 3b). Regional uplift can theoretically be the cause for an increased relief and, therefore, may negatively affect the stability of rock slopes (Galadini, 2006; Martino et al., 2004). However, it remains unclear, which ef-

fect the amount of uplift has. The relation in between uplift gradient and the occurrence of rockfalls exhibits a negative relation for low uplift gradients and a positive relation for medium to high gradients (Table 2, Figure 3c).

6.4.2 Seismicity

Seismicity may represent a potential trigger of rockfalls (e.g., Keefer, 1984; Marzorati et al., 2002) or may lead to rock mass strength reduction as a long term predisposing factor (Jaboyedoff et al., 2003). In the study area the seismicity on land is in general too low in order to trigger rockfalls (Keefer, 1984) and it should primarily be considered as a long term predisposing factor. However, the analysis results of earthquake density do not indicate any clear relation in between the location of rockfalls and earthquakes.

6.5 Topography

As described above the registered impacts on the road instead of the source areas cause major problems when analysing the DEM or derivatives of it, like resulting in positive spatial relations of rockfalls to low slope angles, planar or profile curvature around zero as well as low roughness values. Those properties can consequently not be used for describing relations to the occurrence of rockfall sources. However, the analyses of relative relief and slope aspect resulted in statistically and geologically significant spatial relations. Areas with a relative relief larger than $1020\,\mathrm{m}$ but smaller than $1620\,\mathrm{m}$ are prone to rockfalls, for areas with lower or higher relief the rockfall susceptibility is decreasing (Table 2, Figure 3d). In addition, it can be demonstrated that a slope aspect from 206° to 332° (SW-NW) is prone to develop rockfalls, whereas other slope orientations have a negative relation to the occurrence of rockfalls (Table 2, Figure 3e). A small positive correlation is also found for a slope aspect from 107 to 134° (ESE-SE). As described above the climate in the study area is primarily influenced by large weather systems mainly coming from west. This results in a larger exposure of west-facing slopes to precipitation. However, this cannot be the only reason, since the spatial relation becomes less clear when analysing the general valley trends with a coarser grid. These slope orientations experience also the most intense melt water production, because of the combined favoured exposure to wind and solar radiation (Sandersen et al., 1996). On the other hand, Bjerrum and Jørstad (1968) and Sandersen et al. (1996) state that frost shattering is the most important factor for rockfalls in Norway. Diurnal freeze and thaw cycles are in general most effective on slopes facing SE to SW (Baillifard et al., 2004; Matsuoka and Sakai, 1999; Santi et al., 2009), however frost weathering of rocks depends on more factors than solely temperature and solar radiation (Matsuoka and Murton, 2008; Matsuoka, 2008).

6.6 Climate

A strong negative spatial correlation in between the occurrence of rockfalls and normal annual average temperatures lower than $0.5\,^\circ\mathrm{C}$ has been identified. Higher temperatures, however, do not have any clear spatial relation to the occurrence of rockfalls.

Low normal annual total precipitation values are increasing the rockfall susceptibility, and very low values below $740\,\mathrm{mm/year}$ as well as values above $1100\,\mathrm{mm/year}$ have a negative relation to the occurrence of rockfalls (Figure 3f). Sandersen et al. (1996) state that the precipitation is one of the most significant factors controlling rockfalls besides freeze-thaw cycles. However, this cannot be confirmed by analyzing normal annual values. It might be rather extreme events that have an influence on the development of rockfalls.

7 Resulting susceptibility maps

Controlling parameters that have a clear and significant spatial relation to the occurrence of rockfalls were selected and regrouped into fewer classes, based on observed relations, so that the groups represent coherent relations with respect to the occurrence of rockfalls. Breakpoints that maximise the spatial association between rockfalls and controlling parameters and that are statistically significant have been identified based on calculated weights (W^+ and W^-) and studentised contrasts $stud(C)$. The final classifications with the corresponding weights are summarized in Table 2. These controlling parameter maps were used to produce susceptibility maps based on the Weights-of-Evidence method for the training area. More than 50 different susceptibility maps with different parameter combinations were produced, testing the influence of each controlling parameter. Conditional independence was tested for all models and models where this assumption was violated were rejected. The model with the best performance was defined based on success rate curves and validated with a prediction rate curve (Figure 4a). This model includes the controlling parameters tectonostratigraphic position, quaternary geology, geological lineament density, relative relief and slope aspect and has an area under the success rate curve of 0.75. Success and prediction rate curves are very similar; however, it is noticeable that the success rate curve is slightly lower than the prediction rate curve. This is in general the opposite since the success rate curve is obtained using the data with that the model was calculated, whereas for the prediction rate curve the validation data is used, that has not been included for producing the model. It indicates that the validation data fits the model better than the training data. The prediction rate curve reveals that the model detects 70% of rockfalls from the validation data set within 30% of the training area.

Finally, a susceptibility map was calculated for the entire land area of the study area using the model obtained and val-

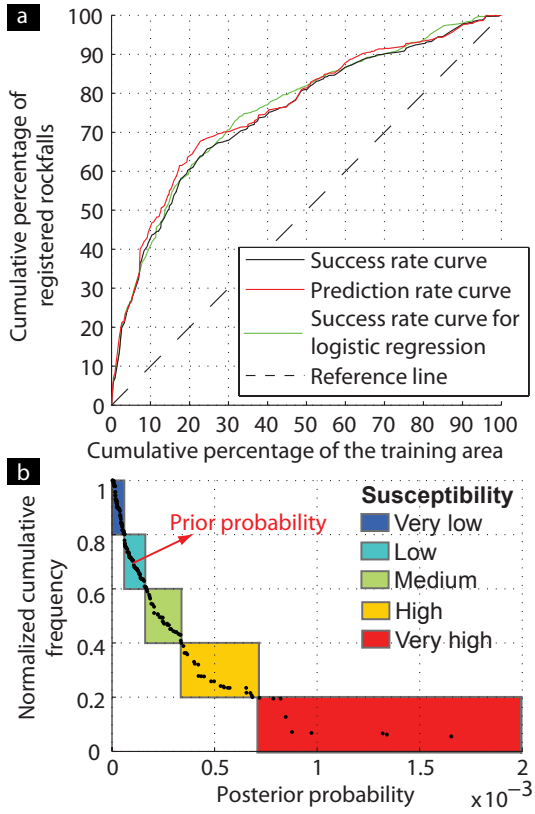

Fig. 4. a) Success rate and prediction rate curve for the best performing Weights-of-Evidence model as well as success rate curve for logistic regression model using the same parameters as the Weights-of-Evidence model. All three curves are very similar. b) Distribution of the posterior probability for all registered rockfalls. 70% of the rockfalls have a posterior probability larger than the prior probability of 0.0001. Posterior probabilities are classified into five susceptibility classes, indicated by coloured boxes, based on equally percentages of registered rockfalls for each class. Each susceptibility class contains 20% of the registered rockfalls.

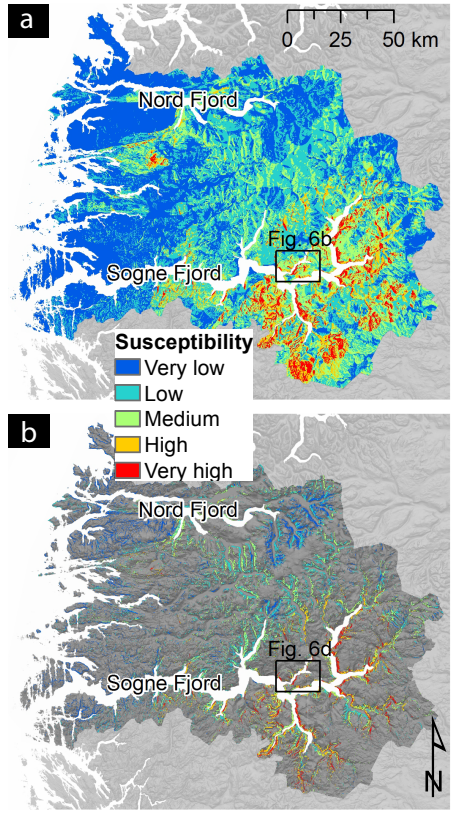

Fig. 5. Resulting susceptibility maps based on the controlling parameters tectono-stratigraphic position, quaternary geology, geological lineament density, relative relief and slope aspect. a) Susceptibility for the entire land area and b) for the physically determined source zones from Derron (2010).

idated within the training area (Figure 5a). The final susceptibility map is characterized by in general lower susceptibilities close to the coast and higher susceptibilities further inland. In addition, an increasing susceptibility from north to south can be observed.

Especially the entire inner fjord system of Sogne Fjord displays higher rockfall susceptibilities. At last the obtained susceptibility map was intersected with the source areas from the physically based rockfall susceptibility map (Figure 5b and Figure 6). The resulting susceptibility map is now restricted to areas that are steep enough to generate rockfalls. This is an important step, because the slope angle has not been included into the model so far. The physically determined rockfall source areas are now updated with relative probabilities.

8 Discussion

It has been questioned whether the existing slope failure inventory in Norway is suitable for statistical analysis or not because of its strong restrictions, mainly temporal and spatial discontinuity and incompleteness. However, temporal and spatial censoring of data is a problem that most inventories face including underreporting of data, incomplete data, inadequate sample time intervals or protective measures in high susceptible zones (Hungr et al., 1999). This study aimed to

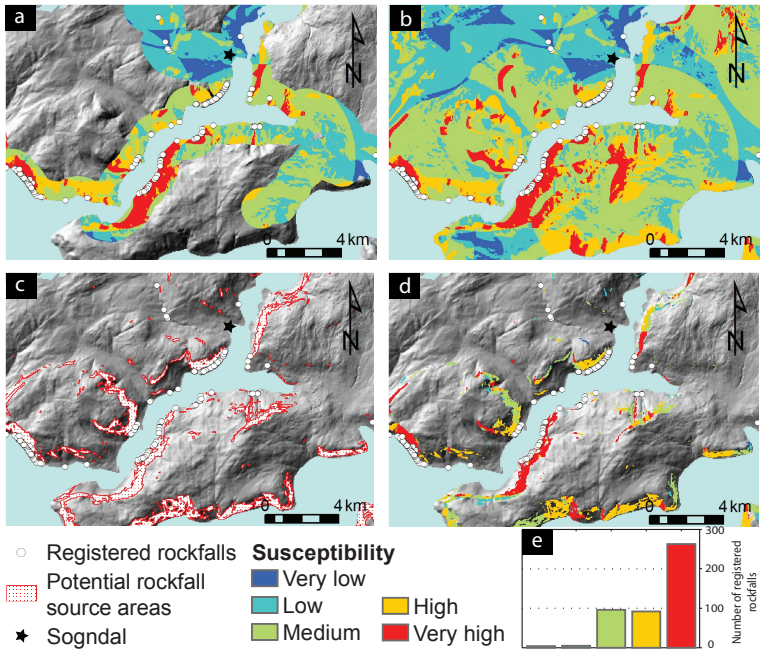

Fig. 6. Detail of the different susceptibility maps. For the location see Figure 5. a) Susceptibility within a road buffer of 1 km, which has been used as training area for analyzing the spatial relation between rockfalls and controlling parameters as well as for validation of the model. b) Susceptibility for the entire land area based on the model set up from a). c) Rockfall susceptibility map based on Derron (2010). d) Combined rockfall susceptibility map displaying the physically determined source zones from Derron (2010) updated with probabilistically assessed susceptibilities. e)Distribution of susceptibility for the registered rockfalls within the displayed area.

investigate the feasibility of statistic and probabilistic methods for analysing the inventories existing in Norway focusing on rock slope failures. The results confirm that the existing data in fact can be used to gain further knowledge about the controlling factors for rock slope failures in Norway based on statistical analysis in spite of strong restrictions. The results are robust with respect to changes of the study area as well as of the inventory and the restrictions have thus a limited influence. This study demonstrated the possibility of using road inventories for statistical analyses and should encourage for further analysis of the remaining inventory covering entire Norway in order to study regional variations within the controlling parameters.

Even if this study claims to be quantitative, a certain degree of subjectivity remains, when choosing the parameters for the final susceptibility map. Spatial relations of the controlling parameters were judged based on expert knowledge whether they are geologically reasonable or not. Detailed geological knowledge about the study area is always required in order to be able to produce credible susceptibility maps. This small scale susceptibility map should be primarily used as a first order susceptibility map in order to detect hot spot areas, where critical factor combinations occur. More detailed investigations should be performed in areas that were identified as especially critical so that more precise susceptibility maps and additionally hazard maps can be prepared.

By replacing probabilities with relative frequencies it must be assumed that all rockfalls are known and the applied methods are thus strongly dependent on the completeness of the inventory (Schaeben, 2012). This is however assumed to be not the case for this study and will thus lead to an underestimation of the prior probability resulting in a bias of the weights as well as the final susceptibility (Agterberg and Cheng, 2002). Furthermore, the calculation of the susceptibility map with help of the Weights-of-Evidence method depends on the assumption of conditional independence. However, even if the tests for conditional independence do not reveal a strong violation of this assumption, a certain degree of conditional dependence will always be present in natural applications. Conditional dependence will lead to an overestimation of the final susceptibility. Based on our experience Weights-of-Evidence is a very powerful method for data exploration, but its application is limited for combining datasets to a susceptibility map due to the multiple assump-

tion of conditional independence (Böhme, 2007; Schaeben, 2012). As logistic regression is closely related to Weights-of-Evidence, but not based on the assumption of conditional independence, this method yields a good alternative in generating susceptibility maps (Hosmer and Lemeshow, 2000). However, applying logistic regression with the same controlling parameters within the training area, results in a very similar susceptibility map as with the Weights-of-Evidence method, but in total with larger posterior probabilities. Success rate curves display that the results from both methods yield comparable predictabilities (Figure 4a) and susceptibilities are thus most likely not over estimated by the Weights-of-Evidence method. Resulting posterior probabilities are in general very low with the highest posterior probability of 0.0027 for the source zones. For comparison, the prior probability for rockfalls in the study area is 0.0001 for each cell.

9 Conclusions

The spatial relationship between rockfall occurrence and potential controlling parameters in the county of Sogn & Fjordane has been evaluated using the Weights-of-Evidence method. Quaternary geology, tectono-stratigraphic position and geological lineament density have the strongest spatial relation to the occurrence of rockfalls in the study area (Table 2). A rockfall susceptibility map for the entire county of Sogn & Fjordane could be calculated based on the results of the statistical analyses of the controlling parameters. The model with best performance includes the controlling parameters tectono-stratigraphic position, quaternary geology, geological lineament density, relative relief and slope aspect. Combining the statistical susceptibility model with a physically based model restricts the susceptibility map to areas that are steep enough to represent a potential rockfall source. This combination makes it possible to use road inventories, with registered impacts instead of sources, for susceptibility modelling.

Acknowledgements. The authors are grateful to A. Saintot for her help with reclassifying the bedrock maps into rock types as well as assigning tectono-stratigraphic positions. We thank Oddleiv Olesen, Hilmar Bungum and Halfdan P. Kierulf to provide neotectonic data and detailed information about those, as well as M. Panzner for assistance with Matlab to plot the weight statistics.

References

Agterberg, F. P. and Cheng, Q.: Conditional Independence Test for Weights-of-Evidence Modeling, Natural Resources Research, 11, 249–255, 2002.

Agterberg, F. P., Bonham-Carter, G. F., and Wright, D. F.: Statistical pattern integration for mineral exploration, in: Computer Applications in Resource Estimation; Prediction and Assessment for Metals and Petroleum, edited by Gaal, G. and Merriam, D. F., pp. 1–21, Pergamon Press, Oxford-New York, 1990.

Aleotti, P. and Chowdhury, R.: Landslide hazard assessment: summary review and new perspectives, B. Eng. Geol. Environ., 58, 21–44, 1999.

Ambrosi, C. and Crosta, G. B.: Large sackung along major tectonic features in the Central Italian Alps, Eng. Geol., 83, 183–200, 2006.

Armaş, I.: Weights of evidence method for landslide susceptibility mapping. Prahova Subcarpathians, Romania, Nat. Hazards, 60, 937–950, 2012.

Baillifard, F., Jaboyedoff, M., Rouiller, J.-D., Robichaud, G., Locat, P., Locat, J., Couture, R., and Hamel, G.: Towards a GIS-based rockfall hazard assessment along the Quebec City Promontory, Quebec, Canada, in: Landslides: Evaluation and Stabilization, edited by Lacerda, W. A., Ehrlich, M., Fontoura, A. B., and Sayão, A., pp. 207–213, Taylor & Francis Group, London, 2004.

Bjerrum, L. and Jørstad, F. A.: Stability of Rock Slopes in Norway, Tech. Rep. NGI report no. 79, Norwegian Geotechnical Institute, 1968.

Blais-Stevens, A., Behnia, P., Kremer, M., Page, A., Kung, R., and Bonham-Carter, G.: Landslide susceptibility mapping of the Sea to Sky transportation corridor, British Columbia, Canada: comparison of two methods, B. Eng. Geol. Environ., 71, 447–466, 2012.

Blikra, L. H., Longva, O., Braathen, A., Anda, E., Dehls, J. F., and Stalsberg, K.: Rock Slope Failures in Norwegian Fjord Areas: Examples, Spatial Distribution and Temporal Pattern, in: Landslides from Massive Rock Slope Failure; NATO Science Series, IV. Earth and Environmental Sciences, Vol 49, edited by Evans, S. G., Scarascia Mugnozza, G., Strom, A., and Hermanns, R. L., pp. 475–496, Springer, Dodrecht, Netherlands, 2006.

Böhme, M.: Predictive 3D Mineral Potential Modelling: Application to the VHMS Deposits of the Noranda District, Canada, Diploma thesis, TU Bergakademie Freiberg, Germany, 2007.

Böhme, M., Saintot, A., Henderson, I., Henriksen, H., and Hermanns, R. L.: Rock-slope instabilities in Sogn & Fjordane County, Norway: a detailed structural and geomorphological analysis, in: Slope Tectonics, edited by Jaboyedoff, M., pp. 97–111, Geol. Soc. Spec. Publ., 351, London, 2011.

Bonham-Carter, G. F.: Geographic Information Systems for Geoscientists: Modeling with GIS, Pergamon Press, Ontario, Canada, 1994.

Bonham-Carter, G. F., Agterberg, F. P., and Wright, D. F.: Weigths of evidence modeling: a new approach to mapping mineral potential, in: Statistical Applications in the Earth Sciences, edited by Agterberg, F. P. and Bonham-Carter, G. F., pp. 171–183, Geological Survey of Canada, Report 89-09, 1989.

Braathen, A., Blikra, L. H., Berg, S. S., and Karlsen, F.: Rock-slope failure in Norway; type, geometry, deformation mechanisms and stability, Norw. J. Geol., 84, 67–88, 2004.

Brenning, A.: Spatial prediction models for landslide hazards: review, comparison and evaluation, Nat. Hazard. Earth Sys., 5, 853–862, 2005.

Brideau, M.-A., Stead, D., Kinakin, D., and Fecova, K.: Influence of tectonic structures on the Hope Slide, British Columbia, Canada, Eng. Geol., 80, 242–259, 2005.

Bungum, H., Lindholm, C., Dahle, A., Woo, G., Nadim, F., Holme, J., Gudmestad, O., Hagberg, T., and Karthigeyan, K.: New seis-

mic zoning maps for Norway, the North Sea, and the United Kingdom, Seismol. Res. Lett., 71, 687–697, 2000.

Bungum, H., Olesen, O., Pascal, C., Gibbons, S., Lindholm, C., and Vestøl, O.: To what extent is the present seismicity of Norway driven by post-glacial rebound?, J. Geol. Soc. London, 167, 373–384, 2010.

Burrough, P. A. and McDonnell, R. A.: Principles of Geographic Information Systems, Oxford University Press, Oxford, 1998.

Chung, C.-J. F. and Fabbri, A. G.: Validation of spatial prediction models for landslide hazard mapping, Nat. Hazards, 30, 451–472, 2003.

Dehls, J. F., Olesen, O., Bungum, H., Hicks, E. C., Lindholm, C. D., and Riis, F.: Neotectonic map: Norway and adjacent areas, 1:3,000,000, Geological Survey of Norway, 2000.

Derron, M.-H.: Method for the Susceptibility Mapping of Rock Falls in Norway, Tech. rep., Geological Survey of Norway, 2010.

Duarte, R. M. and Marquínez, J.: The influence of environmental and lithologic factors on rockfall at a regional scale: an evaluation using GIS, Geomorphology, 43, 117–136, 2002.

Dunlop, S.: Rockslides in a changing climate: Establishing relationships between meteorological conditions and rockslides in southwestern Norway for the purposes of developing a hazard forecast system, Master thesis, Queen's University, Kingston, Canada, 2010.

Erener, A. and Düzgün, H. S. B.: Improvement of statistical landslide susceptibility mapping by using spatial and global regression methods in the case of Møre and Romsdal (Norway), Landslides, 7, 55–68, 2010.

Fell, R., Corominas, J., Bonnard, C., Cascini, L., Leroi, E., and Savage, W. Z.: Guidelines for landslide susceptibility, hazard and risk zoning for land use planning, Eng. Geol., 102, 85–98, 2008.

Fjeldskaar, W., Lindholm, C., Dehls, J. F., and Fjeldskaar, I.: Postglacial uplift, neotectonics and seismicity in Fennoscandia, Quaternary Sci. Rev., 19, 1413–1422, 2000.

Frattini, P., Crosta, G. B., Carrara, A., and Agliardi, F.: Assessment of rockfall susceptibility by integrating statistical and physically-based approaches, Geomorphology, 94, 419–437, 2008.

Gabrielsen, R. H., Braathen, A., Dehls, J., and Roberts, D.: Tectonic lineaments of Norway, Norw. J. Geol., 82, 153–174, 2002.

Galadini, F.: Quaternary tectonics and large-scale gravitational deformations with evidence of rock-slide displacements in the Central Apennines (central Italy), Geomorphology, 82, 201–228, 2006.

Gutenberg, B. and Richter, C. F.: Magnitude and energy of earthquakes, Annals of Geophysics, 53, 7–12, 2010.

Guzzetti, F.: Landslide Hazard and Risk Assessment, Ph.D. thesis, Rheinische Friedrich-Wilhelms-Universität Bonn, Germany, 2005.

Guzzetti, F., Carrara, A., Cardinali, M., and Reichenbach, P.: Landslide hazard evaluation: a review of current techniques and their application in a multi-scale study, Central Italy, Geomorphology, 31, 181–216, 1999.

Hasekioğulları, G. D. and Ercanoglu, M.: A new approach to use AHP in landslide susceptibility mapping: a case study at Yenice (Karabuk, NW Turkey), Nat. Hazards, 63, 1157–1179, 2012.

Henderson, I. H. C. and Saintot, A.: Regional spatial variations in rockslide distribution from structural geology ranking: an example from Storfjord, western Norway, in: Slope Tectonics, edited by Jaboyedoff, M., pp. 79–95, Geol. Soc. Spec. Publ., 351, London, 2011.

Hermanns, R. L., Fischer, L., Oppikofer, T., Böhme, M., Dehls, J. F., Henriksen, H., Booth, A., Eilertsen, R., Longva, O., and Eiken, T.: Mapping of unstable and potentially unstable slopes in Sogn og Fjordane (work report 2008-2010), Tech. Rep. 2011.055, Geological Survey of Norway, 2011.

Hervás, J. and Bobrowsky, P.: Mapping: inventories, susceptibility, hazard and risk, in: Landslides - Disaster Risk Reduction, edited by Sassa, K. and Canuti, P., pp. 321–349, Springer, Berlin, 2009.

Hosmer, D. W. and Lemeshow, S.: Applied Logistic Regression, John Wiley and Sons, Inc., New York, 2nd edn., 2000.

Hungr, O., Evans, S., and Hazzard, J.: Magnitude and frequency of rock falls and rock slides along the main transportation corridors of southwestern British Columbia, Can. Geotech. J., 36, 224–238, 1999.

Jaboyedoff, M., Baillifard, F., and Derron, M.-H.: Preliminary note on uplift rates gradient, seismic activity and possible implications for brittle tectonics and rockslide prone areas: The example of western Switzerland, Bulletin de Géologie de l'Université de Lausanne, 88, 401–420, 2003.

Jaboyedoff, M., Baillifard, F., Derron, M.-H., Couture, R., Locat, J., and Locat, P.: Modular and evolving rock slope hazard assessment methods, in: Landslides and Avalanches: ICFL 2005 Norway, edited by Senneset, K., Flaate, K., and Larsen, J. O., pp. 187–194, Taylor & Francis Group, London, 2005.

Jaedicke, C., Solheim, A., Blikra, L. H., Stalsberg, K., Sorteberg, A., Aaheim, A., Kronholm, K., Vikhamar-Schuler, D., Isaksen, K., Sletten, K., Kristensen, K., Barstad, I., Melchiorre, C., Høydal, O. A., and Mestl, H.: Spatial and temporal variations of Norwegian geohazards in a changing climate, the GeoExtreme Project, Nat. Hazard. Earth Sys., 8, 893–904, 2008.

Jaedicke, C., Lied, K., and Kronholm, K.: Integrated database for rapid mass movements in Norway, Nat. Hazard. Earth Sys., 9, 469–479, 2009.

Kayastha, P., Dhital, M., and Smedt, F. D.: Application of the analytical hierarchy process (AHP) for landslide susceptibility mapping: A case study from the Tinau watershed, west Nepal, Comput. Geosci., 52, 398–408, 2012a.

Kayastha, P., Dhital, M. R., and Smedt, F. D.: Landslide susceptibility mapping using the weight of evidence method in the Tinau watershed, Nepal, Nat. Hazards, 63, 479–498, 2012b.

Keefer, D. K.: Landslides caused by earthquakes, Geol. Soc. Am. Bull., 95, 406–421, 1984.

Kierulf, H. P., Ouassou, M., Simpson, M. J. R., and Vestøl, O.: A continuous velocity field for Norway, J. Geodesy, 87, 337–349, 2013.

Kildal, E. S.: Bedrock map Florø, 1:250,000, Geological Survey of Norway, 1970.

Koistinen, T., Stephens, M. B., Bogatchev, V., Nordgulen, Ø., Wenneström, M., and Korhonen, J.: Geological Map of the Fennoscandian Shield, 1:2,000,000, Geological Surveys of Finland, Norway an Sweden and the North-West Department of Natural Resources of Russia, 2001.

Lee, S., Choi, J., and Min, K.: Landslide susceptibility analysis and verification using the Bayesian probability model, Environ. Geol., 43, 120–131, 2002.

Leroi, E.: Landslide hazard-risk maps at different scales: objectives, tools and developments, in: Proceedings of the 7th International Symposium on Landslides, Trondheim, edited by Senneset, K.,

pp. 17–21, Balkema, Rotterdam, 1996.

Loye, A., Jaboyedoff, M., and Pedrazzini, A.: Identification of potential rockfall source areas at a regional scale using a DEM-based geomorphometric analysis, Nat. Hazard. Earth Sys., 9, 1643–1653, 2009.

Marquínez, J., Duarte, R. M., Farias, P., and Sánchez, M. J.: Predictive GIS-based model of rockfall activity in mountain cliffs, Nat. Hazards, 30, 341–360, 2003.

Martino, S., Moscatelli, M., and Mugnozza, G. S.: Quaternary mass movements controlled by a structurally complex setting in the central Apennines (Italy), Eng. Geol., 72, 33–55, 2004.

Marzorati, S., Luzi, L., and Amicis, M. D.: Rock falls induced by earthquakes: a statistical approach, Soil Dyn. Earthq. Eng., 22, 565–577, 2002.

Matsuoka, N.: Frost weathering and rockwall erosion in the southeastern Swiss Alps: Long-term (1994-2006) observations, Geomorphology, 99, 353–368, 2008.

Matsuoka, N. and Murton, J.: Frost weathering: recent advances and future directions, Permafrost Periglac., 19, 195–210, 2008.

Matsuoka, N. and Sakai, H.: Rockfall activity from an alpine cliff during thawing periods, Geomorphology, 28, 309–328, 1999.

Neuhäuser, B., Damm, B., and Terhorst, B.: GIS-based assessment of landslide susceptibility on the base of the Weights-of-Evidence model, Landslides, 9, 511–528, 2012.

NGU Berggrunnskart: NGU Berggrunn - Nasjonal berggrunnsdatabase, http://geo.ngu.no/kart/berggrunn/, 2013.

NGU Løsmassekart: NGU Løsmasser - Nasjonal løsmassedatabase, http://geo.ngu.no/kart/losmasse/, 2013.

Olesen, O., Dehls, J., Bungum, H., Riis, F., Hicks, E., Lindholm, C., Blikra, L. H., Fjeldskaar, W., Olsen, L., and Longva, O.: Neotectonics in Norway, Final Report, Tech. Rep. 2000.002, Geological Survey of Norway, 2000.

Porwal, A., Carranza, E. J. M., and Hale, M.: Extended weights-of-evidence modelling for predictive mapping of base metal deposit potential in Aravalli province, western India, Explor. Min. Geol., 10, 273–287, 2001.

Ragnhildstveit, J. and Helliksen, D.: Bedrock map Bergen, 1:250,000, Geological Survey of Norway, 1997.

Roberts, D. and Gee, D. G.: An introduction to the structure of the Scandinavian Caledonides, in: The Caledonide orogen–Scandinavia and related areas, edited by Gee, D. G. and Sturt, B. A., vol. 1, pp. 55–68, John Wiley & Sons, 1985.

Ruff, M. and Czurda, K.: Landslide susceptibility analysis with a heuristic approach in the Eastern Alps (Vorarlberg, Austria), Geomorphology, 94, 314–324, 2008.

Saintot, A., Henderson, I., and Derron, M.-H.: Inheritance of ductile and brittle structures in the development of large rock slope instabilities: examples from western Norway, in: Slope tectonics, edited by Jaboyedoff, M., pp. 27–78, Geol. Soc. Spec. Publ., 351, London, 2011.

Sandersen, F., Bakkehøi, S., Hestnes, E., and Lied, K.: The influence of meteorological factors on the initiation of debris flows, rockfalls, rockslides and rockmass stability, in: Proceedings of the 7th International Symposium on Landslides, Trondheim, edited by Senneset, K., pp. 97–114, Balkema, Rotterdam, 1996.

Santi, P. M., Russell, C. P., Higgins, J. D., and Spriet, J. I.: Modification and statistical analysis of the Colorado Rockfall Hazard Rating System, Eng. Geol., 104, 55–65, 2009.

Sawatzky, D. L., Raines, G. L., Bonham-Carter, G. F., and Looney, C. G.: Spatial Data Modeller (SDM): ArcMAP 9.3 geoprocessing tools for spatial data modelling using weights of evidence, logistic regression, fuzzy logic and neural networks., 2009.

Schaeben, H.: Comparison of Mathematical Methods of Potential Modeling, Math. Geosci., 44, 101–129, 2012.

Sezer, E. A., Pradhan, B., and Gokceoglu, C.: Manifestation of an adaptive neuro-fuzzy model on landslide susceptibility mapping: Klang valley, Malaysia, Expert Syst. Appl., 38, 8208–8219, 2011.

Shirzadi, A., Saro, L., Joo, O. H., and Chapi, K.: A GIS-based logistic regression model in rock-fall susceptibility mapping along a mountainous road: Salavat Abad case study, Kurdistan, Iran, Nat. Hazards, 64, 1639–1656, 2012.

Sigmond, E. M.: Bedrock map Odda, 1:250,000, Geological Survey of Norway, 1999.

Soeters, R. and van Westen, C. J.: Slope stability: recognition, analysis and zonation, in: Landslides Investigation and Mitigation, edited by Turner, A. K. and Schuster, R. L., vol. Special Report 247, pp. 129–177, Transportation Research Board, National Research Council, National Academy Press, Washington, DC, 1996.

Solli, A. and Nordgulen, Ø.: Bedrock map of Norway and the Caledonides in Sweden and Finland, 1:2,000,000, Geological Survey of Norway, 2008.

Tanarro, L. M. and Muñoz, J.: Rockfalls in the Duratón canyon, central Spain: Inventory and statistical analysis, Geomorphology, 169-170, 17–29, 2012.

Tveito, O. E., Førland, E., Heino, R., I., and others Hanssen-Bauer: Nordic temperature maps, Tech. Rep. 09/00 KLIMA, Norwegian Meteorological Institute, 2000.

Tveten, E., Lutro, O., and Thorsnes, T.: Bedrock map Ålesund, 1:250,000, Geological Survey of Norway, 1998.

van Westen, C. J.: The modelling of landslide hazards using GIS, Surv. Geophys, 21, 241–255, 2000.

van Westen, C. J., Rengers, N., and Soeters, R.: Use of Geomorphological Information in Indirect Landslide Susceptibility Assessment, Nat. Hazards, 30, 399–419, 2003.

van Westen, C. J., Asch, T. W. J. V., and Soeters, R.: Landslide hazard and risk zonation – why is it still so difficult?, B. Eng. Geol. Environ., 65, 167–184, 2005.

Vestøl, O.: Determination of postglacial land uplift in Fennoscandia from leveling, tide-gauges and continuous GPS stations using least squares collocation, J. Geodesy, 80, 248–258, 2006.

Zahiri, H., Palamara, D., Flentje, P., Brassington, G., and Baafi, E.: A GIS-based weights-of-evidence model for mapping cliff instabilities associated with mine subsidence, Environ. Geol., 51, 377–386, 2006.

Appendix B

Paper II

Reference to the paper

Böhme, M., Saintot, A., Henderson, I., Henriksen, H. and Hermanns, R.L.: Rock-slope instabilities in Sogn & Fjordane County, Norway: a detailed structural and geomorphological analysis, in: M. Jaboyedoff (Ed.), Slope Tectonics. Geological Society, London, Special Publications, 351, pp. 97-111, 2011.

Note on contributions

The candidate wrote this paper and carried out all analyses. All authors participated in the fieldwork and contributed to finalize the manuscript.

Is not included due to copyright

Appendix C

Paper III

Reference to the paper

Böhme, M., Hermanns, R.L., Oppikofer, T., Fischer, L., Bunkholt, H.S.S., Eiken, T., Pedrazzini, A., Derron, M.-H., Jaboyedoff, M., Blikra, L.H., Nilsen, B.: Analyzing complex rock slope deformation at Stampa, western Norway, by integrating geomorphology, kinematics and numerical modeling. Engineering Geology, 154, 116-130, 2012.

Note on contributions

The candidate wrote this paper and carried out all analyses. Fieldwork and the collection of structural data in the study area was carried out by the candidate together with Reginald L. Hermanns, Luzia Fischer and Thierry Oppikofer. The first geomorphological field mapping was conducted by Lars H. Blikra. The differential Global Navigation Satellite System data was processed by Trond Eiken and initial analysis was conducted by Halvor S. S. Bunkholt. The candidate conducted the final analyses of the differential Global Navigation Satellite System results as presented in the publication. Andrea Pedrazzini and Bjørn Nilsen assisted the candidate with the numerical analyses. Thierry Oppikofer provided the results of the rotation analysis of block A1. Reginald L. Hermanns carried out the sampling for terrestrial cosmogenic nuclide dating and discussed the results with the candidate. All authors contributed to discuss the results and finalize the manuscript.

Engineering Geology 154 (2013) 116–130

Contents lists available at SciVerse ScienceDirect

Engineering Geology

journal homepage: www.elsevier.com/locate/enggeo

Analyzing complex rock slope deformation at Stampa, western Norway, by integrating geomorphology, kinematics and numerical modeling

Martina Böhme [a,b,*], Reginald L. Hermanns [a], Thierry Oppikofer [a], Luzia Fischer [a], Halvor S.S. Bunkholt [a], Trond Eiken [c], Andrea Pedrazzini [d], Marc-Henri Derron [d], Michel Jaboyedoff [d], Lars H. Blikra [e], Bjørn Nilsen [b]

[a] Geological Survey of Norway, Leiv Eirikssons vei 39, 7040 Trondheim, Norway
[b] Norwegian University of Science and Technology, 7491 Trondheim, Norway
[c] University of Oslo, 0316 Oslo, Norway
[d] Institute of Geomatics and Risk Analysis, University of Lausanne, 1015 Lausanne, Switzerland
[e] Åknes/Tafjord Beredskap IKS, Ødegårdsvegen 176, N-6200 Stranda, Norway

ARTICLE INFO

Article history:
Received 11 July 2012
Received in revised form 26 October 2012
Accepted 24 November 2012
Available online 19 December 2012

Keywords:
GPS
Terrestrial cosmogenic dating
Rockslide
Structural geology
Continuum modeling
Discontinuum modeling

ABSTRACT

The unstable rock slope, Stampa, above the village of Flåm, Norway, shows signs of both active and postglacial gravitational deformation over an area of 11 km^2. Detailed structural field mapping, annual differential Global Navigation Satellite System (GNSS) surveys, as well as geomorphic analysis of high-resolution digital elevation models based on airborne and terrestrial laser scanning indicate that slope deformation is complex and spatially variable. Numerical modeling was used to investigate the influence of former rockslide activity and to better understand the failure mechanism. Field observations, kinematic analysis and numerical modeling indicate a strong structural control of the unstable area. Based on the integration of the above analyses, we propose that the failure mechanism is dominated by (1) a toppling component, (2) subsiding bilinear wedge failure and (3) planar sliding along the foliation at the toe of the unstable slope. Using differential GNSS, 18 points were measured annually over a period of up to 6 years. Two of these points have an average yearly movement of around 10 mm/year. They are located at the frontal cliff on almost completely detached blocks with volumes smaller than 300,000 m^3. Large fractures indicate deep-seated gravitational deformation of volumes reaching several 100 million m^3, but the movement rates in these areas are below 2 mm/year. Two different lobes of prehistoric rock slope failures were dated with terrestrial cosmogenic nuclides. While the northern lobe gave an average age of 4,300 years BP, the southern one resulted in two different ages (2,400 and 12,000 years BP), which represent most likely multiple rockfall events. This reflects the currently observable deformation style with unstable blocks in the northern part in between Joasete and Furekamben and no distinct blocks but a high rockfall activity around Ramnanosi in the south. With a relative susceptibility analysis it is concluded that small collapses of blocks along the frontal cliff will be more frequent. Larger collapses of free-standing blocks along the cliff with volumes >100,000 m^3, thus large enough to reach the fjord, cannot be ruled out. A larger collapse involving several million m^3 is presently considered of very low likelihood.

1. Introduction

In order to understand the deformation of a complex unstable rock slope and to develop a coherent geomechanical model the integration of different data sources and results from different analysis methods is necessary (e.g. Zangerl et al., 2010; Gischig et al., 2011). Numerical modeling techniques are especially helpful to understand the failure mechanisms of complex rock slope deformations, where basic kinematic analyses often present an oversimplification (Stead et al., 2006). However, especially for structurally controlled instabilities, the latter are still essential for a first evaluation of the slope situation (Coggan et al., 1998; Stead et al., 2006). Kinematic models yield valuable information as inputs for more advanced numerical models. It has been demonstrated in numerous studies that structural control plays an important role for large rock slope instabilities (e.g. Terzaghi, 1962; Cruden and Varnes, 1996; Hermanns and Strecker, 1999; Agliardi et al., 2001; Sartori et al., 2003; Jaboyedoff et al., 2009). The influence of inherited structures, mainly pre-existing joint sets and the metamorphic foliation, has been pointed out to be especially important in western Norway, where the study area is

* Corresponding author at: Geological Survey of Norway, Leiv Eirikssons vei 39, 7040 Trondheim, Norway. Tel.: +47 73904242; fax: +47 73921620.
E-mail addresses: martina.bohme@ngu.no (M. Böhme), reginald.hermanns@ngu.no (R.L. Hermanns), thierry.oppikofer@ngu.no (T. Oppikofer), luzia.fischer@ngu.no (L. Fischer), halvor.bunkholt@ngu.no (H.S.S. Bunkholt), trond.eiken@geo.uio.no (T. Eiken), Andrea.Pedrazzini@unil.ch (A. Pedrazzini), Marc-Henri.Derron@unil.ch (M.-H. Derron), Michel.Jaboyedoff@unil.ch (M. Jaboyedoff), lhb@aknes.no (L.H. Blikra), bjorn.nilsen@ntnu.no (B. Nilsen).

0013-7952/$ – see front matter © 2012 Elsevier B.V. All rights reserved.
http://dx.doi.org/10.1016/j.enggeo.2012.11.016

located (Braathen et al., 2004; Böhme et al., 2011; Henderson and Saintot, 2011; Saintot et al., 2011).

Historical records and geological studies of western Norway show a high concentration of post-glacial gravitational slope failures as well as current rock slope instabilities (Blikra et al., 2006; Böhme et al., 2011; Saintot et al., 2011). Several catastrophic failures causing tsunamis in the inner fjord areas of western Norway resulted in large loss of life in the last century (Furseth, 2006). The unstable rock slope, Stampa, above the village Flåm, Aurland municipality, is one of the largest actively deforming rockslide areas known today in Norway (Braathen et al., 2004). An area of up to 11 km^2 that extends 7 km N–S and 2 km E–W exhibits signs of both active and postglacial gravitational deformation (Figs. 1 and 2). Movement rates vary considerably over the entire unstable area, ranging from average 3D movement vectors of 15 mm/year at one delimited block down to below significance level (Hermanns et al., 2011a).

We carried out detailed structural field mapping, yearly differential Global Navigation Satellite System (GNSS) surveys from 2005 to 2011, as well as an analysis of a high-resolution digital elevation model (HR-DEM) based on airborne laser scanning (ALS) data and several terrestrial laser scanning (TLS) surveys. In addition, continuum and discontinuum numerical modeling were used to understand the influence of former rockslide activity as well as the deformation of the unstable slope.

2. Overview of the study area

The unstable rock slope, Stampa, is located on the eastern slope at the southern end of Aurland Fjord, a branch of Sogne Fjord in western Norway (Fig. 2). The bedrock in this area consists of Lower Palaeozoic and Precambrian metamorphic rocks. During the Caledonian Orogeny, the rocks were intensely reworked by a general NW–SE oriented crustal shortening that resulted in a thrust sheet transport towards SE onto the Precambrian basement (Roberts and Gee, 1985). The instability is completely located within phyllites that are thrusted over the Precambrian basement. A Caledonian thrust boundary forms the contact between the phyllites and the overlying Jotun Nappe to the west (Fig. 2).

Quarternary glaciations have had a strong impact on the Norwegian topography. Glacial erosion resulted in long U-shaped valleys and many deep fjords. The valleys of the study area are assumed to have been ice-free since 10,800 cal. years BP (Mangerud et al., 2011). Deglaciation has resulted in a sudden unloading of the glacially steepened slopes. This, in addition to post-glacial tectonic activity, including isostatic rebound and large magnitude earthquakes (Dehls et al., 2000; Fjeldskaar et al., 2000; Olesen, 2004), may have generated a large amount of gravitational structures in western Norway (Blikra et al., 2006; Saintot et al., 2011).

The unstable area is located directly at the corner where the valley changes its orientation from NNE–SSW towards N–S (Fig. 2). This change in orientation is likely to have caused a different stress pattern in the unstable slope during glaciation and deglaciation compared to straight valleys elsewhere and might thus explain the location of the instability exactly at this place (Panizza, 1973).

Large rockslide deposits have been mapped within Aurland Fjord reaching up to almost 4 km along the fjord and dating back to the end of the last glaciation (Blikra et al., 2006). Additionally, at least one further rockslide reached down to the fjord dating older than ca. 2800 years BP (Bøe et al., 2004). Multiple lobes of smaller rockslide deposits cover the slope below the entire deformation front (Fig. 2). Instabilities and collapses have been observed within these deposits, but those are not part of this study.

The gravitational slope deformations above Flåm were first studied in the early 2000s, when geomorphological maps were produced, bathymetric and seismic data were collected in Aurland Fjord and a first structural model was presented (Domaas et al., 2002; Braathen et al., 2004; Olesen, 2004; Blikra et al., 2006). A differential GNSS campaign started in 2005, whereas detailed investigations and

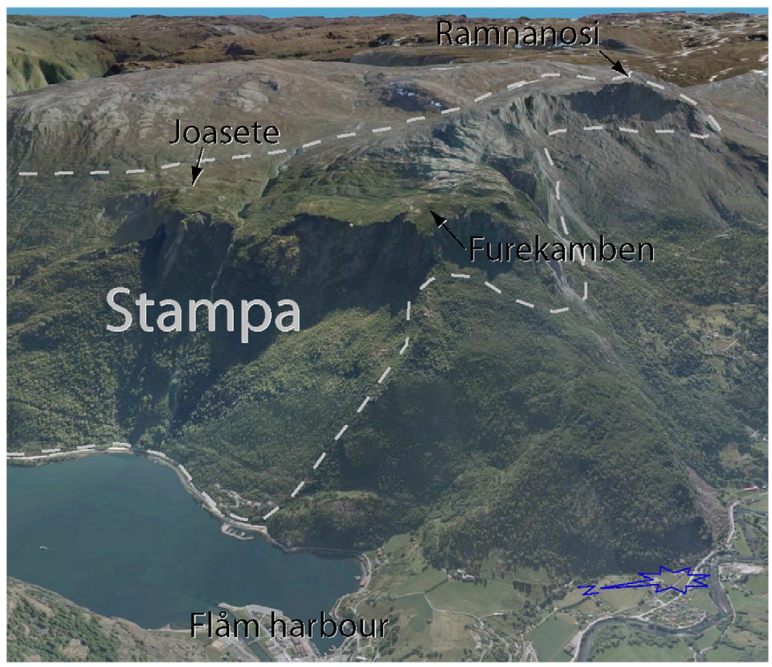

Fig. 1. Aerial oblique view of the unstable slope, Stampa, above the village Flåm (www.norgei3d.no).

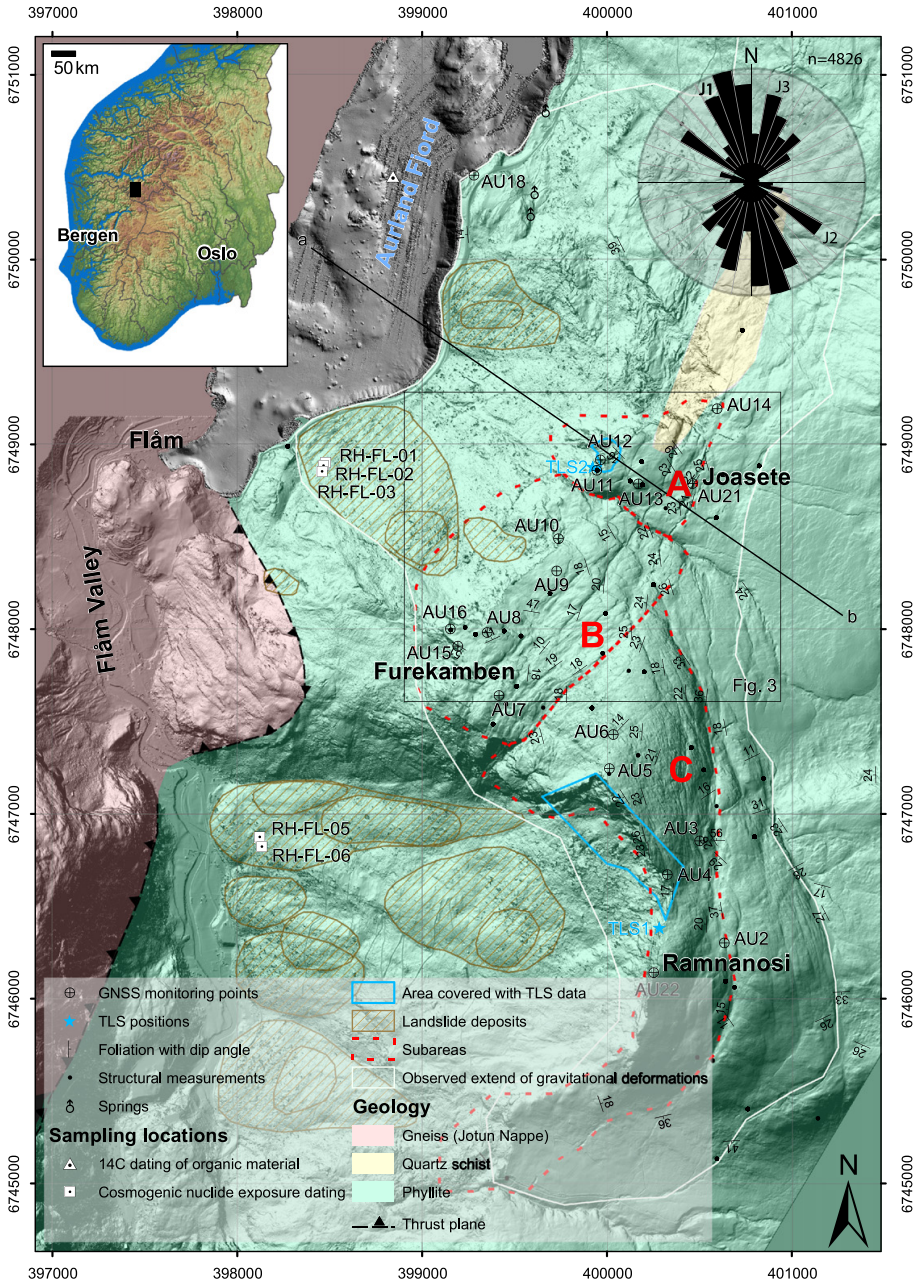

Fig. 2. Hillshade of the HR-DEM based on ALS data on land and bathymetric data for the fjord bottom. Lines a-b mark the profile used for numerical modeling (Figs. 10 and 11). Rose diagram of digitalized lineaments and open fractures from the HR-DEM (segments with 10 m length). The inset shows the location of the study area in southern Norway. (For interpretation of the references to color in this figure legend, the reader is referred to the web version of the article.)

mapping were first commenced in 2008. Besides the studies presented here, airborne and ground based electromagnetic investigations have been undertaken in recent years (Pfaffhuber et al., 2010, 2011).

The unstable area above Flåm was divided into three subareas (A, B and C) based on geomorphological observations (Fig. 2). Subarea A, representing the northernmost part of the unstable area north and west of Joasete, displays the most advanced stage of deformation. The largest open fractures striking NE–SW and forming graben structures are located in this region. Two nearly freestanding blocks (block A1 and A2; Fig. 3) with the highest measured horizontal movement rates of 8.5 and 10.8 mm/year, respectively, are situated

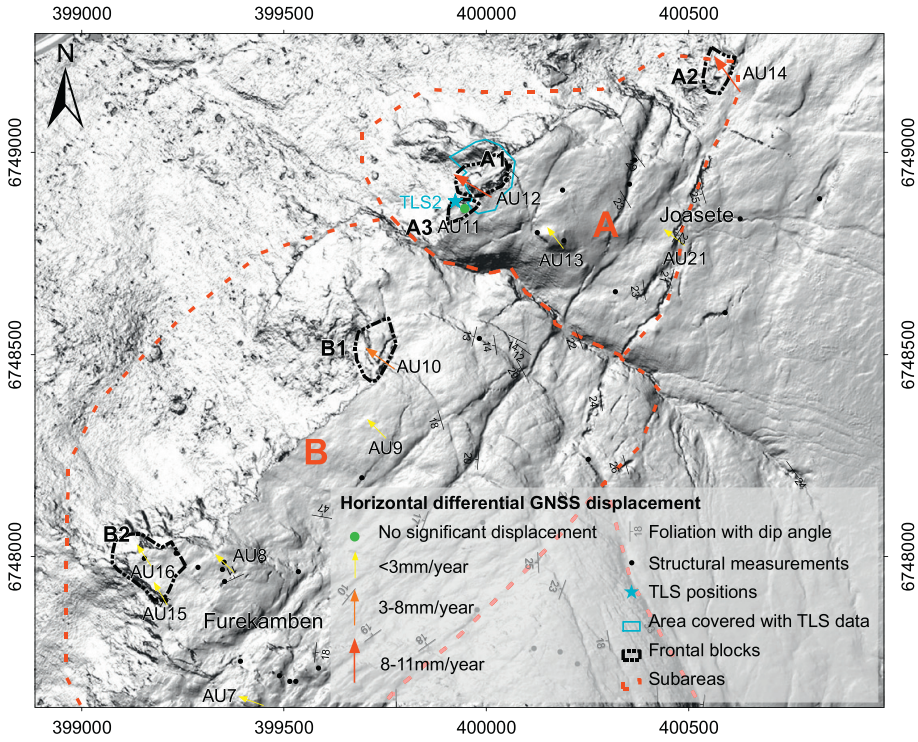

Fig. 3. Hillshade detail of subarea A and B between Joasete and Furekamben (see Fig. 2 for location). The subareas and analyzed blocks A1, A2, A3, B1 and B2 are outlined. (For interpretation of the references to color in this figure legend, the reader is referred to the web version of the article.)

along the cliff in subarea A. The central part of the unstable slope between Joasete and Furekamben, subarea B, is characterized by smaller scale open fractures and large surface depressions (Fig. 2). Two clearly delimited blocks are located close to the cliff (block B1 and B2; Fig. 3), but the detachment of these blocks is not as well developed as for block A1 and A2 in subarea A. The area south of Furekamben and around Ramnanosi, subarea C, reveals a different deformation pattern and is characterized by an up to 200 m high, west-facing cliff with very high rockfall activity. Two extensive surface depressions have developed along slope parallel structures that can be traced up to 3 km on the hillshade of the HR-DEM (Fig. 2; Braathen et al., 2004).

3. Structural analysis and volume estimations

3.1. Methods

Detailed structural field mapping was undertaken between 2008 and 2010. More than 2500 orientation measurements of joints and foliation were recorded at 122 localities (Figs. 2 and 4). Terrestrial laser scanning (TLS) surveys were carried out in 2008 and 2009 on two different locations, TLS 1 focusing on the cliffs at Ramnanosi and TLS 2 focusing on block A1 (Fig. 2). A detailed structural analysis of the TLS data was conducted using the Coltop3D software (www.terranum.ch; Jaboyedoff et al., 2007). In addition, the total rotational movement of block A1 was analyzed based on quantifying the differences in orientation of the discontinuity sets on the unstable block and on the stable part obtained from the structural analysis of the TLS data (Hermanns et al., 2011a; Oppikofer et al., 2012).

A high-resolution digital elevation model (HR-DEM) with 1 m resolution based on airborne laser scanning (ALS) data as well as very detailed aerial photographs provided the basis for a detailed analysis of the unstable area. Open fractures and lineaments were digitized and their orientations determined. Five frontal blocks were analyzed more in detail based on the HR-DEM and the structural knowledge obtained from field data (blocks A1, A2, A3, B1 and B2; Fig. 3). Using the PolyWorks software (InnovMetric, 2011) lateral and backbounding structures for those blocks and subarea A were determined and potential basal failure surfaces were estimated by fitting planes to

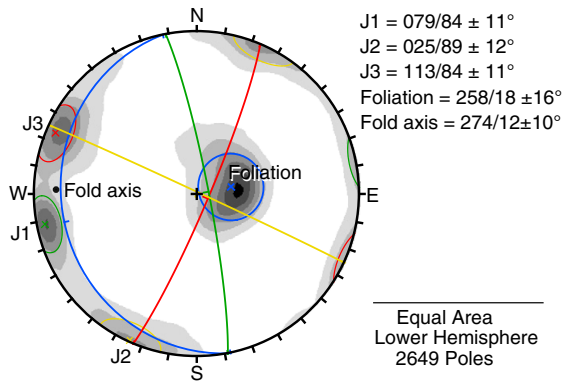

Fig. 4. Density stereonet of the field data (1% contour intervals). In addition, 1σ variability cones and mean surfaces for the major discontinuity sets are displayed.

the point cloud following the method proposed by Oppikofer (2009). Accurate volume calculations were possible based on these limits. In addition, volumes for larger unstable subareas where calculated with the Sloping Local Base Level (SLBL) method (Derron et al., 2005; Jaboyedoff and Derron, 2005). All blocks and subareas are internally fractured and might not fail at once, but rather in several smaller events. The calculated volumes have thus to be considered as the upper limit for the different block volumes.

3.2. Results

All orientation data of discontinuity surfaces in this publication are given as dip direction and dip angle in degrees. The variability of the discontinuity sets is reported as one standard deviation.

3.2.1. Joints

The analysis of the three different sources of structural data revealed three main joint sets that are all steep and very constant in orientation across the whole unstable area; J1 striking NNW–SSE, J2 striking WNW–ESE and J3 striking NNE–SSW (Table 1; Figs. 2 and 4). Most open gravitational fractures, graben structures and lineaments, which are visible on the HR-DEM and in the field, developed along those main sets or a combination of two of them. Furthermore, unstable blocks at the frontal cliff are mainly delimited by these three discontinuity sets (Table 2). This shows that gravitational slope deformation is strongly influenced by these pre-existing joint sets.

3.2.2. Foliation

The metamorphic foliation of the phyllites is strongly folded with varying types and degrees of folding (Fig. 5), ranging from centimeter-scale close folds to meter-scale open folds, but with a constant shallow fold axis plunging on average $274/12 \pm 10°$. Despite this complex folding pattern, the foliation develops preferentially surfaces with an average orientation of $258/18 \pm 16°$, thus down towards the Flåm Valley (Figs. 4 and 5b). The entire study area has similar average values for the orientation of foliation, besides some few outstanding localities, which are mostly localities with a strong folding (Fig. 5a).

The orientation of the foliation obtained from TLS data coincides with our field measurements (Table 1). However, TLS 1 data indicate steeper foliation surfaces than those measured in the field. Our field data as well as TLS 2 give an average dip of 18°, while TLS 1 data give foliation dip angles around 35°. This difference is significant for stability evaluation. Field data was almost exclusively collected on top of the plateau, since the steeper slopes are not accessible. In contrast, TLS data samples the vertical cliffs and vertical variations in discontinuity orientations might thus explain differences between the two data sets, especially taking into account the locally high degree of small scale folding. However, it cannot fully be asserted whether the measured surfaces in the TLS 1 dataset are foliation surfaces or not.

3.2.3. Detailed analysis of frontal blocks

The back-bounding and lateral structures of subarea A as well as for the five delimited blocks could be mapped on the HR-DEM and the basal limits were assumed parallel to the outcropping slope below the toe of the cliff (Table 2). Volume calculations based on these limits result in a volume of 31 million m^3 for the entire subarea A, and accordingly smaller volumes for the single blocks in this subarea: 280,000 m^3 for block A1, 130,000 m^3 for block A2 and 100,000 m^3 for block A3. Based on a run-out estimation with CONEFALL (Jaboyedoff and Labiouse, 2011), Block A1 could reach the fjord during a complete failure. A tsunami hazard assessment indicates that this volume would cause a run up of 3–4 m in the village of Flåm (NGI, 2009). However, since block A1 has high internal fracturing, it is uncertain if it will release in one part or successive smaller events.

The detachment of blocks B1 and B2 is not as well developed as for the blocks A1 and A2 in subarea A. In any case they can still be delimited by visible structures that follow pre-existing joint sets and a volume of 280,000 m^3 for block B1 and 380,000 m^3 for block B2 have been calculated based on these limits (Table 2). Since it is difficult to define basal limits for larger areas like subarea B, the volume of it has been estimated with the SLBL technique, resulting in 300 million m^3 (Table 2).

4. Kinematic analysis

4.1. Method

Simple kinematic feasibility tests for planar sliding, wedge failure and toppling have been made based on the criteria defined by Richards et al. (1978) and Hoek and Bray (1981). However, we used a larger direction tolerance of 45° for toppling failure and no direction tolerance at all for planar failure to be more conservative. This study investigates rockslides with complex structures and a small direction limitation might thus not be suitable (Oppikofer, 2009). In addition, a low friction angle of 20° has been used due to the possibility of breccia or gouge containing material with low frictional strength (e.g. Henderson et al., 2010). Mean slope values of an entire subarea have been used for the kinematic analysis, since this study is focusing on large instabilities.

4.2. Results

Kinematic analyses indicate that both planar failure along foliation and wedge failure along the foliation and J2 are feasible in all subareas, taking into account the high variability of foliation (Fig. 6). Furthermore, toppling is kinematically possible along J3 and partly along J1. This agrees with the analyzed blocks A1, A2, A3 and B1, where back-bounding structures formed along J3 and lateral release surfaces parallel to J1 (Table 2).

Since the foliation is strongly folded, it varies considerably within small distance. It can therefore be excluded that one single continuous sliding surface long enough to permit planar or also wedge failure of large rock slope instabilities can develop along the foliation. Hence, it is necessary that this unstable area is affected by a more complex failure mechanism than planar sliding along foliation or also wedge failure including the foliation. A more complex basal failure surface

Table 1
Summary of the main discontinuity sets. Orientation data are given as dip direction/dip angle $\pm 1\sigma$ variability in degrees. The orientations from TLS data are for all joint sets within the limits of the variability of the field data. For TLS 1 discontinuity set J3 is not visible due to the scanning direction, which is parallel to these surfaces. Foliation orientations are identical for field data and TLS 2, but steeper for TLS 1. Orientations for ALS data represent digitized lineaments and open fractures from the HR-DEM for which no dip angles have been determined.

Discontinuity set	Field data				TLS 1	TLS 2	ALS
	Mean orientation	Spacing [m]	Persistence [m]	JRC	Mean orientation	Mean orientation	Mean orientation
J1	$079/84 \pm 11°$	0.5–2	1–3	7.5	$243/89 \pm 9°$	$080/78 \pm 13°$	076
J2	$025/89 \pm 12°$	0.5–3	1–2	16	$205/72 \pm 10°$	$007/54 \pm 25°$	035
J3	$113/84 \pm 11°$	0.5–2	0.5–1	7	–	$144/56 \pm 20°$	109
Foliation	$258/18 \pm 16°$	–	–	–	$243/35 \pm 11°$	$261/18 \pm 16°$	–

Table 2
Overview of subareas and different unstable blocks. Volumes are calculated based on limiting structures except for Subarea B, where the SLBL method was used to estimate the volume. Values for GNSS points with no significant vertical or horizontal movement are shown in italics (Table 3).

		GNSS-point	3D movement vector		Volume [m³]	Limiting structures		
			Value [mm/year]	Direction (trend/plunge)		Back bounding fracture	Lateral release fractures	Basal failure surface
Subarea A	Entire subarea	AU13	*2.4*	322/*25*	31 Million	310/80 (J3)	Free face	300/27
		AU21	*2.0*	308/*25*		285/80 (J3)		
	Block A1	AU12	9.5	301/28	280,000	281/75 (J3)	226/46 331/74	302/38
	Block A2	AU14	15.2	324/45	130,000	120/90 (J3)	247/74 (J1) 036/80 (J2)	259/18 333/29
	Block A3	AU11	*4.7*	*308*/65	100,000	331/74 313/74 (J3)	270/80 (J1) 016/75 (J2)	283/41
Subarea B	Entire subarea	AU7	*2.6*	290/*30*	300 Million	Volume calculation based on SLBL		
		AU8	*2.5*	314/*28*				
		AU9	*2.2*	315/*18*				
	Block B1	AU10	4.4	306/24	380,000	300/76 (J3)	258/80 (J1)	005/18
	Block B2	AU15	3.9	330/53	280,000	310/40	240/80	310/40
		AU16	3.6	326/58				

has to develop, which probably follows the foliation in some parts, but steps down additionally along pre-existing joints with viable orientations, fold hinges or breaking through intact rock similar as observed in other locations in Norway (Fig. 7a; Jaboyedoff et al., 2011; Oppikofer et al., 2011). Failure surfaces parallel to foliation but stepping down along fold hinges or pre-existing joints were observed on smaller blocks in the field (Fig. 7b and c). However, structures related to regional detachment zones or faults that are not visible in the field data may be important for the failure system.

5. Displacement measurements

5.1. Method

Differential GNSS surveys have been undertaken yearly since the establishment of the first survey points in 2005. At that time, 3 fixed points were installed in stable areas and 16 rover points in potentially unstable regions. Two additional rover points (AU15 and AU16) were installed in a potentially unstable area at Furekamben in 2006. The locations of all GNSS-points are illustrated in Fig. 2.

GNSS-points with a significant movement are in this publication defined as points with a registered average movement larger than the average movement error $3\sigma_m$.

$$3\sigma_m = 3 \cdot \frac{\sqrt{2 \cdot \left(\frac{1}{n}\sum_{i=1}^{n}\sigma_i\right)^2}}{\Delta t}$$

where

σ_i	position error of each measurement
n	number of measurements
Δt	time in between first and last measurement

The average movement error $3\sigma_m$ varies in this study from 0.6 to 2.6 mm/year in horizontal direction and 1.1 to 3.9 mm/year in vertical direction (Table 3).

Movement rates and directions vary significantly from year to year as most points have observed displacements close to the level of accuracy of the measurement method. Variations between yearly measurements might display random measurement errors (Hermanns et al., 2011a). Robust linear regressions over the entire time series were thus applied to determine average yearly movement rates. The movement trend and plunge were computed for every GNSS-point with significant horizontal and respectively vertical displacement based on the regression results. However, with only seven sets of readings, the regression is still influenced by single years measurements and a longer time series is necessary to increase the statistical significance of the regression results.

5.2. Results

The yearly differential GNSS measurements indicate that in total 16 points have a significant average horizontal movement over the entire measurement period from 2005 to 2011 (Fig. 8a). However, only 5 points indicate a clear gravitational downslope deformation with a consistent movement trend over time in the horizontal movement (Table 3; e.g. Fig. 9a and b). Even if the other points with significant movement do not reveal a constant movement trend on a yearly basis, their long-term movement trend over the entire six-year measurement period is towards WNW to NW (290–330°, average: 310°), which is consistent with a downslope movement (Fig. 3).

Significant average yearly horizontal movement rates range from 0.8 to 10.8 mm/year. The two GNSS-points, AU12 and AU14, with the highest horizontal movement rates of 8.5 and 10.8 mm/year towards 301° and 324°, respectively, are located close to each other in

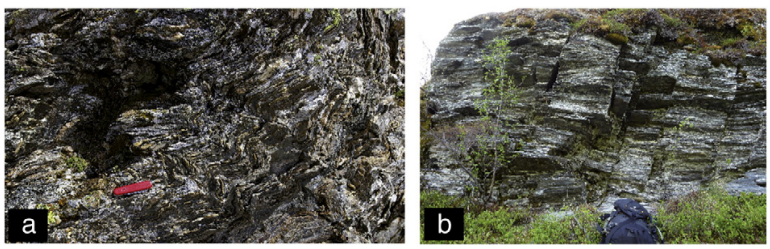

Fig. 5. Metamorphic foliation of the phyllites. a) Strongly folded foliation as it can be observed at several locations of the study area. b) Large open folds develop preferentially shallow dipping foliation surfaces.

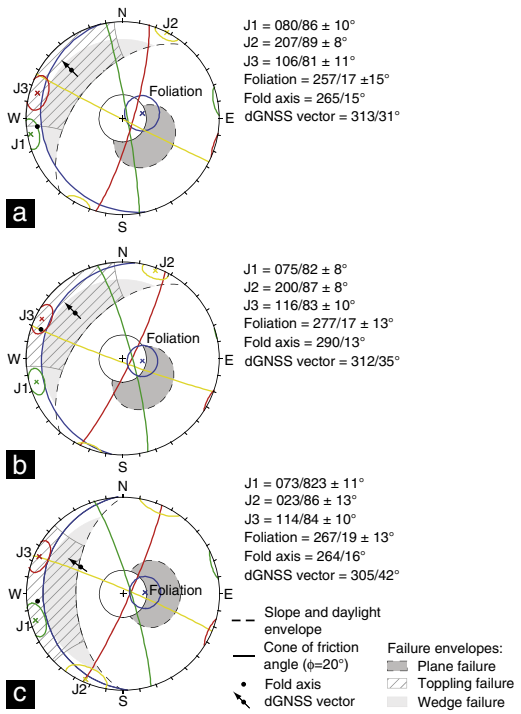

Fig. 6. Kinematic analysis of a) subarea A, b) subarea B, and c) subarea C. 1σ variability cones and mean surfaces for the major discontinuity sets are displayed. Planar sliding along foliation as well as wedge failure along the foliation and J2 are feasible in all subareas, taking into account the high variability of foliation. Additionally toppling along J3 is feasible in all three subareas and along J1 in subarea C and partially in subarea A. Average orientations of differential GNSS vectors for each subarea are plotted on the stereonet.

subarea A on defined blocks that are almost completely detached from the surrounding bedrock (block A1 and A2; Fig. 3). The same observation applies for GNSS-point AU10 in subarea B, which has an average horizontal movement of 4.0 mm/year towards 306° and is located close to the cliff on a delimited block (B1; Fig. 3). All other GNSS-points have horizontal movement rates around 2 mm/year or lower (Fig. 8a; Table 3).

Only 9 GNSS-points have a significant average vertical movement over the entire measurement period from 2005 to 2011, but only point AU14 reveals a consistent movement trend over time in the vertical movement (Table 3; Fig. 8b and 9d). Higher average 3D movement rates, compared to horizontal movement rates, indicate that the vertical movement rate is an important component in the deformation mechanism (Table 3). However, the interpretation of vertical differential GNSS results is difficult for most points due to annual systematic trends. The GNSS signal propagation velocity was modeled based on standard atmosphere, and deviations from this, especially in temperature and relative humidity, have a systematic impact on the large height differences between fixed points and rover points (up to 1400 m). Temperature inversion layers in the valley between fixed and rover points can have a similar effect. This leads to very inconsistent vertical movement patterns that cannot be explained geologically even for points with statistically significant vertical measurement results. The measurements from 2007 exemplify this, since most points have an exceptional upward movement in 2007, which is most likely due to atmospheric effects (Fig. 9c and d). Calculated movement plunges have thus to be handled with caution for all points, except GNSS point AU14, which is the only point with a consistent vertical movement trend (Fig. 9d). The resulting 3D movement for AU 14 is 15.2 mm towards 324/45 (Table 3).

All blocks display internal fracturing and it cannot be excluded that the single GNSS-points on each block record only the movement of a smaller part of each block and might not be representative for the entire block.

6. Dating of rockslide deposits

Terrestrial cosmogenic nuclides (TCN) dating was used in the Flåm study area to help further constraining the chronology and nature of rockslide events at two different lobes, belonging either to single rockslide events or to creeping lobes of successive rockfall deposits. TCN dating has been previously used for separating complex rock avalanche deposits of several generations into various events (Hermanns et al., 2001, 2004). A comprehensive review of TCN dating is provided by Gosse and Phillips (2001). This novel method provided absolute dates for two deposits in the study area.

6.1. Method

A total of 6 samples were taken from boulders with 4–12 m in diameter from two lobes (3 samples per lobe) in the study area (Fig. 2). The samples were collected following the guidelines recommended by Gosse and Phillips (2001), recording the rationale for sample selection, description of sampled rock block, geologic description of sample, location, orientation, sample thickness, and shielding geometry. The samples were prepared and concentrated at the Dalhousie University Cosmogenic Nuclide Exposure Dating Facility in Halifax, Canada. All except one sample had enough quartz to obtain a reliable result. The derived ages were calculated using the program CRONUS

Fig. 7. a) Schematic sketch of proposed basal failure surface along foliation, but stepping down along joint sets J1 and J3 or fold hinges. b and c) Step-path failure mode as observed in the field on smaller blocks.

Table 3
Summary of differential GNSS results. Average movement values as well as movement trend and plunge are calculated based on linear regression. In italics: results that are not significant, and in bold: points that show a consistent movement trend (Fig. 8).

GNSS-point	Average horizontal movement [mm/year]	Average horizontal movement error $3\sigma_m$ [mm/year]	Significant horizontal movement	Average vertical movement [mm/year]	Average vertical movement error $3\sigma_m$ [mm/year]	Significant vertical movement	Average 3D movement [mm/year]	Average 3D movement error $3\sigma_m$ [mm/year]	Movement trend [°]	Movement plunge [°]
AU2	0.8	0.7	Yes	−1.2	1.1	Yes	1.5	1.3	287	56
AU3	*0.9*	*1.7*	*No*	*−0.8*	*2.9*	*No*	*1.2*	*3.4*	*255*	*42*
AU4	1.2	0.7	Yes	−1.6	1.2	Yes	2.0	1.3	301	53
AU5	1.4	0.7	Yes	−1.5	1.2	Yes	2.1	1.4	297	48
AU6	**1.7**	0.7	Yes	*−1.1*	*1.2*	*No*	*2.0*	*1.4*	**303**	*33*
AU7	**2.3**	0.8	Yes	*−1.3*	*1.4*	*No*	*2.6*	*1.6*	**290**	*30*
AU8	2.2	0.8	Yes	*−1.2*	*1.4*	*No*	*2.5*	*1.6*	314	*28*
AU9	2.1	0.9	Yes	*−0.7*	*1.5*	*No*	*2.2*	*1.7*	315	*18*
AU10	**4.0**	0.9	Yes	−1.8	1.5	Yes	4.4	1.8	**306**	24
AU11	*2.0*	*2.6*	*No*	−4.3	3.9	Yes	*4.7*	*4.7*	*308*	65
AU12	**8.5**	2.2	Yes	−4.4	3.4	Yes	9.5	4.0	**301**	31
AU13	2.1	0.9	Yes	*−1.0*	*1.5*	*No*	*2.4*	*1.8*	322	*25*
AU14	**10.8**	1.1	Yes	**−10.7**	1.8	Yes	15.2	2.1	**324**	**47**
AU15	2.3	1.0	Yes	−3.1	1.8	Yes	3.9	2.1	330	53
AU16	1.9	1.1	Yes	−3.1	2.0	Yes	3.6	2.3	326	58
AU18	1.6	1.3	Yes	*−0.9*	*2.2*	*No*	*1.8*	*2.6*	322	*31*
AU21	1.8	0.9	Yes	*−0.9*	*1.5*	*No*	*2.0*	*1.8*	308	*25*
AU22	1.4	0.6	Yes	*−1.0*	*1.1*	*No*	*1.7*	*1.2*	317	*35*

^{10}Be exposure age calculator (Balco et al., 2008) and therefore were first calculated using global production rates and scaling models by Lal (1991) and Stone (2000). In a second step the ages were calibrated to local production rates determined within Norway; one in northern Norway (Fenton et al., 2011) and another in southern Norway (Goehring et al., 2012).

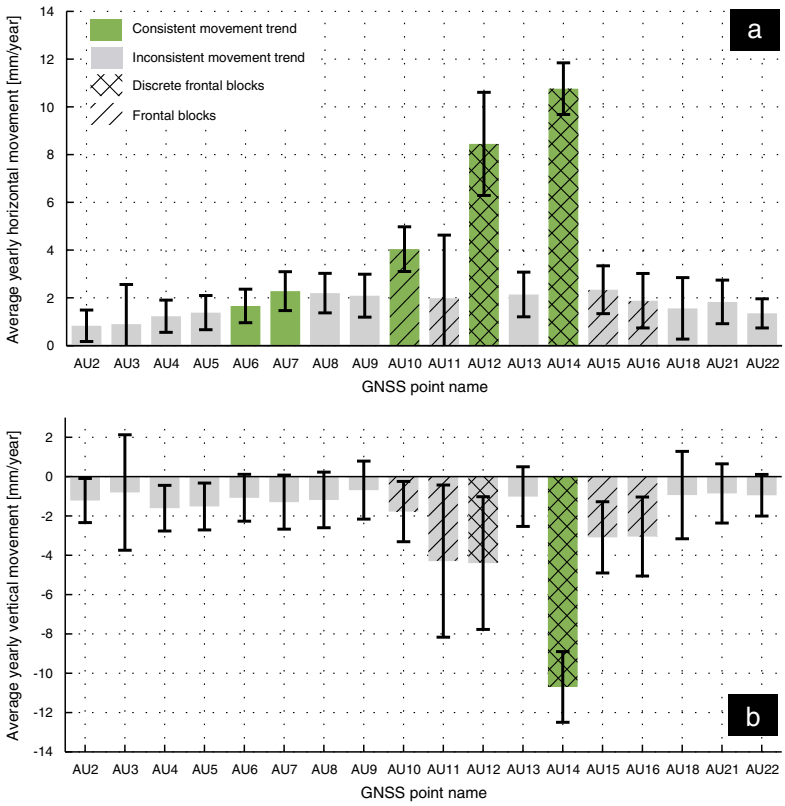

Fig. 8. Results of the differential GNSS surveys. Average yearly horizontal (a) and vertical (b) movement rates for each point obtained by robust linear regression of all measured points between 2005 and 2011. Error bars indicate $\pm 3\sigma_m$. Sixteen points have a significant horizontal movement, while only 9 points have a significant vertical movement. Points that have a consistent movement trend over time are shown in green and the location of the GNSS points on either frontal blocks or distinct frontal blocks along the cliff is indicated with hatched symbols. (For interpretation of the references to color in this figure legend, the reader is referred to the web version of the article.)

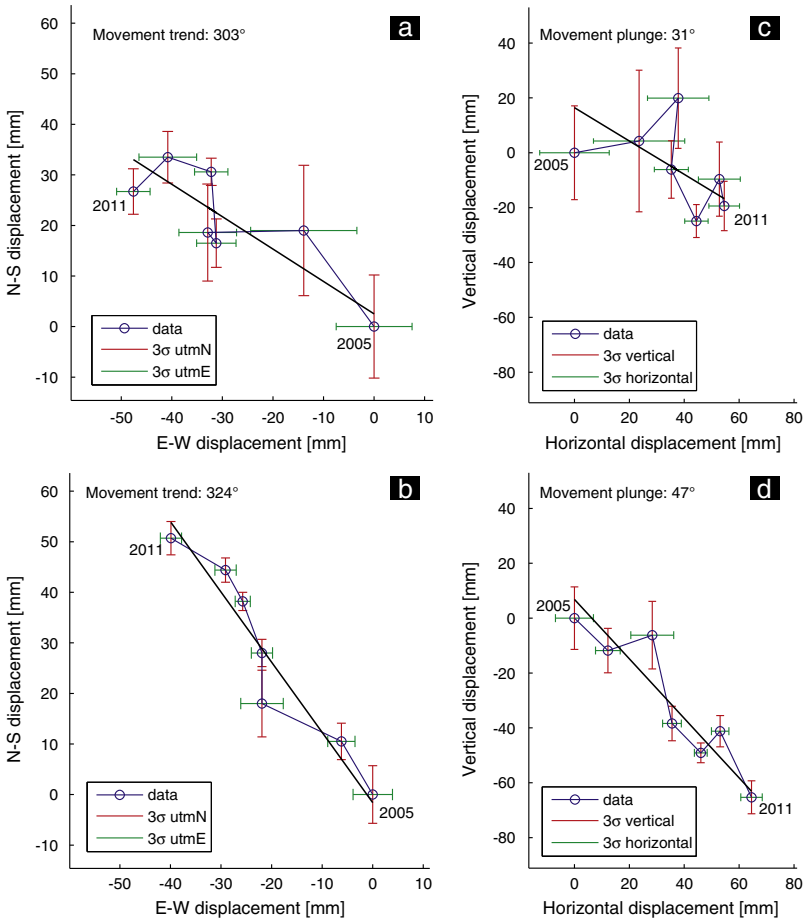

Fig. 9. Examples of the results of the differential GNSS surveys. a and c) Differential GNSS registrations for point AU12 and b and d) for point AU14. a and b) Display map plots of the horizontal movement, whereas c and d) present the vertical movement with respect to the horizontal movement. Data registration started at the coordinate [0,0] in 2005. Black regression lines indicate a consistent horizontal movement trend toward NW for AU12 and NNW for AU14. A consistent plunge of 47° can be observed for AU14, but AU12 displays an inconsistent vertical movement trend (Fig. 8). GNSS points AU12 and AU14 are situated on discrete frontal blocks with limited volumes. (For interpretation of the references to color in this figure legend, the reader is referred to the web version of the article.)

6.2. Results

Results from the dating are presented in Table 4. As expected all ages point towards a post-glacial origin for the deposits. Ages obtained using local production rates are slightly older than those using global production rates. The results from both lobes vary significantly.

The three samples from the northern lobe below Joasete nearly coincide within 1σ uncertainties and indicate a mean age close after the mid-Holocene climate optimum ending around 5,000 years BP. This may coincide with a minimum age of 2,840–2,720 cal years BP of organic material extracted from a sediment core above the deposits of a rock avalanche deposited into Aurland Fjord (Fig. 2; Blikra et al., 2006; Bøe et al., 2004) and suggests that the organic material extracted from the marine core post dates the same rock avalanche deposit dated onshore.

The southern lobe below Ramnanosi has very contrasting ages, one age is of the latest Holocene (2,400 years BP) while the other of the late Pleistocene (12,000 years BP). These ages are ambiguous. One interpretation is that this lobe is build up by multiple rockfall activity over a long period. This agrees with the currently observable deformation style at Ramnanosi with a high rockfall activity, but no larger unstable blocks comparable to those described in subareas A and B. Alternatively they can represent the deposit of a single event, where the older sample has an inherited surface exposure age of pre-failure exposure or the younger age might represent a boulder

Table 4
Ages obtained by ^{10}Be cosmogenic nuclide dating on samples in the Flåm Valley and 1σ uncertainty levels. Sample height is measured by altimeter with 1 m resolution; sample locations are shown in Fig. 2.

	RH-FL-01	RH-FL-02	RH-FL-03	RH-FL-05	RH-FL-06
Sample height [m]	92	115	126	135	166
Age [years] calibrated to Lal (1991) and Stone (2000)	4223	3665	3374	2230	11,130
Age [years] calibrated to Fenton et al. (2011)	4884	4239	3902	2579	12,873
Age [years] calibrated to Goehring et al. (2012)	4557	3955	3641	2407	12,012
Uncertainty [years] (1σ)	483	334	338	224	1119

that tilted due to post landslide creeping. Such effects have been reported by Ivy-Ochs et al. (2009) for the Flims rockslide.

7. 2D numerical analyses

7.1. General method

Two different numerical approaches were conducted in this study. First, a continuum model was used to analyze the stress distribution within the slope and to investigate the influence of unloading the slope due to a prehistoric rockslide. In a second step, the potential failure mechanism was investigated in more detail using a discontinuum model with the aim to reproduce the current slope morphology from an assumed pre-deformation topography.

A profile parallel to the main measured movement trend was constructed through subarea A so that it includes block A1 (Fig. 2). For this profile, a pre-deformation topography was assumed, where all graben structures have been closed (Figs. 10 and 11a). In-situ stress measurements from this region indicate a horizontal to vertical stress ratio of around one, i.e. moderate tectonic horizontal stress in addition to the vertical component induced by gravity (Hanssen, 1998). Thus an in-situ stress ratio of one was assumed for this study in both numerical models.

7.2. Continuum modeling setup

The two-dimensional finite element software Phase^2 (Rocscience, 2012) was used for the continuum model. A Mohr–Coulomb plastic approach was applied to model the rock mass before and after failure of a prehistoric rockslide in a two-stage analysis. The topography prior to this prehistoric rockslide was reconstructed based on today's morphology. By including a ubiquitous joint model in the strength factor calculation (Rocscience, 2012) the influence of foliation and vertical joint sets (J1 and J3) on the strength factor was investigated. The strength factor in Phase^2 is defined as the ratio of rock strength to induced stress at every point in the mesh.

The rock strength has been derived based on 14 existing uniaxial compression tests of samples from the same lithological unit (Hanssen et al., 1990). The uniaxial compressive strength of these samples varies from 10 to 125 MPa with a mean and median of 47 MPa. Young's modulus E, Young's modulus for intact rock E_i, Poisson's ratio ν and the Hoek–Brown intact material constant mi were estimated from literature with similar rock types or tabled values (Table 5; Agliardi et al., 2001, 2009; Kulhawy, 1975). The geological strength index (GSI; Hoek et al., 2002) was estimated in the field to be 40–60 and a value of 50 was used to calculate the rock mass parameters. A disturbance factor D of 0.5 was assumed in order to account for effects of mechanical weathering due to melting-freezing cycles of water as well as fractures induced from glacial erosion and deglaciation (e.g. Jaboyedoff et al., 2012). The Mohr–Coulomb parameters and the rock mass parameters were assessed with RocLab (Rocscience, 2007) based on the Hoek–Brown failure criterion (Table 5; Hoek et al., 2002). The residual parameter for cohesion was estimated based on Edelbro (2009) by multiplying the peak values with 0.3, while the residual friction angle was chosen to be equal to the peak friction angle as suggested by the same author.

7.3. Discontinuum modeling setup

The discontinuum modeling approach was carried out using the two-dimensional distinct element code UDEC (Itasca, 2004) in order to be able to model the deformation of a structurally controlled rock slope instability (Eberhardt et al., 2004; Brideau et al., 2006). A linearly elastic model was assumed for intact rock block behavior and discontinuities are modeled using the Mohr–Coulomb failure criterion with residual strength.

Foliation and joint networks were generated based on average apparent dip values from field measurements of subarea A (Table 6). However, joint set J2 was not included since its dip direction deviates too much from the profile trend. The spacing of the joints was estimated in the field, but needed to be increased for the modeling (Tables 1 and 6). The location and orientation of four graben structures are known from the geomorphologic mapping on the HR-DEM and were thus explicitly introduced as single joints in addition to the joint network with lower peak strength properties that were set equal to the corresponding residual strength values (Table 6). Inclinations of these graben structures have been estimated by fitting planes to the ALS point cloud using PolyWorks (InnovMetric, 2011). In the field it could be observed that discontinuities are non-persistent to different degrees. This is accounted for in the numerical model by applying Jennings' equivalent cohesion and friction criterion (Jennings, 1970). This means that the discontinuities were modeled as fully persistent, but with higher peak strength properties that account for the combined effect of non-persistent joints and intact rock bridges (Fischer et al., 2010; Gischig et al., 2011; Jaboyedoff et al., 2012).

There are large uncertainties in the model associated with the assigned rock mass and discontinuity strength parameters (Tables 5 and 6). A basic sensitivity analysis was thus undertaken in order to investigate the influence in changes of the different parameters. In addition the discontinuity networks have a relatively large variability of dip and dip direction in the field. This was not directly included in the modeling, but different geometrical configurations were tested in order to investigate the influence of the presence of different discontinuity sets as well as differing discontinuity inclinations on the modeling results. Since the largest uncertainties are due to the locally high degree of folding of the foliation, different dip angles and spacing of the foliation were modeled. In addition, models with and without introducing foliation or the graben structures were run.

7.4. Continuum modeling results

Continuum modeling was used to investigate the stress distribution in the slope and to investigate the influence of a prehistoric rockslide. The finite element simulation illustrates clearly that significant changes in the stress field of the slope after the modeled failure of the prehistoric rockslide are restricted to the frontal area (Fig. 10a). It indicates an increase of mean stress at the slope crest and a decrease on the middle of the slope, at the foot of the modeled prehistoric rockslide.

The importance of an anisotropic rock mass strength could be highlighted by introducing ubiquitous joint sets in the strength factor calculation (Fig. 10b and c). Modeling results indicate that the presence of discontinuities was necessary to develop the prehistoric failure as well as the current morphology with distinct graben structures. Without introducing discontinuities, the strength factor stays significantly above one for the entire studied profile. However, the introduction of ubiquitous joint sets results in lowered strength factors in regions that coincide with the extent of the prehistoric rockslide and the approximate location of the largest graben structure situated at Joasete (Fig. 10b). There are only minor regions along the slope with strength factors below one after the prehistoric failure (Fig. 10c). It can thus be concluded that the weakness zones, along which today's graben structures formed, have developed already prior to the prehistoric slope failure and might thus at the present stage only be remnants of a former instability.

7.5. Discontinuum modeling results

Discontinuum modeling was used to further investigate the possible failure mechanisms. The modeling results highlight a clear structural dependence of the failure mechanisms: testing different geometrical configurations confirmed that all observable structures

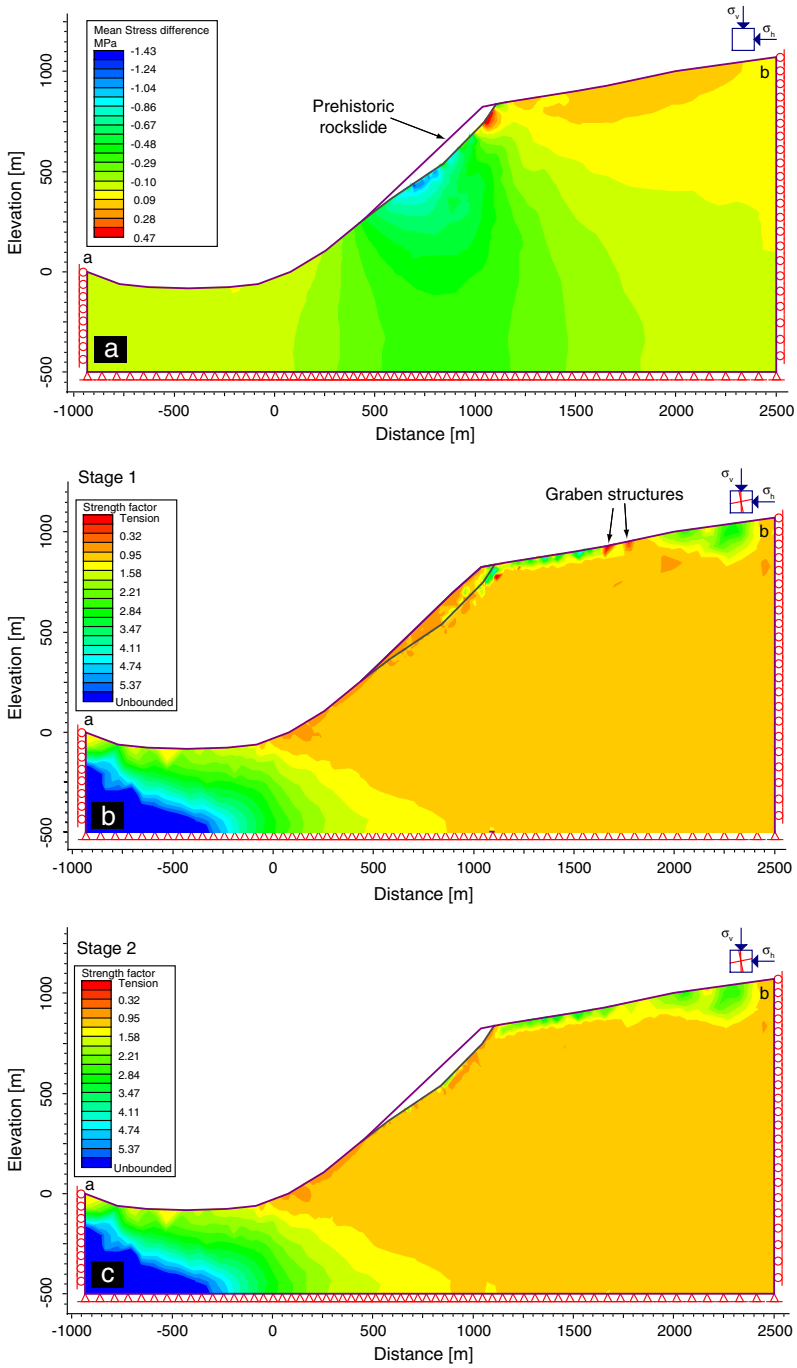

Fig. 10. Continuum modeling results. See Fig. 2 for profile location. a) Mean stress difference after failure of the prehistoric rockslide. An increase of mean stresses at the slope crest and decrease at the central part of the slope can be observed. However, only the frontal area is affected by changes in the stress field. b and c) Strength factor after introducing ubiquitous joint sets. b) Situation before failure of the prehistoric rockslide and c) situation after the failure. The prehistoric rockslide area is clearly delimited by a low strength factor (b). In addition zones with a low strength factor, corresponding approximately to the location of today's graben structures can be observed (b). These weakness zones are not present any longer after the failure of the prehistoric rockslide (c). (For interpretation of the references to color in this figure legend, the reader is referred to the web version of the article.)

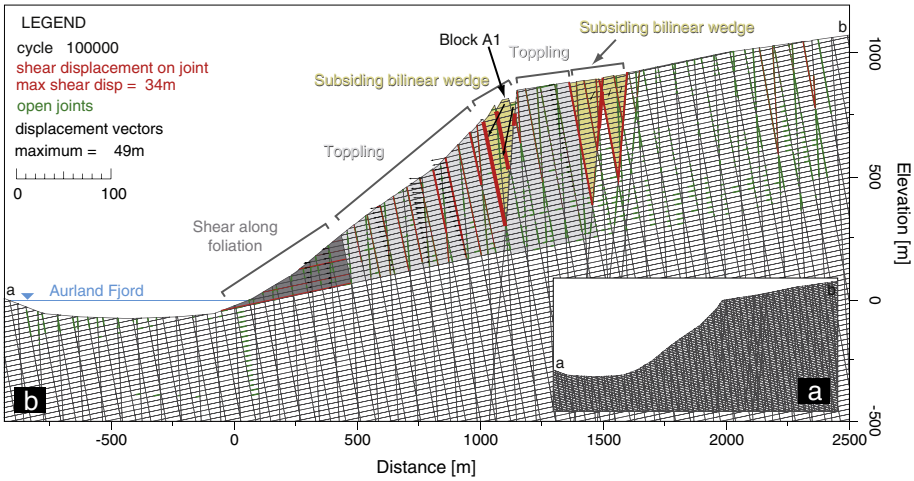

Fig. 11. Discontinuum modeling results. See Fig. 2 for profile location. a) Starting model for numerical simulation in UDEC. b) Final UDEC model displaying a morphology similar to the observed morphology in the field with the formation of block A1 at the slope crest and grabens in the back. Typical apertures of block interfaces for toppling are visible at the base of the toppling columns (in green). Thicknesses of the red lines displaying the shear displacement indicate the relative amount of shear displacement along the corresponding joint, with thicker lines for higher shear displacement. For clarity reasons just some displacement vectors are displayed in order to present the main characteristics of the displacement pattern. Toppling is confirmed by linearly increasing displacement vectors from bottom to top. (For interpretation of the references to color in this figure legend, the reader is referred to the web version of the article.)

need to be included into the model in order to (1) get the highest deformation at the slope crest at block A1 and (2) to be able to reproduce today's morphology (Fig. 11b). The discontinuities forming today's graben structures have to be explicitly introduced with a low strength into the model in order to really form graben structures and to obtain a downward movement of the frontal block A1. This confirms again that these structures need to be initiated already at an earlier stage, for example prior to the prehistoric slope failure. As mentioned before, the graben structures formed along joint set J3, which was included as a joint network in the numerical model. However, during modeling the variation in dip angle and dip direction was not taken into account and the mean dip direction of J3 is opposite to the manually introduced weak structures.

Sensitivity analysis confirmed that changing the strength parameters of the rock mass as well as those of the discontinuity sets, does not change the general failure mechanism. Different discontinuity strength parameters result mainly in different amounts of calculated displacement, like for example the formation of smaller or larger graben structures.

The results of the numerical modeling highlight a complex failure mechanism, that is a combination of (1) a toppling component over the entire unstable area along J1 and J3, (2) the formation of grabens based on a subsiding bilinear wedge between J1 or J3 and the graben structures similar as described by Norrish and Wyllie (1996) and (3) planar sliding along foliation on different horizons at the toe of the slope (Fig. 11b). The bilinear wedge formation can be observed in the field on the cliff in between Furekamben and Ramnanosi which forms a natural cross section through the studied area. Such a bilinear wedge was also reported for the 2006 Eiger rockslide in Switzerland (Oppikofer et al., 2008; Jaboyedoff et al., 2012). The specific discontinuity configuration of the studied profile with steep joints dipping into the mountain, combined with a flatter foliation is characteristic for block toppling (e.g. Wyllie, 1980; Nichol et al., 2002; Wyllie and Mah, 2004). Toppling is indicated by linearly increasing displacements from the bottom upwards and typical apertures of block interfaces (Fig. 11b; Lanaro et al., 1997). In theory a block toppling failure has a stepped base (Wyllie and Mah, 2004), but this is in this study disrupted by the graben structures. Within the numerical model no continuous basal failure surface developed below the entire unstable area.

Table 5
Rock mass properties used for continuum and discontinuum modeling.

Density [kg/m^3]	2800
Uniaxial compressive strength *UCS* [MPa]	47
GSI	50
mi	10
Disturbance factor *D*	0.5
Young's modulus for intact rock E_i [GPa]	30
Tensile strength [MPa]	0.06
Cohesion [MPa]	2
Residual cohesion [MPa]	0.6
Friction angle [°]	26
Residual friction angle [°]	26
Young's modulus *E* [GPa]	15
Poisson's ratio ν	0.1
Bulk modulus *K* [GPa]	6.25
Shear modulus *G* [GPa]	6.82

Table 6
Discontinuity properties used in UDEC for discontinuum modeling.

Discontinuities	Foliation	J1	J3	Graben structures
Apparent dip [°]	12	−87	−80	85
Spacing [m]	20	80	60	–
Peak tensile strength [kPa]	0.5	0.5	0.5	0
Residual tensile strength [kPa]	0	0	0	0
Peak cohesion [MPa]	1	0.5	0.5	0.01
Residual cohesion [MPa]	0.1	0.01	0.01	0.01
Peak friction angle [°]	30	32	32	20
Residual friction angle [°]	15	20	20	20
Joint normal stiffness [GPa/m]	7	7	7	7
Joint shear stiffness [GPa/m]	1	1	1	1

8. Discussion of the geomechanical model

Movement trends from the differential GNSS analysis are consistent with a wedge failure along foliation and J2 as well as toppling along J3 taking into account the variability of the involved structures, but not with a planar sliding along foliation (Fig. 6). However, calculated movement plunges are too steep for both mechanisms. As demonstrated by the numerical modeling results, combined toppling and subsiding bilinear wedge failure result in steeper displacement vectors (Fig. 11b).

The analysis of the total rotational movement of block A1 based on discontinuity orientations resulted in a total toppling movement of 15° towards 308° (Hermanns et al., 2011a; Oppikofer et al., 2012). This rotation is consistent with the measured differential GNSS movement vector of AU12 on block A1 (Table 3), but oblique to the expected toppling movement along J3 (Table 2), which is forming the back-bounding escarpment. A lateral restriction by joint set J2 may explain this deviation.

Numerical discontinuum modeling demonstrated that toppling along J1 and J3 as well as bilinear wedge failure along J1, J3 and the graben structures are the dominant failure mechanisms for subarea A. However, it has to be kept in mind that the numerical models are still simplified and conceptual, so that details might be different in reality. Nevertheless, the general failure mechanisms that have been observed in the modeling results were not sensitive to changes in the input parameters as shown by a basic sensitivity analysis. In addition, large regional faults may be of importance for the failure system, but these have not been found in the field.

The used apparent dip angle of foliation is less than the friction angle (Table 6) and sliding failure is thus unlikely. However, planar sliding along the foliation is present at the toe of the unstable slope within the discontinuum model due to the actively pushing rock mass behind. Signs for planar sliding cannot be directly observed in the field because of thick scree coverage of the lower parts of the slope. Movements of this scree deposits have been reported and a local collapse in 1979 resulted in 11 m total displacement (Domaas et al., 2002).

The here proposed failure model is similar to the complex field model with planar fault geometry suggested by Braathen et al. (2004), also called slide-topple (Brideau and Stead, 2009; Hermanns and Longva, 2012). This combined failure mechanism depends on the interaction between basal and rear structures and involves sliding at the toe of the unstable rock mass and toppling in the upper part, as observed in this study. However, in contrast to simple toppling the displacement pattern for this failure mechanism would be characterized by non-linearly increasing displacements from the bottom upwards as demonstrated by Brideau and Stead (2009). This could not be observed in the results of the numerical model within this study. In addition, according to Brideau and Stead (2009) the dip of the rear structures has to be shallower than 70° in order to develop a slide-topple mechanism, which is not the case for the discontinuities observed in the study area.

The largest uncertainty in the discontinuum model is the assumption of a straight foliation without including variability. Field observations show a high variability of the foliation orientation and locally high degrees of folding. Those are difficult to include into the model directly, but have been partially accounted for by applying higher strength properties for the foliation. However, especially high degrees of folding with distinct fold hinges may have a strong influence on the deformation mechanism, like described in Chapter 4.2 and Fig. 7a. In addition, no orientation data from below the surface exist since all measurements are from the top of the plateau. Potential vertical changes, like indicated by TLS 1, have thus not been considered. However, even cored boreholes would only give very local information about the variability of foliation with depth. In general it might be difficult to model a complex failure mechanism like observed at Stampa along a single profile in 2D. Numerical analyses in 3D would probably improve the understanding of the entire slope instability (Brideau et al., 2011).

The potential influence of groundwater and seasonal pore pressure build up was not taken into account in the numerical models due to the lack of data on hydrological conditions. However, especially the introduction of a general porewater pressure as well as a potential pore pressure build up during snow melt will lower the shear strength of the failure surfaces and thus influence the geomechanical model. In addition ice wedging may act as an important factor in the instability development, especially because of the well-developed joint network at Stampa.

9. Relative failure susceptibility and implications for hazard

The village of Flåm is a popular tourist destination during summer, receiving around 450,000 visitors and more than 130 cruise ships each year. Due to the high public interest and the large amount of potentially affected persons, questions about the likelihood of a catastrophic failure are important to answer. Based upon geomorphological studies of prehistoric events, structural variability and differential GNSS movements it is interpreted that slope deformation and collapse of the slope in future will be similar to the past. Small collapses of blocks $<100{,}000\ m^3$ along the frontal cliffs where structures allow for slope disintegration (i.e. partial release of blocks A1, A2, A3, B1 and B2), can occur more frequent. These failures have deposited on the slope in the past and did not reach down to the fjord or village (Fig. 2). Medium-sized slope collapses of blocks $>100{,}000\ m^3$ along the cliff with volumes large enough to reach the fjord cannot be ruled out (i.e. blocks A1, A2, A3, B1 and B2). At least two such events have occurred since the end of the last glaciation. One of them was dated older than 3000 years BP (Table 4; Bøe et al., 2004; Hermanns et al., 2011b). Large rockslide deposits on the fjord bottom, which date back to the end of the last glaciation (Blikra et al., 2006), indicate that a collapse involving a larger volume (i.e. entire subarea A or B) is of very low likelihood and most likely linked to major climatic changes like glacial-interglacial cycles.

These failure scenarios can be supported by the differential GNSS results. Movements of ≥ 4 mm/year can only be found for clearly delimited frontal blocks, but not inside the subareas. Long-term movement rates determined by cosmogenic nuclide dating of exposed sliding surfaces of other active unstable rock slopes in Norway indicated that these slow movement rates (<4 mm/year) may be present since the end of the last glaciation without any significant acceleration (Hermanns et al., 2012). Thus these slow movement rates represent most likely long-term movement rates and are not critical for a failure in the near future assuming aseismic conditions. In this region neo-tectonic activity has not been reported until now. A significant increase of movement rates will therefore be necessary before a catastrophic failure (Crosta and Agliardi, 2003).

10. Summary and conclusions

This study of the Stampa slope demonstrated the importance of integrating different data sources and analysis methods in order to understand the deformation mechanism of a complex unstable rock slope. Only the joint interpretation of all results led to a coherent model of the deformation and failure mechanism.

All analyses indicated that gravitational slope deformation in the study area is strongly influenced by inherited structures, like pre-existing joint sets and the metamorphic foliation of the phyllites. Large open fractures or surface depressions developed along the main joint sets or a combination of two of them. The analyzed blocks are clearly delimited by pre-existing joint sets. Numerical modeling also supports a structurally controlled failure, where discontinuities with a low strength dominate the rock mass behavior. Continuum modeling results suggest that the weakness zones, along which today's graben

structures formed, have developed already prior to a prehistoric slope failure and are today probably only remnants of a former instability.

The integrated structural and kinematic analysis as well as numerical modeling indicate a complex failure system involving the following mechanisms (1) a toppling component, (2) a subsiding bilinear wedge failure and (3) planar sliding along the foliation at the toe of the unstable slope. Frontal blocks may have a stepped basal failure surface following the foliation and stepping down along J1 and J3. Planar sliding at the toe of the unstable slope indicated by numerical discontinuum modeling can however not be confirmed by other results or field observations, due to thick scree deposits that cover the entire lower part of the slope.

Geomorphological analysis and cosmogenic nuclide dating confirmed that the northern region between Joasete and Furekamben, subarea A and B, has potential for medium-scale gravitational slope failures of blocks with volumes up to various 100,000 m^3, while the area around Ramnanosi, subarea C, will most likely only be affected by small-volume rockfall events. The larger subareas which have movement rates below 4 mm/year exhibit probably long-term movement rates and are not critical for catastrophic failure without significant external changes.

Acknowledgments

The authors are grateful to A. Günther for support in the field and the master student Å. Tukkensæter from the Norwegian University of Science and Technology, who was involved in the fieldwork of 2009. Partial funding was received by the Research Council of Norway through the International Centre for Geohazards (ICG). Their support is gratefully acknowledged. This is ICG contribution no. 406. The authors would also like to acknowledge constructive comments on this article from C.R. Froese, an anonymous reviewer and the journal editor, G.B. Crosta.

References

Agliardi, F., Crosta, G.B., Zanchi, A., 2001. Structural constraints on deep-seated slope deformation kinematics. Engineering Geology 59 (1–2), 83–102.

Agliardi, F., Zanchi, A., Crosta, G.B., 2009. Tectonic vs. gravitational morphostructures in the central Eastern Alps (Italy): constraints on the recent evolution of the mountain range. Tectonophysics 474 (1–2), 250.

Balco, G., Stone, J.O., Lifton, N.A., Dunai, T.J., 2008. A complete and easily accessible means of calculating surface exposure ages or erosion rates from ^{10}Be and ^{26}Al measurements. Quaternary Geochronology 3 (3), 174–195.

Blikra, L.H., Longva, O., Braathen, A., Anda, E., Dehls, J.F., Stalsberg, K., 2006. Rock slope failures in Norwegian Fjord Areas: examples, spatial distribution and temporal pattern. In: Evans, S.G., Mugnozza, G., Strom, A., Hermanns, R.L. (Eds.), Landslides from Massive Rock Slope Failure. NATO Science Series, IV. Earth and Environmental Sciences, vol. 49. Springer, Dodrecht, Netherlands, pp. 475–496.

Bøe, R., Longva, O., Lepland, A., Blikra, L.H., Sønstegaard, E., Hadlidason, H., Bryn, P., Lien, R., 2004. Postglacial mass movements and their causes in fjords and lakes in western Norway. Norsk Geologisk Tidsskrift 84 (1), 35–56.

Böhme, M., Saintot, A., Henderson, I.H.C., Henriksen, H., Hermanns, R.L., 2011. Rock-slope instabilities in Sogn & Fjordane County, Norway: a detailed structural and geomorphological analysis. In: Jaboyedoff, M. (Ed.), Slope Tectonics. Geological Society, London, Special Publications, pp. 97–111.

Braathen, A., Blikra, L.H., Berg, S.S., Karlsen, F., 2004. Rock-slope failure in Norway; type, geometry, deformation mechanisms and stability. Norwegian Journal of Geology 84 (1), 67–88.

Brideau, M., Stead, D., 2009. The role of rear release surfaces, block size and lateral confinement on rock slope failure mechanisms. Proceedings of the 62nd Canadian Geotechnical Conference, pp. 489–496.

Brideau, M., Stead, D., Couture, R., 2006. Structural and engineering geology of the East Gate Landslide, Purcell Mountains, British Columbia, Canada. Engineering Geology 84 (3–4), 183–206.

Brideau, M., Pedrazzini, A., Stead, D., Froese, C., Jaboyedoff, M., van Zeyl, D., 2011. Three-dimensional slope stability of South Peak, Crowsnest Pass, Alberta, Canada. Landslides 8, 139–158.

Coggan, J.S., Stead, D., Eyre, J.M., 1998. Evaluation of techniques for quarry slope stability assessment. Transactions of the Institution of Mining and Metallurgy. Section B: Applied Earth Science 107, B139–B147.

Crosta, G.B., Agliardi, F., 2003. Failure forecast for large rock slides by surface displacement measurements. Canadian Geotechnical Journal 40 (1), 176–191.

Cruden, D.M., Varnes, D.J., 1996. Landslide types and process. In: Turner, A.K., Schuster, R.L. (Eds.), Landslides Investigation and Mitigation. Transportation Research Board, National Research Council, National Academy Press, Washington, DC, pp. 36–75.

Dehls, J.F., Olesen, O., Olsen, L., Harald Blikra, L., 2000. Neotectonic faulting in northern Norway; the Stuoragurra and Nordmannvikdalen postglacial faults. Quaternary Science Reviews 19 (14–15), 1447–1460.

Derron, M.-H., Jaboyedoff, M., Blikra, L.H., 2005. Preliminary assessment of rockslide and rockfall hazards using a DEM (Oppstadhornet, Norway). Natural Hazards and Earth System Sciences 5 (2), 285–292.

Domaas, U., Rosenvold, B.S., Blikra, L.H., Johansen, H., Grimstad, E., Sørlie, J.E., Gunleiksrud, O., Engen, A., Lægreid, O., 2002. Studie av fjellskred og dalsidestabilitet i fyllittområder (Study of rockslides and valley-side-stability in phyllite regions). Norges forskningsråd.

Eberhardt, E., Stead, D., Coggan, J.S., 2004. Numerical analysis of initiation and progressive failure in natural rock slopes—the 1991 Randa rockslide. International Journal of Rock Mechanics and Mining Sciences 41 (1), 69–87.

Edelbro, C., 2009. Numerical modelling of observed fallouts in hard rock masses using an instantaneous cohesion-softening friction-hardening model. Tunnelling and Underground Space Technology 24 (4), 398–409.

Fenton, C.R., Hermanns, R.L., Blikra, L.H., Kubik, P.W., Bryant, C., Niedermann, S., Meixner, A., Goethals, M.M., 2011. Regional ^{10}Be production rate calibration for the past 12ka deduced from the radiocarbon-dated Grøtlandsura and Russenes rock avalanches at 69° N, Norway. Quaternary Geochronology 6 (5), 437–452.

Fischer, L., Amann, F., Moore, J.R., Huggel, C., 2010. Assessment of periglacial slope stability for the 1988 Tschierva rock avalanche (Piz Morteratsch, Switzerland). Engineering Geology 116 (1–2), 32–43.

Fjeldskaar, W., Lindholm, C., Dehls, J.F., Fjeldskaar, I., 2000. Postglacial uplift, neotectonics and seismicity in Fennoscandia. Quaternary Science Reviews 19 (14–15), 1413–1422.

Furseth, A., 2006. Skredulykker i Norge. Tun Forlag, Oslo, Norway.

Gischig, V., Amann, F., Moore, J.R., Loew, S., Eisenbeiss, H., Stempfhuber, W., 2011. Composite rock slope kinematics at the current Randa instability, Switzerland, based on remote sensing and numerical modeling. Engineering Geology 118 (1–2), 37–53.

Goehring, B.M., Lohne, Ø.S., Mangerud, J., Svendsen, J.I., Gyllencreutz, R., Schaefer, J., Finkel, R., 2012. Late glacial and holocene ^{10}Be production rates for western Norway. Journal of Quaternary Science 27 (1), 89–96.

Gosse, J.C., Phillips, F.M., 2001. Terrestrial in situ cosmogenic nuclides: theory and application. Quaternary Science Reviews 20 (14), 1475–1560.

Hanssen, T.H., 1998. Rock stresses and tectonic activity, in: Alten, T., Hermann, S., Beitnes, A. and Berg, K. (Eds.), Fjellsprengningsteknikk: Oslo, 26 november 1998; Bergmekanikk: Oslo, 27 november 1998; Geoteknikk: Oslo, 27 november 1998. Norsk betongforening, Oslo., pp. 29.1.

Hanssen, T.H., Stjern, G., Sørløkk, T., 1990. Bergartens mekaniske egenskaper STF36 F90048 SINTEF Bergteknikk, Trondheim.

Henderson, I.H.C., Saintot, A., 2011. Regional spatial variations in rockslide distribution from structural geology ranking: an example from Storfjord, western Norway. In: Jaboyedoff, M. (Ed.), Slope Tectonics. Geological Society, London, Special Publications, pp. 79–95.

Henderson, I.H.C., Ganerød, G.V., Braathen, A., 2010. The relationship between particle characteristics and frictional strength in basal fault breccias: implications for fault-rock evolution and rockslide susceptibility. Tectonophysics 486, 132–149.

Hermanns, R.L., Longva, O., 2012. Rapid rock-slope failures. In: Clague, J.J., Stead, D. (Eds.), Landslides: Types, Mechanisms and Modeling. Cambridge University Press, Cambridge, UK.

Hermanns, R.L., Strecker, M.R., 1999. Structural and lithological controls on large Quaternary rock avalanches (sturzstroms) in arid northwestern Argentina. Geological Society of America Bulletin 111 (6), 934–948.

Hermanns, R.L., Niedermann, S., Garcia, A.V., Gomez, J.S., Strecker, M.R., 2001. Neotectonics and catastrophic failure of mountain fronts in the southern intra-Andean Puna Plateau, Argentina. Geology 29 (7), 619.

Hermanns, R.L., Niedermann, S., Ivy-Ochs, S., Kubik, P.W., 2004. Rock avalanching into a landslide-dammed lake causing multiple dam failure in Las Conchas valley (NW Argentina)—evidence from surface exposure dating and stratigraphic analyses. Landslides 1 (2), 113–122.

Hermanns, R.L., Bunkholt, H.S.S., Böhme, M., Fischer, L., Oppikofer, T., Rønning, J.S., Eiken, T., 2011a. Foreløpig fare- og risikovurdering av ustabile fjellparti ved Joasete-Furekamben-Ramnanosi, Aurland kommune. NGU report 2011.025. Geological Survey of Norway, Trondheim, Norway.

Hermanns, R.L., Fischer, L., Oppikofer, T., Böhme, M., Dehls, J.F., Henriksen, H., Booth, A., Eilertsen, R., Longva, O., Eiken, T., 2011b. Mapping of unstable and potentially unstable slopes in Sogn og Fjordane (work report 2008–2010). NGU report 2011.55. Geological Survey of Norway, Trondheim, Norway.

Hermanns, R.L., Redfield, T.F., Bunkholt, H., Fischer, L., Oppikofer, T., Gosse, J., Eiken, T., 2012. Cosmogenic nuclide dating of slow moving rockslides in Norway in order to assess long-term slide velocities. In: Eberhardt, E., Froese, C., Turner, A.K., Leroueil, S. (Eds.), Landslides and Engineered Slopes. Protecting Society through Improved Understanding: Proceedings of the 11th International & 2nd North American Symposium on Landslides, Banff, Canada, 3–8 June 2012. CRC Press, pp. 849–854.

Hoek, E., Bray, J., 1981. Rock Slope Engineering, 3rd ed. E & FN Spon, London.

Hoek, E., Carranza-Torres, C., Corkum, B., 2002. Hoek–Brown failure criterion—2002 edition. Proceedings 5th North American Rock Mechanics Symposium and 17th Tunneling Association of Canada Conference: NARMS-TAC, pp. 267–271.

InnovMetric, 2011. PolyWorks: 3D scanner and 3D digitizer software from InnovMetric Software Inc. http://www.innovmetric.com/polyworks/3D-scanners/home.aspx?lang=en (accessed 03/21 2011).

Itasca, 2004. UDEC-Universal Distinct Element Code v4.0: Numerical modeling code for advanced geotechnical analysis of soil, rock, and structural support in two dimensions. Itasca Consulting Group, Minneapolis.

Ivy-Ochs, S., Poschinger, A.V., Synal, H., Maisch, M., 2009. Surface exposure dating of the Flims landslide, Graubünden, Switzerland. Geomorphology 103 (1), 104–112.
Jaboyedoff, M., Derron, M.-H., 2005. A new method to estimate the infilling of alluvial sediment of glacial valleys using a sloping local base level. Geografica Fisica e Dinamika Quaternaria 28, 37–46.
Jaboyedoff, M., Labiouse, V., 2011. Technical Note: Preliminary estimation of rockfall runout zones. Natural Hazards and Earth System Sciences 11, 819–828.
Jaboyedoff, M., Metzger, R., Oppikofer, T., Couture, R., Derron, M.-H., Locat, J., Turmel, D., 2007. New insight techniques to analyze rock-slope relief using DEM and 3D-imaging cloud points: COLTOP-3D software. In: Eberhardt, E., Stead, D., Morrison, T. (Eds.), Rock mechanics: Meeting Society's challenges and demands. Proceedings of the 1st Canada — U.S. Rock Mechanics Symposium, Vancouver, Canada, 27–31 May 2007. Taylor & Francis, London, pp. 61–68.
Jaboyedoff, M., Couture, R., Locat, P., 2009. Structural analysis of Turtle Mountain (Alberta) using digital elevation model: Toward a progressive failure. Geomorphology 103 (1), 5–16.
Jaboyedoff, M., Oppikofer, T., Derron, M., Blikra, L.H., Böhme, M., Saintot, A., 2011. Complex landslide behaviour and structural control: a three-dimensional conceptual model of Åknes rockslide, Norway. Geological Society Special Publication 351, 147–161.
Jaboyedoff, M., Derron, M.-H., Jakubowski, J., Oppikofer, T., Pedrazzini, A., 2012. Mt. Eiger, European Alps. In: Clague, J.J., Stead, D. (Eds.), Landslides: Types, Mechanisms and Modeling. Cambridge University Press, Cambridge, UK.
Jennings, J.E., 1970. A mathematical theory for the calculation of the stability of slopes in open cast mines. In: van Rensburg, P.W.J. (Ed.), Planning Open Pit Mines, Proceedings, Johannesburg, Johannesburg, pp. 87–102.
Kulhawy, F.H., 1975. Stress deformation properties of rock and rock discontinuities. Engineering Geology 9 (4), 327–350.
Lal, D., 1991. Cosmic ray labeling of erosion surfaces: in situ nuclide production rates and erosion models. Earth and Planetary Science Letters 104 (2–4), 424–439.
Lanaro, F., Jing, L., Stephansson, O., Barla, G., 1997. DEM modelling of laboratory tests of block toppling. International Journal of Rock Mechanics and Mining Sciences 34 (3) (173. e1-173. e15).
Mangerud, J., Gyllencreutz, R., Lohne, Ø., Svendsen, J.I., 2011. Chapter 22 — Glacial History of Norway. In: Ehlers, J., Gibbard, P.L., Hughes, P.D. (Eds.), Quaternary Glaciations - Extent and Chronology; A Closer Look. : Developments in Quaternary Science, vol. 15. Elsevier, pp. 279–298.
NGI, 2009. Beregning av flodbølger for tre potensielle fjellskred fra Stampa. 20081693–1 Norwegian Geotechnical Institute, Oslo.
Nichol, S.L., Hungr, O., Evans, S.G., 2002. Large-scale brittle and ductile toppling of rock slopes. Canadian Geotechnical Journal 39, 773–788.
Norrish, N.I., Wyllie, D.C., 1996. Rock slope stability analysis. In: Turner, A.K., Schuster, R.L. (Eds.), Landslides Investigation and Mitigation. Transportation Research Board, National Research Council, National Academy Press, Washington, DC, pp. 391–425.
Olesen, O., 2004. Neotectonic deformation in Norway and its implications: a review. Norwegian Journal of Geology 84, 3–34.
Oppikofer, T., 2009. Detection, analysis and monitoring of slope movements by high-resolution digital elevation models. Ph.D. thesis. Institute of Geomatics and Analysis of Risk, University of Lausanne, Lausanne, Switzerland.
Oppikofer, T., Jaboyedoff, M., Keusen, H.-R., 2008. Collapse at the eastern Eiger flank in the Swiss Alps. Nature Geoscience 1 (8), 531–535.
Oppikofer, T., Jaboyedoff, M., Pedrazzini, A., Derron, M.-H., Blikra, L.H., 2011. Detailed DEM analysis of a rockslide scar to improve the basal failure surface model of active rockslides. Journal of Geophysical Research 116, F02016.
Oppikofer, T., Bunkholt, H., Fischer, L., Saintot, A., Hermanns, R.L., Carrea, D., Longchamp, C., Derron, M.-H., Michoud, C., Jaboyedoff, M., 2012. Investigation and monitoring of rock slope instabilities in Norway by terrestrial laser scanning. In: Eberhardt, E. (Ed.), Landslides and Engineered Slopes. Protecting Society through Improved Understanding: Proceedings of the 11th International & 2nd North American Symposium on Landslides, Banff, Canada, 3–8 June 2012. CRC Press, pp. 1235–1241.
Panizza, M., 1973. Glacio-pressure implications in the production of landslides in the dolomitic area. Geologia Applicata e Idrogeologia 8 (1), 289–297.
Pfaffhuber, A.A., Grimstad, E., Domaas, U., Auken, E., Foged, N., Halkjær, M., 2010. Airborne EM mapping of rockslides and tunneling hazards. The Leading Edge 29 (8), 956.
Pfaffhuber, A.A., Bazin, S., Domaas, U., Grimstad, E., 2011. Electrical resistivity tomography to follow up an airborne EM rock slide mapping survey—Linking rock quality with resistivity. In: Guizan, C., Loures, L.G., Cetale, M., Zago, N. (Eds.), Proceedings of the Twelfth International Congress of the Brazilian Geophysical Society. SBGf — Sociedade Brasileira de Geofisica, Rio de Janeiro, Brazil.
Richards, L.R., Leg, G.M.M., Whittle, R.A., 1978. Appraisal of stability conditions in rock slopes. In: Bell, F.G. (Ed.), Foundation Engineering in Difficult Ground. Newnes-Butterworth, London, UK, pp. 449–512.
Roberts, D., Gee, D.G., 1985. An introduction to the structure of the Scandinavian Caledonides. In: Gee, D.G., Sturt, B.A. (Eds.), The Caledonide orogen—Scandinavia and related areas. John Wiley & Sons, pp. 55–68.
Rocscience, 2007. RocLab v1.0: Rock Mass Strength Analysis Using the Generalized Hoek–Brown Failure Criterion. Rocscience Inc., Canada.
Rocscience, 2012. Phase^2 v8.0: Finite Element Analysis for Excavations and Slopes. Rocscience Inc., Canada.
Saintot, A., Henderson, I.H.C., Derron, M., 2011. Inheritance of ductile and brittle structures in the development of large rock slope instabilities: examples from western Norway. In: Jaboyedoff, M. (Ed.), Slope Tectonics. Geological Society, London, Special Publications, pp. 27–78.
Sartori, M., Baillifard, F., Jaboyedoff, M., Rouiller, J., 2003. Kinematics of the 1991 Randa rockslides (Valais, Switzerland). Natural Hazards and Earth System Sciences 3 (5), 423–433.
Stead, D., Eberhardt, E., Coggan, J.S., 2006. Developments in the characterization of complex rock slope deformation and failure using numerical modelling techniques. Engineering Geology 83 (1–3), 217–235.
Stone, J.O., 2000. Air pressure and cosmogenic isotope production. Journal of Geophysical Research 105 (B10), 23753–23759.
Terzaghi, K., 1962. Stability of steep slopes on hard unweathered rock. Geotechnique 12, 251–263.
Wyllie, D.C., 1980. Toppling rock slope failures examples of analysis and stabilization. Rock Mechanics and Rock Engineering 13 (2), 89–98.
Wyllie, D.C., Mah, C.W., 2004. Rock Slope Engineering: Civil and Mining. Spon Press/Taylor & Francis Group, London and New York.
Zangerl, C., Eberhardt, E., Perzlmaier, S., 2010. Kinematic behaviour and velocity characteristics of a complex deep-seated crystalline rockslide system in relation to its interaction with a dam reservoir. Engineering Geology 112 (1–4), 53–67.

Appendix D

Paper IV

Reference to the paper

Böhme, M., Hermanns, R.L., Fischer, L., Oppikofer, T., Bunkholt, H.S.S., Derron, M.-H., Carrea, D., Jaboyedoff , M., and Eiken, T.: Detailed assessment of the deep-seated gravitational deformation at Stampa above Flåm, Norway, in: Eberhardt,E., Froese,C., Turner,A.K. and Leroueil,S. (Eds.), Landslides and Engineered Slopes. Protecting Society through Improved Understanding: Proceedings of the 11th International & 2nd North American Symposium on Landslides, Banff, Canada, 3-8 June 2012. CRC Press, pp. 647-652, 2012.

Note on contributions

This publication presents a preliminary stage of the investigations carried out at the unstable rock slope Stampa. The candidate wrote this paper and carried out all presented analyses. Fieldwork and the collection of structural data in the study area was carried out by the candidate together with Reginald L. Hermanns, Luzia Fischer and Thierry Oppikofer. The differential Global Navigation Satellite System data was processed by Trond Eiken and initial analysis was conducted by Halvor S. S. Bunkholt. The candidate conducted the final analyses of the differential Global Navigation Satellite System results as presented in the publication. Dario Carrea processed and analysed the groundbased Lidar data. All authors contributed to discuss the results and finalize the manuscript.

Landslides and Engineered Slopes: Protecting Society through Improved Understanding – Eberhardt et al. (eds)
© 2012 Taylor & Francis Group, London, ISBN 978-0-415-62123-6

Detailed assessment of the deep-seated gravitational deformation at Stampa above Flåm, Norway

M. Böhme
Geological Survey of Norway, Trondheim, Norway
Norwegian University of Science and Technology, Norway

R.L. Hermanns, L. Fischer, T. Oppikofer & H.S.S. Bunkholt
Geological Survey of Norway, Trondheim, Norway

M.-H. Derron, D. Carrea & M. Jaboyedoff
Institute of Geomatics and Risk Analysis, University of Lausanne, Switzerland

T. Eiken
University of Oslo, Norway

ABSTRACT: The unstable rock slope above the village of Flåm shows signs of active and postglacial gravitational deformation over an area of 11 km². We performed detailed structural field mapping, annual differential Global Navigation Satellite System (GNSS) surveys, and generated a detailed topographic model based on airborne and terrestrial laser scanning. Kinematic analyses of the structural data indicates that deformation is complex and varies over the slope. Both sliding and toppling are locally feasible. Using differential GNSS, 18 points were measured annually over a period of up to 6 years. Two of these points show an average yearly movement of around 10 mm/year. They are located at the frontal cliff on almost completely detached blocks. Large fractures indicate deep-seated gravitational deformation of volumes up to 80 million m³, but the movement rates in these areas are below 2 mm/year. Based upon these combined observations, we interpret that small collapses of blocks along the frontal cliff will be more frequent. Larger collapses of free-standing blocks along the cliff with volumes >100,000 m³, thus large enough to reach the fjord, cannot be ruled out. A large collapse involving more than 10 million m³, however, is of very low likelihood at present.

1 INTRODUCTION

Historical records and geological studies show a high concentration of post-glacial gravitational slope failures as well as current rock slope instabilities in western Norway (Blikra et al., 2006, Böhme et al., 2011). Several catastrophic failures causing tsunamis in the inner fjord areas of western Norway resulted in large loss of life in the last century (Furseth 2006).

The unstable rock slope above the village Flåm, Aurland municipality is one of the largest actively deforming rockslide areas known today in Norway (Braathen et al., 2004). It is located at the southern end of Aurlandsfjorden, a branch of Sognefjorden, on the eastern slope above the fjord and the village of Flåm (Fig. 1). An area of up to 11 km² that extends 7 km N-S and 2 km E-W shows signs of active and postglacial gravitational deformation. Slide velocities vary considerably over the entire unstable area, ranging from mean velocities of 11 and 9 mm/year at two delimited blocks down to below significance level (Hermanns et al., 2011a).

Large rockslide deposits have been mapped within the fjord and date back to the end of the last glaciation at ca. 11,000 years BP (Blikra et al., 2006). Additionally, at least one further rockslide reached down to the fjord dating older than 3000 years BP (Bøe et al., 2004, Hermanns et al., 2011a). Multiple lobes of smaller size deposits cover the slope below the entire deformation front (Fig. 1).

An intensive investigation program has been carried out in order to understand this unstable slope. Part of this is detailed structural field mapping, a differential Global Navigation Satellite System (GNSS) survey, as well as the analysis of a detailed digital elevation model (DEM) based on airborne laser scanning (ALS) data and several terrestrial laser scanning (TLS) surveys.

In this study we summarize all data, which results in a detailed and consistent model of the instability with a complex structural setting that

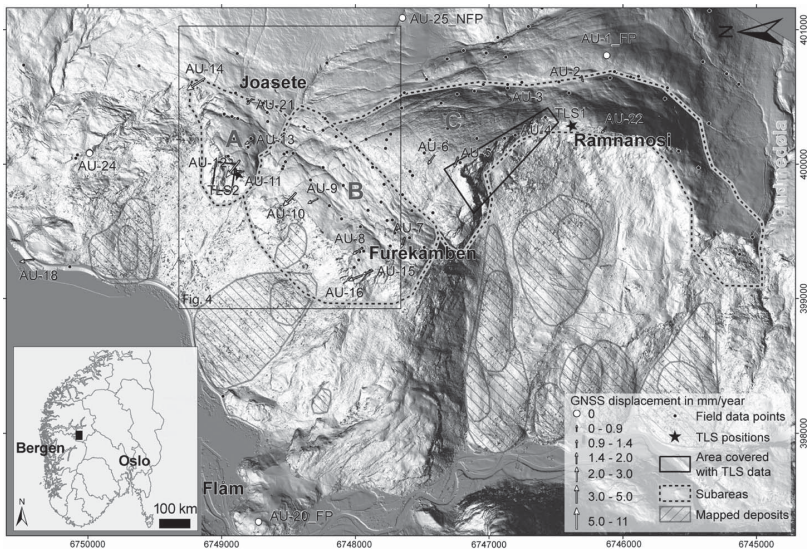

Figure 1. Hillshade of the study area based on ALS data. GNSS points, observation points for structural data, the different subareas as well as mapped rockslide deposits on the slope are illustrated. The inset shows the location of the study area inside southern Norway.

is controlling the deformation pattern of the unstable slope. Three different subareas have been distinguished based on geomorphology, structural variability and velocities (Fig. 1).

2 METHODS

2.1 *Structural analysis*

Detailed structural field mapping was undertaken in the summers of 2008, 2009 and 2010. More than 2500 orientation measurements of joints and foliation were recorded at 122 localities (Fig. 1).

TLS surveys. were carried out in the autumn of 2008 and 2009 on two different locations (TLS 1 and 2, Fig. 1). A detailed structural analysis of the TLS data was conducted using the Coltop3D software (www.terranum.ch, Jaboyedoff et al., 2007).

In addition, a DEM with 1 m resolution based on ALS data, provided the basis for further analyses of the unstable area. Open fractures and lineaments were digitalized and their orientations determined. Certain unstable areas were analyzed in much higher detail based on the detailed DEM and the obtained structural knowledge about the study area. Using PolyWorks software (InnovMetric 2011) lateral and back-bounding structures were determined and potential basal failure surfaces were estimated by fitting planes to the point cloud (see Oppikofer 2009 for method). Accurate volume calculations were possible based on these limits.

Simple kinematic tests for planar sliding, wedge failure and toppling have been made based on the criteria defined by Hoek & Bray (1981). However, we used a larger direction tolerance of 45° for toppling failure and no direction tolerance at all for planar failure to be more conservative. This study investigates rockslides with complex structures and a direction limitation might thus not be suitable (see also Oppikofer 2009).

2.2 *Displacement measurements*

Differential GNSS surveys have been undertaken yearly since the establishment of the first survey points in 2005. At that time, 3 fixed points were installed in stable areas and 16 rover points in potentially unstable regions. Two additional points (AU15 and AU16, Fig. 1) were installed in a potentially unstable area at Furekamben in 2006. One new fixed point (AU25_NFP) as well as a new point on a potentially unstable block (AU24) were established in 2009. The locations of all GNSS-points are illustrated in Figure 1.

Significant movement is in this publication defined as a registered movement larger than the uncertainty of the measurement method. This is under normal conditions varying from 3 to 6 mm for a 99% significance level in horizontal direction and 10 to 20 mm in vertical direction (Hermanns et al., 2011a, b). In addition, a certain gravitational deformation is only given in points where the trend of the movement direction is consistent over time.

The interpretation of vertical differential GNSS results is for most points difficult due to annual systematic trends from unmodeled meteorological effects and large height differences between fixed points and rover points (max. 1400 m). Hence, the uncertainty for the vertical movements is much higher than the uncertainty for the horizontal movements. Additionally, they show inconsistent directions for most points, and have thus not been used in the following analysis.

Movement rates and directions vary significantly from year to year as most points have observed displacements near the level of accuracy of the measurement method. Variations between yearly measurements might display random measurement errors (Hermanns et al., 2011b). Thus normalizing the total horizontal movement between the first and last measurement by the observation time can reduce this uncertainty. Hence, the differential GNSS movement rates in this report are given as average yearly movement rates.

3 RESULTS

3.1 *Structural analysis*

Work on the structural model is based on detailed structural field mapping, as well as on detailed DEMs derived from ALS data and TLS surveys.

All orientation data of discontinuity planes in this publication are given as dip direction and dip angle.

3.1.1 *Joints*

The analysis of the three different sources of structural data revealed three main joint sets that are all steep and very constant in orientation across the whole unstable area (Table 1, Fig. 2). Most open fractures and lineaments, which are visible on the DEM and in the field, developed along those main sets or a combination of two of them. Furthermore, unstable blocks at the frontal cliff are mainly delimited by these three discontinuity sets. This shows that the gravitational slope deformation is strongly influenced by pre-existing joint sets.

3.1.2 *Foliation*

The metamorphic foliation of the phyllites is strongly folded with varying types and degrees of folding, ranging from centimeter-scale, close folds to meter-scale open folds, but with a constant shallow fold axis plunging on average 274/12 ± 10°. Despite this complex folding pattern, the foliation develops preferentially surfaces with an average orientation of 264/18 ± 15°, thus slightly oblique down towards the fjord.

Table 1. Summary of main discontinuity sets. Orientation data are given as dip direction/dip angle ± 1σ variability in degrees.

Discontinuity set	Field data	TLS 1	TLS 2
J1	078/84 ± 9°	243/89 ± 9°	080/78 ± 11°
J2	203/89 ± 9°	205/72 ± 10°	010/71 ± 14°
J3	113/83 ± 11°		108/78 ± 10°
Foliation	264/18 ± 15°	243/35 ± 11°	262/19 ± 16°

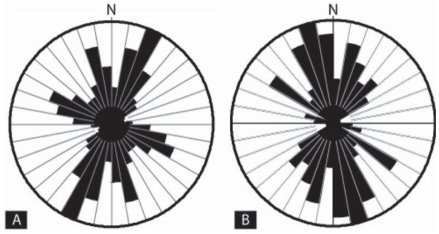

Figure 2. Rose diagrams of A) field data of joints sets and B) digitalized lineaments and open fractures from the ALS derived DEM. Both show the same three main joint sets (Table 1).

The orientation of the foliation obtained from TLS data coincides with our field measurements. However, TLS 1 data indicate steeper foliation planes than those measured in the field (Table 1). Our field data as well as TLS 2 give an average dip of 18°, while TLS 1 data give foliation dip angles around 35°. This difference is significant for stability evaluation, but the TLS data might be influenced by local variations due to the high degree of folding.

3.2 *Displacement measurements*

In total 15 GNSS-points have a significant horizontal total movement over the measurement period from 2005 to 2011 (Fig. 3A). However, only three points indicate a certain gravitational deformation with a coherent trend in the movement (Fig. 3B, C for points AU12 and 14). Even if the other points do not reveal a constant trend, their general movement trend towards WNW to NWN is consistent with the geological model (Fig. 1).

Average yearly movement rates range from 1 to 11 mm. Two monitoring points (AU12 and AU14) show an average yearly movement around 10 mm per year. They are located close to each other in the northern part of the monitored area of the unstable slope on defined blocks that are almost completely detached from the surrounding bedrock (block A1 and A2, see below, Fig. 4).

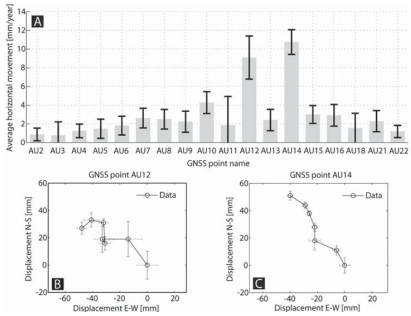

Figure 3. Results of the differential GNSS data. A) Total horizontal movements for each point between 2005 and 2011. Error bars indicate ± 3σ. B) and C) differential GNSS registrations for points AU12 and AU14, respectively. Data registration started at the coordinate [0, 0] in 2005. A coherent trend of the horizontal movement toward NW can be observed.

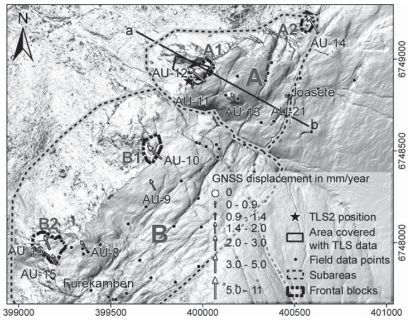

Figure 4. Detail of the study area between Joasete and Furekamben. For location see Fig. 1. Subarea A and B as well as the analyzed blocks A1, A2, B1 and B2 are outlined. Line a-b marks the profile in Fig. 6.

4 DISCUSSION

4.1 *Spatial sub-division based on morphology, structures, deformation, differential GNSS velocity and kinematic analysis*

The unstable area above Flåm can be divided into three subareas (A, B and C) based on the detailed DEM, the structural analysis, geomorphological observations and displacement measurements (Fig. 1).

Furthermore, it can be shown that all GNSS-points with movements >2 mm/year are located on defined blocks, which can be delimited by cracks, cliffs and incised rivers (Figs. 1, 4). For these blocks, lateral and back-bounding structures could be determined and potential basal failure surfaces were estimated. Additionally, volumes for the different subareas and some defined blocks have been calculated. In the following the subareas as well as the single blocks are described in more detail.

It has to be mentioned that all blocks described below show internal fracturing and might not fail at once, rather in several smaller events. The calculated volumes have thus to be considered as the upper limit for a volume estimation. In the same manner it cannot be excluded that the single GNSS-points on each block record only the movement of a smaller part of each block and might not be represantative for the whole block.

4.1.1 *Subarea A*

The northern part of the unstable area, thus the area N and W of Joasete, represents the most advanced stage of deformation (Figs. 1, 4). The largest open fractures, which developed along J1, J2 and J3, are located in this region. Two nearly freestanding blocks (blocks A1 and A2, Fig. 4) with the highest measured movement rates around 10 mm/year are situated at the cliff in this subarea. All other GNSS-points that are located further away from the cliff in this sub-area have movements ≤2 mm/year. The back-bounding and lateral structures could be mapped on the DEM and the basal limits were assumed parallel to the slope below the toe of the cliff.

This results in a volume of 31 million m³ for the entire subarea A, and accordingly smaller volumes for the single blocks, 280,000 m³ for block A1 and 130,000 m³ for block A2. The volume of block A1 is critical as a failure of the entire block could reach the fjord. A tsunami hazard assessment indicates that this volume would cause a run up of 3–4 m in the village of Flåm (NGI 2009). However, since block A1 has high internal fracturing, it is uncertain if it will release in one part or successive smaller events.

Kinematic analysis indicates that potential basal failure surfaces could partially develop along the foliation, taking into account the high variability of foliation (Fig. 5A). Furthermore, toppling is kinematically possible along J3 and partly J1. This can be confirmed by the unstable blocks in this area (A1 and A2). Both blocks have a back-crack along J3 and lateral release surfaces parallel to J1.

4.1.2 *Subarea B*

The central part of the unstable slope between Joasete and Furekamben is characterized by small open fractures and large surface depressions that have developed along J1 and J3. Horizontal movement rates are below 2.6 mm/year for the points farther away from the cliff, but 4.3, 3.0 and 2.9 mm/year for points AU10, 15 and 16, respectively, that are located close to the cliff on delimited blocks (B1 and B2, Fig. 4).

More detailed analyses have been done for the two frontal blocks B1 and B2. However, the detachment of these blocks is not as well developed as for the blocks described for subarea A. In any case

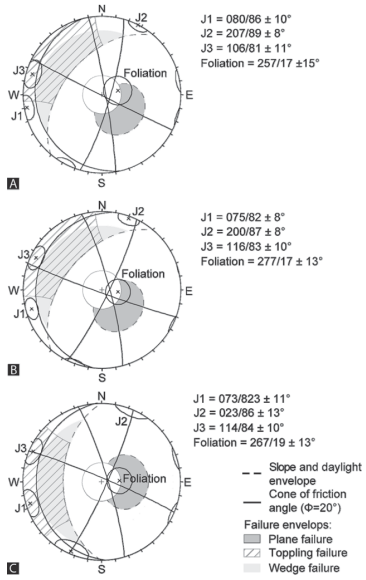

Figure 5. Kinematic analysis of A) subarea A, B) subarea B, and C) subarea C. Planar sliding along foliation as well as toppling along J3 is possible in all subareas. Additionally toppling along J1 is feasible in subarea C and partially in subarea A.

they can still be delimited by visible structures that follow pre-existing joint sets. The basal limits have been estimated based on the outcropping slope below the foot of the blocks. This results in a volume of 280,000 m³ for block B1 and 380,000 m³ for block B2.

The kinematic analysis shows similar results as in subarea A. Sliding is also possible along foliation and toppling along J3 (Fig. 5B).

4.1.3 *Subarea C*

The southern part of the study area, thus the area S of Furekamben and around Ramnanosi, reveals a different deformation pattern. This region is characterized by an up to 200 m high, west-facing cliff with very high rockfall activity. Two extensive surface depressions have developed along slope parallel structures, which most likely represent the foliation, and can be traced up to 3 km on the DEM (Fig. 1). They confine volumes of up to 80 million m³. However, movement rates in this region are smaller than 2 mm/year. Kinematic analysis indicates that sliding along the foliation as well as toppling along J1 and J3 is kinematically feasible in this region (Fig. 5C).

4.2 *Failure mechanism*

The kinematic tests indicate that both toppling and sliding are feasible mechanisms in the different unstable parts of the slope. Since the foliation is strongly folded, it varies considerably within small distance. It can therefore be excluded that a single constant sliding surface can develop along the foliation. Hence, it is necessary that this unstable area is affected by a more complex failure mechanism. A more complex basal limit has to develop which probably follows the foliation in some parts, but steps down additionally along pre-existing joints, fold hinges or breaking through intact rock (Fig. 6). Toppling is possible along different joint sets and is mainly concentrated along the steep cliffs at the deformation front. However, as discussed by Oppikofer et al. (2012) for block A1, toppling alone cannot explain the large open fractures visible in the field or DEM.

Similar as proposed by Braathen et al. (2004), one possible failure mechanism is a combination of sliding and toppling, called "slide-topple" (Brideau & Stead 2009). This combined failure mechanism depends on the interaction between basal and rear structures and involves sliding at the toe of the unstable block and toppling in the upper part.

4.3 *Relative failure susceptibility*

Based upon geomorphological studies of prehistoric events, structural variability and differential GNSS velocities we interpret that slope deformation and collapse of the slope in future will be similar to the past. Small collapses of blocks <100,000 m³ along the frontal cliffs where structures allow for slope disintegration, can occur several times in the next 1000 years. These failures will deposit on the slope and will not reach down to the fjord or village. Medium-sized slope collapses of blocks >100,000 m³ along the cliff with volumes large enough to reach the fjord cannot be ruled out (i.e., blocks A1, A2, B1 and B2). At least two such events have occurred since the end of the last glaciations. One of them was dated older than 3000 years BP (Bøe et al., 2004, Hermanns et al., 2011a). Large rockslide deposits on the fjord bottom, which date back to the end of the last glaciation (Blikra

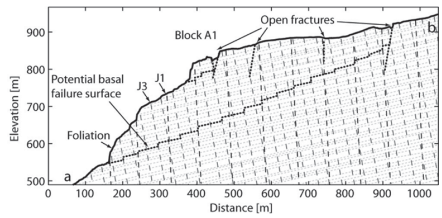

Figure 6. Profile through subarea A including block A1. See Fig. 4 for location. The proposed failure mechanism with basal failure surface along foliation, but stepping down along joint sets J1 and J3 is illustrated.

et al., 2006), indicate that a large collapse involving a volume of more than 10 million m³ is of very low likelihood and most likely linked to major climatic changes like glacial-interglacial cycles.

5 CONCLUSIONS

The structural analysis shows that gravitational slope deformation in the study area is strongly influenced by inherited structures, like pre-existing joint sets and the metamorphic foliation of the phyllites. Several cracks opened along those structures. With kinematic tests it could be confirmed that planar sliding and toppling of blocks is feasible along these discontinuities. Additionally, the analyzed blocks are clearly delimited by pre-existing joint sets. Large open fractures or surface depressions developed along the main joint sets or a combination of two of them.

The study area can be divided into different subareas, based on differential GNSS movement data and stage of development of the slope instabilities. Most advanced deformation is located at the blocks along the cliff in the northern part of the study area, N and W of Joasete (subarea A). Large open fractures characterize this area. Two clearly delimited blocks (blocks A1 and A2) at the front of the cliff have average movement rates around 10 mm/year. Subarea B between Joasete and Furekamben shows less advanced deformation with only minor open fractures, but large surface depressions. Subarea C is characterized by two large surface depressions only, but high rockfall activity at the frontal cliff.

Our work confirms that there are problems with slope instabilities at the area between Joasete, Furekamben and Ramnosi. While the northern region between Joasete and Furekamben has potential for medium-scale gravitational slope failures of blocks with volumes up to various 100,000 m³, the area around Ramnanosi will most likely only be affected by small-volume rockfall events.

ACKNOWLEDGEMENTS

The authors are grateful to A. Günther for support in the field and a master student from the Norwegian University of Science and Technology (Å. Tukkensæter), who was involved in the fieldwork of 2009.

REFERENCES

Blikra, L.H., Longva, O., Braathen, A., Anda, E., Dehls, J.F. & Stalsberg, K., 2006. Rock Slope Failures in Norwegian Fjord Areas: Examples, Spatial Distribution and Temporal Pattern. In S.G. Evans, G. Scarascia Mugnozza, A. Strom & R.L. Hermanns (eds), *Landslides from Massive Rock Slope Failure*; NATO Science Series, IV. Earth and Environmental Sciences, Vol 49. Springer, Dodrecht, Netherlands., pp. 475–496.

Bøe, R., Longva, O., Lepland, A., Blikra, L.H., Sønstegaard, E., Haflidason, H., Bryn, P. & Lien, R., 2004: Postglacial mass movements and their causes in fjords and lakes in western Norway. *Nor. J. Geol.*, Vol. 84 (1), pp. 35–55.

Böhme, M., Saintot, A., Henderson, I., Henriksen, H. & Hermanns, R.L., 2011. Rock-slope instabilities in Sogn & Fjordane County, Norway: a detailed structural and geomorphological analysis. *Geol.Soc.Spec. Pub.* 351, 97–111.

Braathen, A., Blikra, L.H., Berg, S.S. & Karlsen, F., 2004. Rock-slope failures in Norway; type, geometry, deformation mechanisms and stability. *Norw. J. Geol.* 84(1), 67–88.

Brideau, M. & Stead, D. 2009. The role of rear release surfaces, block size and lateral confinement on rock slope failure mechanisms. In: Anonymous *62nd Canadian Geotechnical Conference*, pp. 489–496.

Furseth, A., 2006. *Skredulykker i Norge.*, Oslo: Tun Forlag.

Hermanns, R.L., Bunkholt, H., Böhme, M., Fischer, L., Oppikofer, T. & Eiken, T. 2011b. Foreløpig fare—og risikovurdering av ustabile fjellparti ved Joasete-Furekamben-Ramnanosi, Aurland kommune. *NGU report 2011.025*. Trondheim, Norway: Geological Survey of Norway.

Hermanns, R.L., Fischer, L., Oppikofer, T., Böhme, M., Dehls, J.F. & Henriksen, H. 2011a. Mapping of unstable and potentially unstable slopes in Sogn og Fjordane (work report 2008–2010). *NGU report 2011.55.* Trondheim, Norway: Geological Survey of Norway.

Hoek, E. & Bray, J. 1981. *Rock Slope Engineering*, 3rd edn. London: E & FN Spon.

InnovMetric., 2011. PolyWorks: 3D scanner and 3D digitizer software from InnovMetric Software Inc. http://www.innovmetric.com/polyworks/3D-scanners/home.aspx?lang=en, accessed 10/20 2011.

Jaboyedoff, M., Metzger, R., Oppikofer, T., Couture, R., Derron, M.-H., Locat, J. & Turmel, D. 2007. New insight techniques to analyze rock-slope relief using DEM and 3D-imaging cloud points: COLTOP-3D software. In E. Eberhardt, D. Stead & T. Morrison (eds), *Rock mechanics: Meeting Society's challenges and demands. Proceedings of the 1st Canada—U.S. Rock Mechanics Symposium, Vancouver, Canada, 27–31 May 2007*: 61–68. London: Taylor & Francis.

NGI, 2009. Beregning av flodbølger for tre potensielle fjellskred fra Stampa. NGI report no. 20081693–1, *Norwegian Geotechnical Institute*, Oslo, Norway.

Oppikofer, T. 2009. Detection, analysis and monitoring of slope movements by high-resolution digital elevation models. *Institute of Geomatics and Analysis of Risk, University of Lausanne*, Lausanne, Switzerland.

Oppikofer, T., Bunkholt, H., Fischer, L., Saintot, A., Hermanns, R.L., Carrea, D., Longchamp, C., Derron, M.-H., Michoud, C. & Jaboyedoff, M. 2012, this volume. Investigation and monitoring of rock slope instabilities in Norway by terrestrial laser scanning. In E. Eberhardt (ed.), *Proceedings of the 11th International & 2nd North American Symposium on Landslides, Banff, Canada, 3–8 June 2012*. Balkema.

Appendix E

Paper V

Reference to the paper

Böhme, M. Oppikofer, T., Longva, O., Jaboyedoff, M., Hermanns, R.L., Derron, M.-H.: Analyses of past and present rock slope instabilities in a fjord valley: Implications for hazard estimations. Manuscript, submission planned to Earth and Planetary Science Letters.

Note on contributions

The candidate wrote this paper and carried out all analyses. Thierry Oppikofer provided the inventory of ancient rockslide scars and potential instabilities for Tafjord. He also calculated volumes and defined relative susceptibilities for all potential instabilities in the Storfjorden region. Oddvar Longva made the database of rockslide deposits on the fjord bottom available for analyses. The primary idea of a combined analysis of the three inventories is from Michel Jaboyedoff. Reginald L. Hermanns carried out the sampling for terrestrial cosmogenic nuclide dating and discussed the results with the candidate. All authors contributed to finalize the manuscript.

Analyses of past and present rock slope instabilities in a fjord valley: Implications for hazard estimations

M. Böhme[a,b,*], T. Oppikofer[a], O. Longva[a], M. Jaboyedoff[c], R.L. Hermanns[a], M.-H. Derron[c]

[a] *Geological Survey of Norway, Leiv Eirikssons vei 39, 7040 Trondheim, Norway*
[b] *Department of Geology and Mineral Resources Engineering, Norwegian University of Science and Technology, 7491 Trondheim, Norway*
[c] *Center for Research on Terrestrial Environment, University of Lausanne, 1015 Lausanne, Switzerland*

Abstract

For quantitative hazard estimations it is necessarry to define the magnitude-frequency distribution and a temporal model of the landslide frequency. This is often complicated for large rock slope failures due to the lack of significant numbers of large rock slope failures in inventories of a given homogeneous region or sparse information about the timing.

An inventory of in total 108 rock slope failure deposits within the fjords of the Storfjord region including a relative rockslide chronostratigraphy formed the basis for this study. Terrestrial cosmogenic nuclide dating of rockslide failure surfaces validated the previously obtained relative ages for two fjord deposits. However, a third dated failure surface exposes potential limitations of this inventory due to conflicting cosmogenic nuclide and relative ages. The temporal distribution of rock slope failures is characterized by a rapid decrease in number and size of rock slope failures directly after deglaciation followed by a constant frequency from 9,000 years BP for the entire Storfjord region and already from 10,000 years BP for the Tafjord region. The largest volumes have failed directly after deglaciation and volumes larger than 5×10^6 m^3 have not been registered within the last 9,000 years.

In addition, 17 ancient rockslide scars and 17 potential rock slope instabilities have been mapped at the northeastern flank of Tafjord, which is a branch of the Storfjord. Magnitude-frequency relations have been developed for fjord deposits, ancient scars and potential instabilities, resulting in very similar distributions over the entire volume range. All three inventories are representing rock slope failures within the same lithology, the same topography and are consequently underlying the same processes that lead to destabilisation and finally failure. The compilation of the three inventories is independent and based on different methodologies. The similarity of the magnitude-frequency distributions is thus verifying the different inventories. Hence the obtained magnitude-frequency relation can be assumed as correct for rock slope failures of the studied magnitudes larger than 0.01×10^6 m^3 for the northeastern flank of Tafjord and can thus be used to assess the rockslide hazard for the study area. Present day annual expectable frequencies for different volume classes have been assessed based on the obtained magnitude-frequency relation of the fjord deposits. For example, the annual frequency for rock slope failures of $V \geq 1 \times 10^6$ m^3 originating from the northeastern flank of Tafjord is 1/2,535 based on a lognormal distribution and 1/2,147 for a power-law model. Finally, semi quantitative hazard estimations have been obtained for potential unstable rock slopes within the Tafjord region based on a qualitative susceptibility ranking. The resulting annual probabilities are very low and range from 1/10,000 to 1/48,000. However, the uncertainties of the resulting regional as well as site specific hazard estimates are very high as indicated by large confidence intervals, making the results partially difficult to use for further risk assessments.

Keywords:
Magnitude-frequency relation, Temporal distribution, Paraglacial rock slope failures, Rockslide, Storfjord region, Tafjord, Norway

1. Introduction

Quantitative hazard estimations for large rock slope instabilities are difficult to obtain due the lack of significant numbers of large events in inventories of a given homogeneous region. Magnitude-frequency distributions for past rock slope failures have been analysed over several orders of magnitudes, but always with very limited numbers of large events (e.g., Brunetti et al., 2009; Dussauge-Peisser et al., 2002; Dussauge et al., 2003; Guzzetti et al., 2003; Hantz et al., 2003; Hungr et al., 1999; Malamud, 2004; Santana et al., 2012). This is mainly due to the fact that historical inventories cover a too short time period in order to capture low frequency-high magnitude events adequately. Pre-historic rock slope failures need to be included to cover the entire volume spectra of potential rock slope failures. However, for those, information about the timing is sparse.

Many mountainous regions that have been glaciated during the last glaciation, are characterized by large-scale post-glacial rock slope failures (e.g., Ballantyne and Stone, 2013; Korup et al., 2007). It is well accepted that rock slope failures decrease

*Corresponding author
Email addresses: martina.bohme@ngu.no (M. Böhme), thierry.oppikofer@ngu.no (T. Oppikofer), oddvar.longva@ngu.no (O. Longva), michel.jaboyedoff@unil.ch (M. Jaboyedoff), reginald.hermanns@ngu.no (R.L. Hermanns), derron@unil.ch (M.-H. Derron)

in number and size with the time elapsed since deglaciation (e.g., Abele, 1974; Ballantyne, 2002a,b; Cruden and Hu, 1993; Hermanns and Longva, 2012; McColl, 2012), but the exact temporal pattern has only been constructed for few inventories and is still debated (e.g., Ballantyne and Stone, 2013; Cruden and Hu, 1993). However, in order to access the present day landslide hazard of a certain region, it is necessary to develop a temporal model of the landslide frequency and magnitude distribution, since these vary non-linearly with time.

During the last century Norway has suffered several natural disasters with large losses of life due to rockslides and related tsunamis (Furseth, 2006). Those are the cause that special attention is payed to the Åknes rockslide in western Norway (Figure 1), which is assumed to be the most hazardous rockslide in Norway at present (Ganerød et al., 2008). The Åknes rockslide is a large rockslide with an estimated maximum volume of $30 - 40 \times 10^6$ m^3, showing velocities of $3 - 10$ cm per year. Its failure might cause a catastrophic tsunami in the fjord endangering several communities. A large international project focusing on the investigation, monitoring, and early warning of the Åknes rockslide and other large unstable rock slopes in the inner Storfjord region started in 2005 (Blikra, 2008).This project resulted in a large amount of data as an outcome of numerous site specific investigations (e.g., Ganerød et al., 2008; Eidsvig et al., 2011; Jaboyedoff et al., 2011; Lacasse, 2008; Oppikofer et al., 2009). In addition, more regional investigations considering the entire fjord system have been undertaken within the Åknes/Tafjord project. These comprise systematic studies of post-glacial rock slope failures including their deposits on the fjord bottom (Longva et al., 2009) and presently potential unstable rock slopes (Henderson and Saintot, 2011; Saintot et al., 2011). Oppikofer (2009) analysed ancient rockslide scars and potential instabilities in detail for a smaller part of the study area, namely the northeastern flank of Tafjord between the villages Fjøra and Tafjord (Figure 2).

These regional investigations resulted in a unique dataset with three independent types of inventories for the Tafjord including fjord deposits, ancient rockslide scars and potential instabilities. The fjord deposits cover the entire post-glacial period and yield thus a complete inventory of post-glacial rock slope failures within the entire fjord system including information on relative ages and volumes. Analysed ancient scars are the equivalents of the fjord deposits on the slopes, whereas the detection and the volume calculations depend on completely different methods. Both, fjord deposits and scars are representing and characterizing the past rock slope failure activity, whereas the scars are missing temporal information. The potential instabilities instead are representing the future thread and are aimed to be quantified with respect to potential hazard. Detailed analysis of the temporal distribution of the fjord deposits allows developing a model for expectable present rock slope failure frequency. Magnitude-frequency relations of the three inventories can be analysed and a possible link between them may help to characterize and quantify hazard within the Tafjord region.

Furthermore, terrestrial cosmogenic nuclide (TCN) dating was used in order to validate the relative ages of three fjord deposits. Since the ages of the fjord deposits are only relative ages and principally based on seismostratigraphy, there was a demand for double-checking those with absolute dates. For this, three failure surfaces, which are supposed to form the source zone for the corresponding deposits on the fjord bottom, were dated with TCN. Hermanns et al. (2009) confirmed the age of one mapped fjord deposit at the end of Tafjord by dating the equivalent rock avalanche deposits on land with TCN. Failure surfaces of pre-historic failures have been previously dated by Hermanns et al. (2004) and Ivy-Ochs et al. (2009), demonstrating the applicability of this method.

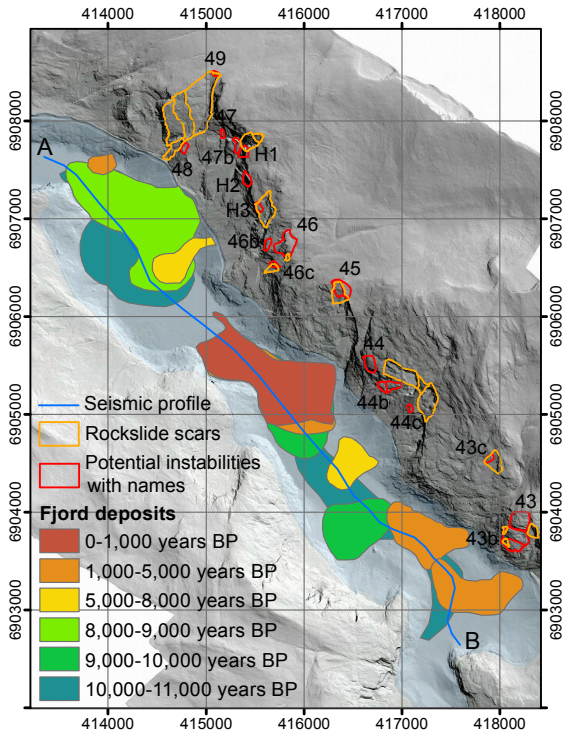

Figure 2: Map of the Tafjord region showing all three inventories for the northeastern flank of Tafjord. Line A-B marks the seismic profile illustrated in Figure 3. Fjord deposits are adapted from Longva et al. (2009) and rockslide scars as well as potential instabilities from Oppikofer (2009).

2. Study area and inventories

2.1. Regional setting of the study area

The study area is located in western Norway within the inner Storfjord region, comprising Sunnylvs Fjord, Geiranger Fjord, Norddals Fjord, Tafjord and the southern part of Storfjord (Figure 1).

Historical data and geological studies display a high concentration of both post-glacial gravitational slope failures and potential instabilities in the Norwegian county of Møre & Romsdal (Blikra et al., 2006; Henderson and Saintot, 2011; Saintot

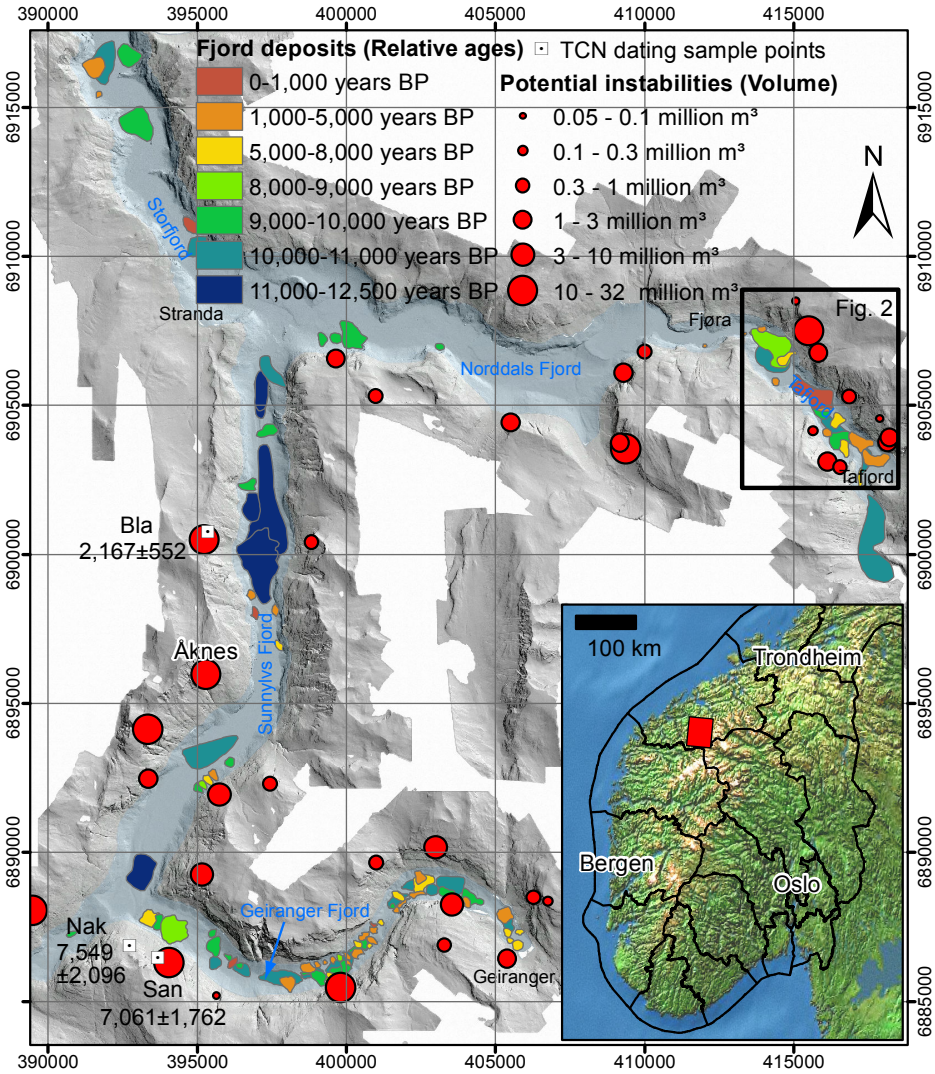

Figure 1: Overview of the study area. The inset shows the location of the study area in southern Norway. Relative deposit ages are given in calibrated ^{14}C years BP and average TCN ages in years BP with 2σ uncertainty levels. TCN sample locations: Nak - Nakkeneset, San - Nokkenibba, Bla - Blåhornet.

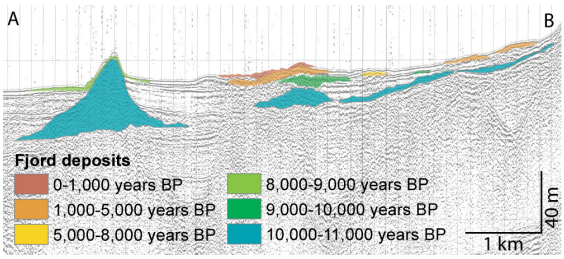

Figure 3: Example of a seismic reflection profile with interpreted deposits from Tafjord. See Figure 2 for profile location.

et al., 2011). Several catastrophic failures causing tsunamis in the inner fjord areas of western Norway resulted in large loss of life in the last century (Furseth, 2006).

The bedrock mainly consisting of granodioritic-dioritic gneisses of the Precambrian basement overlain by augen gneiss and minor mica schist of the Caledonian thrust sheets in the eastern part. The rocks of the study area have undergone intense reworking by a general NW-SE oriented crustal shortening during the Caledonian Orogeny (Roberts and Gee, 1985). In addition, a significant amount of brittle tectonic events affected the bedrock of the study area, like the Permo-Triassic and Jurassic rifting phases. This tectonic history resulted in a high density of ductile, semi-ductile and brittle structures within the study area.

The topography is strongly influenced by the Quaternary glaciations. Long U-shaped valleys and deep fjords with steep slopes are dominating landforms. This steep terrain in combination with heavily fractured exposed bedrock indicates that this area is susceptible to rock slope failures. A clear structural control of rock slope failures as well as unstable rock slopes is visible in the field (Henderson and Saintot, 2011; Oppikofer, 2009; Oppikofer et al., 2011; Saintot et al., 2011). Deglaciation has in addition resulted in a sudden unloading of the glacially steepened slopes. This, in addition to post-glacial tectonic activity, including isostatic rebound and large magnitude earthquakes (Bøe et al., 2004; Fjeldskaar et al., 2000; Olesen et al., 2004), may have contributed to the high concentration of rock slope failures in the study area.

Deglaciation took place in the period 13,000 to 11,000 calibrated ^{14}C years BP (Aarseth et al., 1997; Fareth, 1987; Larsen et al., 1991). However, the innermost fjords where not completely ice-free, when the glaciers re-advanced during the Younger Dryas at 11,000-10,000 calibrated ^{14}C years BP (Aarseth et al., 1997). The retreat from the Younger Dryas was rapid and the fjords were probably ice-free around 10,000 calibrated ^{14}C years BP (Longva et al., 2009).

2.2. Rockslide deposits on the fjord bottom

Longva et al. (2009) mapped rockslide and rock avalanche deposits in the inner parts of Storfjord and its tributary fjords based on a complete swath bathymetry and high-resolution reflection-seismic profiles (Figure 1, Figure 3). The inventory contains a total of 108 rockslide and rock avalanche deposits including the surficial area and volume estimations for each deposit. A relative slide chronostratigraphy has been established based on seismostratigraphic position, one dated core in Tafjord (Bøe et al., 2004), regional deglaciation history and freshness of surface morphology (Longva et al., 2009). Deposit ages are given in calibrated ^{14}C years BP throughout this publication.

2.2.1. Limitations

Relative ages are just given as age classes with a variable width, ranging from 1,000 to 4,000 years. This leaves a large uncertainty about the actual age of each deposit, especially for classes with a large width. Volume calculations are rough estimations based on surficial area, average thickness of the deposits extracted from the seismic lines and expert judgement. The smallest registered fjord deposit is 20, 000 m^3 and may thus be seen as the smallest detectable size. However, this detection limit is most likely also a function of the age of the deposits. Larger failures leave larger traces, which will be visible over a longer time period. Smaller events might only be detected from the last few thousand years and the observation period will therefore be shorter, leading to undersampling small deposits for older time periods. In addition, small deposits may not be detectable, when they are covered with considerable larger ones. Deposits in the inner fjords, namely Tafjord and Geiranger Fjord, are assumed to have been removed during glacial re-advance. Hence the inventory can only be assumed to be complete for deposits younger than the maximum re-advance stage at 10,500 years BP (Fareth, 1987). In many cases it is difficult to distinguish between rockfall and smaller rockslide deposits. Furthermore, several small single deposits may be registered as one large or one large as several small, the latter being however less likely.

2.3. Rockslide scars in the Tafjord region

Oppikofer (2009) identified 17 scars of ancient rockslides at the northeastern flank of Tafjord from field observations and analysed them with the help of a high-resolution digital elevation model (HR-DEM) and aerial photographs (Figure 2). The ante-rockslide topography has been reconstructed in 3D based on the continuity of the present topography besides the scar using the PolyWorks software (InnovMetric, 2011). A detailed description of the method can be found in Oppikofer (2009). Volumes of ancient rockslides have been determined by calculating the difference in between the ante-rockslide and present topography. Based on morphologic observations some scars have been divided into several smaller rockslide scars as a consequence of multiple rock slope failures.

2.3.1. Limitations

In many cases it is uncertain whether an identified scar resulted from a single or several events. One particular scar area may have been the source for multiple rock slope failures (Hermanns et al., 2006). Subsequent failures may remove scars from previous failures, which are then not any longer observable.

The smallest detected ancient rockslide has an estimated volume of $29,000\,m^3$, but the inventory can be assumed to be complete for ancient rockslides larger than $50,000\,m^3$. In addition, there exists an uncertainty in the constructed ante-rockslide topography. This has been tried to eliminate by testing different methods for the reconstruction (Oppikofer, 2009). Furthermore, it is not completely certain if all scars are post-glacial.

2.4. Potential instabilities in the Tafjord region

Oppikofer (2009) identified 17 potential rock slope instabilities at the northeastern flank of Tafjord by field surveys and analysis of the HR-DEM as well as aerial photographs (Figure 2). Bounding structures were determined by fitting planes to the morphological limits of the instability on the airborne laser scanning point cloud using the PolyWorks software (InnovMetric, 2011). A detailed description of the method can be found in Oppikofer (2009). Volume calculations were then possible based on these limits. Different scenarios have been defined for some potential instabilities. This made it necessary to use two different datasets for the following analyses, one containing the largest scenarios and one the smallest, in order to illustrate the possible range of volumes.

2.4.1. Limitations

The smallest registered potential instability is $43,000\,m^3$, since potential instabilities $< 10,000\,m^3$ have not been considered. Especially for larger instabilities the lower limits are very uncertain and volume estimations might be imprecise. Furthermore, it cannot be assured whether each instability may fail as a single event or several smaller events.

2.5. Potential instabilities in the Storfjord region

Henderson et al. (2006), Henderson and Saintot (2011) and Saintot et al. (2011) identified 36 potential unstable rock slopes in the Storfjord region by systematic aerial photograph analyses and field surveys (Figure 1). Investigations on these sites include geomorphological, engineering geological and structural field mapping as well as periodic monitoring on 8 potential unstable rock slopes using differential Global Navigation Satellite Systems and terrestrial laser scanning. As for the instabilities in Tafjord, different scenarios have been defined for some potential instabilities mainly based on geomorphological observations. Volumes of each unstable rock slope were assessed by Oppikofer et al. (submitted) with the sloping local base level technique (Derron et al., 2005; Jaboyedoff and Derron, 2005). Oppikofer et al. (submitted) defined relative susceptibilities for all potential instabilities in the Storfjord region using the hazard and risk classification system for unstable rock slopes in Norway (Hermanns et al., 2013). The susceptibility ranking is obtained by considering a series of geomorphological, engineering geological and structural criteria, as well as signs of activity. The outcome of the classification system is a score ranging from 0 (very low susceptibility) to 12 (very high susceptibility). Uncertainties on the susceptibility score can be evaluated owing to the use of probabilities for each of the criteria (Hermanns et al., 2013).

2.5.1. Limitations

Volumes are rough estimations based on the aerial surface of the unstable rock slope and an assumed basal failure surface. This lower limits are in most cases very uncertain, since no data in depth exist. Furthermore, even if a few different scenarios have been defined for some sites, several sites may fail in even more and smaller events, than the defined scenarios which are visible on the present topography.

3. Methods

3.1. Terrestrial cosmogenic nuclide dating

It was aimed to sample failure surfaces of different ages and at least one failure surface within each tributary fjord arm, except Tafjord (Figure 1). Deposit ages within Tafjord are assumed to be well constrained due to a dated sediment core (Bøe et al., 2004) and a dated rock avalanche on land (Hermanns et al., 2009). In total three failure surfaces above definite fjord deposits, that showed a good preservation of the failure surface and that were accessible for sampling have been selected (Figure 4). In total 9 samples were collected, three for each failure surface. The samples were collected following the guidelines recommended by Gosse and Phillips (2001), recording the rationale for sample selection, description of sampled failure surface, geologic description of sample, location, orientation, sample thickness, and shielding geometry. The samples were prepared and concentrated at the Dalhousie University Cosmogenic Nuclide Exposure Dating Facility in Halifax, Canada. Total Be and ^{10}Be were determined at the PRIME accelerator mass spectrometry facility at Purdue University in Indiana, USA. The derived ages were calculated using the program CRONUS ^{10}Be exposure age calculator (Balco et al., 2008) and therefore were calculated using global production rates and scaling models by Lal (1991) and Stone (2000). A more comprehensive review of TCN dating is provided by Gosse and Phillips (2001).

3.2. Temporal analysis of fjord deposits

The temporal distribution of number and volumes of the fjord deposits has been analysed graphically in order to define the expectable present day frequency and magnitude of rock slope failures in the study area. Ballantyne (2002a) defined a "geological norm" by analysing the paraglacial landscape response. Different models about how the frequency of rock slope failures may change following deglaciation have been proposed in literature, namely exhaustion, steady state decline, rapid response and constant frequency model (Ballantyne, 2002a,b; Ballantyne and Stone, 2013; Cruden and Hu, 1993). In contrast to this, Blikra et al. (2006) argue, based on 15 radiocarbon dated or indirectly dated rock avalanche deposits, that rock slope failures are spread over the entire post-glacial period, with higher frequencies during the more recent half of the Holocene in western Norway. In order to rule out different frequency models and to assess the hazard for large rock slope failures within the Storfjord and Tafjord region a frequency, which is relevant for the present situation has to be determined.

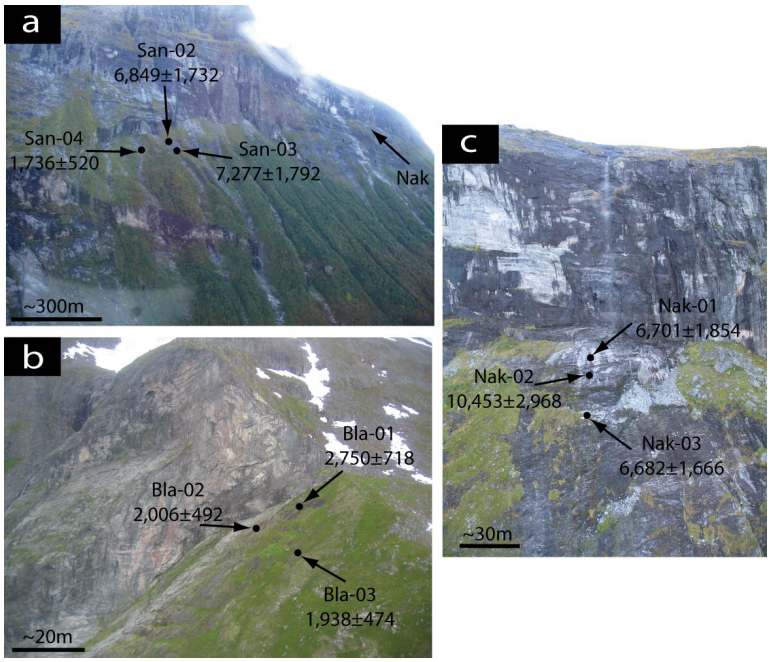

Figure 4: Sampled failure surfaces in the Storfjord region. a) Failure surface and sample loacations at Nokkenibba, b) failure surface and sample loacations at Blåhornet and c) failure surface and sample loacations at Nakkeneset. Ages are given in years BP with 2σ uncertainty levels.

3.3. Volume-frequency analyses

Magnitude-frequency relations of rock slope failures have been studied by several authors (e.g., Brunetti et al., 2009; Dussauge-Peisser et al., 2002; Dussauge et al., 2003; Guzzetti et al., 2003; Hantz et al., 2003; Hungr et al., 1999; Malamud, 2004; Santana et al., 2012). A simple inverse power-law model is most frequently fitted to the magnitude-cumulated frequency distribution of rock slope failures with a typical exponent b in the range of 0.4 to 0.7 (see Santana et al., 2012, for an overview):

$$f(V \geq x) = ax^{-b} \tag{1}$$

where $f(V \geq x)$ is the cumulated frequency of rockslides exceeding a given volume x and a is a constant.

However, in most of these studies, the power-law fits only the tails of the magnitude-frequency distributions above different volume thresholds. Especially in magnitude-frequency analyses of landslides in general, a roll-over effect with positive power-law exponents for small volumes has been observed. In order to fit the entire range of landslide magnitudes, Stark and Hovius (2001) propose a double Pareto distribution and Malamud (2004) an inverse Gamma distribution. Other distributions as for example Lognormal (e.g., ten Brink et al., 2009; Chaytor et al., 2009; Haas et al., 2012) and Weibull distributions (e.g., Crosta, 2007) have been applied to describe magnitude-frequency relations.

Volume-frequency relations have been analysed for all three different datasets from Tafjord. In order to be able to compare the different datasets, cumulative frequencies have been normalized by the number of events in each inventory. Since a volume increase of 25% can be expected for the deposits with respect to the unstable rock mass on the slope (Hungr and Evans, 2004), the volumes of the fjord deposits have been reduced by 20% for the magnitude-frequency analysis, in order to obtain comparable volumes to the ancient scars and potential instabilities. Ancient rockslide scars and fjord deposits are expected to show a similar volume-frequency distribution, since they represent the same rock slope failures. However, since not necessarily the same volumes are measured, there may be differences in the volume-frequency distributions.

4. Results and discussion

4.1. Terrestrial cosmogenic nuclide dating

Results from TCN dating are presented in Table 1. The average ages for the two failure surfaces within Geiranger Fjord, $7,061 \pm 1,762$ years for Nokkenibba (San-02 and 03) and $7,549 \pm 2,096$ years for Nakkeneset (Nak-01, 02 and 03), correspond well with the previously determined age intervals of the fjord deposit that suggest ages of 8,000-9,000 and 5,000-8,000 years BP, respectively. Sample San-04, that was also sampled

Table 1: Ages obtained by ^{10}Be cosmogenic nuclide dating from samples of failure surfaces within the Storfjord area. Sample height is measured by altimeter with 1 m resolution. Sample locations are shown in Figure 1 and sampled surfaces are displayed in Figure 4. Average ages are calculated as a weighted mean based on uncertainties. Sample San-04 is not considered for the average since it is interpreted to belong to a different sliding surface (Section 4.1). Relative ages of corresponding fjord deposits are based on Longva et al. (2009). Nak - Nakkeneset, San - Nokkenibba, Bla - Blåhornet.

	Nak-01	Nak-02	Nak-03	San-02	San-03	San-04	Bla-01	Bla-02	Bla-03
Sample height [m]	633	624	607	455	448	434	919	917	890
Age [yr]	6,701	10,453	6,682	6,849	7,277	1,736	2,750	2,006	1,938
2σ uncertainty [yr]	1,854	2,968	1,666	1,732	1,792	520	718	492	474
Average age [yr]	Nak: $7,549 \pm 2,096$			San: $7,061 \pm 1,762$			Bla: $2,167 \pm 552$		
Relative age of fjord deposit [cal. ^{14}C yr]	5,000 - 8,000	5,000 - 8,000	5,000 - 8,000	8,000 - 9,000	8,000 - 9,000	8,000 - 9,000	11,000 - 12,500	11,000 - 12,500	11,000 - 12,500

at the assumed failure surface for the corresponding fjord deposit, exhibits a much younger age. However, a detailed morphological analysis of the HR-DEM indicates that this sampling location may belong to a different failure surface than San-02 and San-03 (Figure 4). The fjord deposit inventory may thus be incomplete not only for old, small rock slope failures, but also for relatively young, small ones. The sampled failure surface within Sunnylvs Fjord below the mountain Blåhornet yields an average age of $2,167 \pm 552$ years. This is contradictory to the age of the fjord deposit of 11,000-12,500 years BP. The age of this fjord deposit is relatively good constrained due to the vicinity of a terminal moraine. A younger, smaller slide may have occurred on the sampled surface. A minimum volume of $9,000\,\mathrm{m}^3$ can be assumed based on a morphological coherent surface including the sampled points and a minimum thickness of 1.5 m. At a depth of 1.5 m the production rate of ^{10}Be is only $1/8$ and has thus a limited influence on the obtained age. This minimum volume is far below the detectable deposit size. In addition, a relative small deposit on top of the large old one is not detectable due to the morphological prominence of the larger deposit.

4.2. Temporal analysis of fjord deposits

Figure 5 displays how the frequency of rock slope failures varied since the last deglaciation. There are few registered fjord deposits for the time period 11,000-12,5000 years BP (Figure 5a) and the complete lack of deposits for this time period in the Tafjord (Figure 5b), due to the assumption that all deposits in the innermost fjords are younger than the glacial re-advance during the Younger Dryas. Tafjord is one of the innermost fjords where the fjord deposits are assumed to have been removed during glacial re-advance. A large frequency directly after deglaciation can be observed, continued by smaller frequencies. The different temporal models mentioned in section 3.2 were tested by fitting curves to the cumulated number of slope failures (from youngest to oldest) over time, where the exponential curve represents the exhaustion model, the quadratic curve the steady state decline model and the linear curve the constant frequency model (Figure 5c and d). The linear curve is just fitted to data points younger than 9,000 years BP and thus excluding data points representing the rapid response directly after deglaciation. For Tafjord the rapid response may be shorter, only until 10,000 years BP (Figure 5b). However, due to the large age intervals and a small number of data points, it is difficult to obtain a robust model. All models give similar quality with R^2-values between 0.89 and 0.95. A steady state decline model, however, yields the best fit for both the entire study area and the Tafjord subset. All models, particularly the exhaustion model, overestimate the number of events for the youngest time period 0-1,000 years BP, which is most likely the most representative for the present situation. The exhaustion model can be excluded, since the principle assumption for this model, that each slope raptures only once (Cruden and Hu, 1993), is violated. Multiple rock slope failures have occurred at several localities in Norway also in Tafjord (Hermanns et al., 2006). Finally, a constant frequency model following a rapid response as suggested by Ballantyne and Stone (2013) has been implemented in this study, in order to have a sufficient number of fjord deposits to be able to define magnitude-frequency relations. This model is also in agreement with the volume distribution presented in the next paragraph. The constant yearly frequencies of 0.0063 ± 0.0013 for the entire Storfjord region and 0.0011 ± 0.0002 for the northeastern flank of Tafjord form the geological norm.

Plotting the distribution of failed volumes for each time period presents, as expected, the largest total failed volumes directly after deglaciation (Figure 6a and b). From 9,000 years BP a geological norm can be assumed for the entire study area and already from 10,000 years BP for the Tafjord region. The geological norm gives a total failed volume of $4.4 \pm 0.5 \times 10^6\,\mathrm{m}^3$ per millennia for the entire Storfjord region and $1.9 \pm 0.2 \times 10^6\,\mathrm{m}^3$ per millennia for the northeastern flank of Tafjord, representing the presently expectable total failure volumes per millennia. It has to be emphasized that no single rock slope failure $> 5 \times 10^6\,\mathrm{m}^3$ has been registered during the last 10,000 years in the entire studied fjord system. The denudation rate due to rock slope failures from the northeastern flank of Tafjord for the last 10,000 years BP is 0.07 mm/y, compared to 0.94 mm/y for the time period directly after deglaciation (Figure 6b). The first value is comparable with the rockwall retreat rates of 0.04 to 0.11 determined by Laute and Beylich (2012) for the time after the Little Ice Age in the Erdalen and Bødalen valleys in western Norway.

Plotting the magnitude-frequency distribution for the geolog-

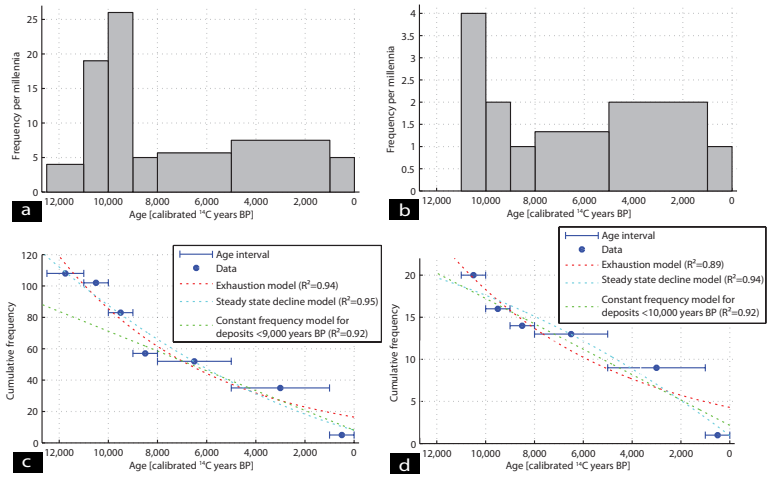

Figure 5: Temporal distribution of all fjord deposits (a and c) and deposits originating from the northeastern flank of Tafjord only (b and d). Different models of time dependent behaviour of the number of rock slope failures after deglaciation have been fitted to the cumulative frequency (c and d). All models have a similar quality of fit, but a steady state decline model shows the best fit for both data sets. The frequency for the youngest time period is overestimated by all models. However, due to the large age intervals and a small number of datapoints, there remains a significant element of speculation in those models.

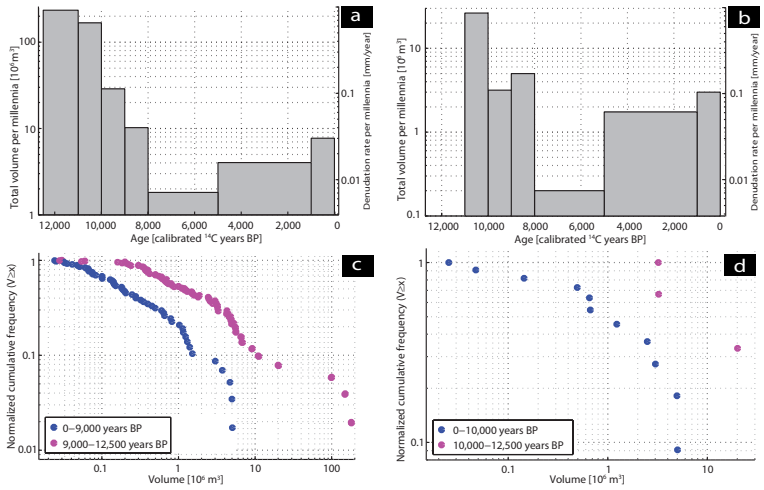

Figure 6: Volume distribution and denudation rate over time for all fjord deposits (a) and fjord deposits originating from the northeastern flank of Tafjord (b). The largest total volumes failed directly after deglaciation. The geological norm for the totally failed volumes is approached at 9,000 years BP for all deposits and at 10,000 years BP for the Tafjord deposits. Magnitude-frequency distributions of all fjord deposits (c) and Tafjord deposits (d) divided into rapid response following deglaciation and present geological norm.

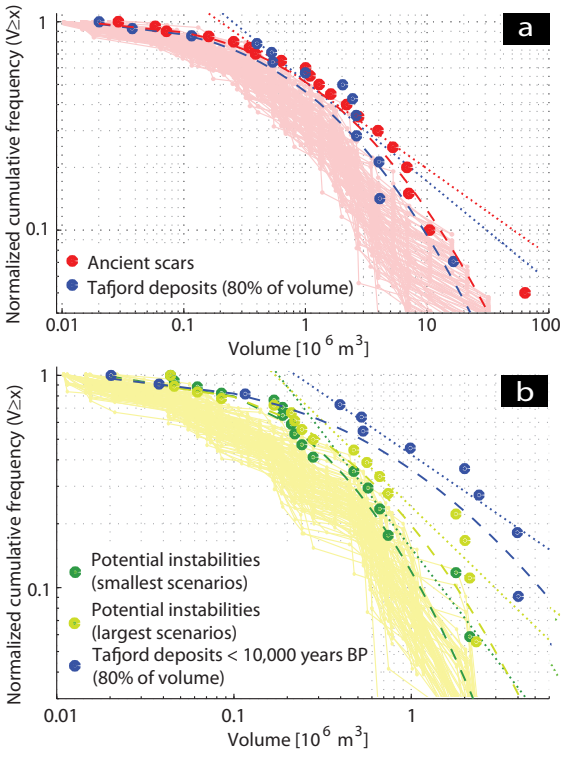

Figure 7: Comparison of volume-frequency distributions of (a) ancient rockslide scars and fjord deposits and (b) potential instabilities and fjord deposits younger than 10,000 years. Fitted lognormal distributions are displayed with dashed lines and power-law models with dotted lines. Power-law tails are fitted to $V \geq 0.3 \times 10^6$ m^3. a) Both distributions are almost identical, with slopes increasing continuously towards larger volumes. 100 simulations with segmented volumes of the ancient rockslide scars into 1-4 parts are displayed in pink. b) The distribution of potential instabilities differ from the distribution of fjord deposits younger than 10,000 years BP for volumes $> 0.2 \times 10^6$ m^3. 100 simulations with segmented volumes of the largest scenarios of the potential instabilities into 1-4 parts are displayed in yellow. The smallest scenarios plot within the limits of these simulations.

ical norm and rapid response separately indicates a shift of the latter towards larger volumes (Figure 6c and d). This may confirm the general decrease of failure magnitude after the rapid response following deglaciation. However, this effect could partly also be explained by undersampling of small events for the oldest time periods.

4.3. Volume-frequency analyses

All three datasets of the Tafjord region present similar volume-frequency relations with similar slopes increasing towards larger volumes on a log-log plot (Figure 7). This continuously increasing slope is, however, contradictory to usually fitted power-law models and may instead be closer to a lognormal distribution.

Kolmogorov-Smirnov tests indicate that all three datasets are consistent with a lognormal distribution (Table 2). In addition, power-law models have been fitted for volumes $\geq 0.3 \times 10^6$ m^3 (Table 2). However, it is not definite where to set the lower bound of the power law. The resulting power-law exponents range from 0.4 to 1.1. Power law exponents for Tafjord deposits and ancient scars are within the range of reported values of 0.4 to 0.7 (Santana et al., 2012), but the exponents for the potential instabilities, especially the smallest scenarios, are larger.

As described in Section 2.3.1 registered single scars may have been the source for several smaller rock slope failures. Equally, it cannot be assured whether a potential instability will fail in one single or several smaller events (Section 2.4.1). In order to test this, 100 new datasets were produced by segmenting the registered volumes of ancient rockslides and the largest scenarios of the potential instabilities randomly into 1 to 4 parts. The resulting magnitude-frequency plots display that the original dataset represents an upper limit with all simulations plotting below (Figure 7). The smallest scenarios of the potential instabilities plot within the limits of this simulation (Figure 7b).

The magnitude-frequency distribution of ancient scars and fjord deposits are almost identical (Figure 7a). However, the magnitude-frequency distributions of potential instabilities differ from the distribution of fjord deposits younger than 10,000 years BP for volumes $> 0.2 \times 10^6$ m^3 (Figure 7b; Table 2).

Different factors that may influence the power-law exponent have been discussed, proposing mechanical properties of the rock mass (Dussauge et al., 2003), degree of fracturing of the rock mass (Hungr et al., 1999; Katz et al., 2011) and topography (Dussauge et al., 2003; Frattini and Crosta, 2013) as possible influencing factors. However, the geomechanical, geomorphological and geographic setting are the same for all three inventories in Tafjord and the underlying processes can be assumed identical. Thus, consistency in the distributions may serve as a measure of correctness of the proportions of different volumes within each inventory. Based on the equal distributions of ancient scars and fjord deposits, those two datasets can thus be assumed as correct.

4.4. Implications for hazard

Frequencies of past failures can be used to assess the hazard for a certain region for certain volume classes given that the inventory is complete (Guthrie and Evans, 2005) and under the assumption that the environmental factors that caused past rockslides remain constant in future. The comparison of the volume-frequency distributions of ancient scars and fjord deposits has been used to verify the fjord deposit inventory. This allows using the fjord deposits to infer on the future hazard that is posed by potential instabilities in the study area. Consequently, the frequency per time period for a certain volume class has been assessed based on the frequency of fjord deposits that are younger than 10,000 years BP for the northeastern flank of Tafjord (Table 3):

$$f(V \geq x, T) = f(V \geq x) \times f(T) \quad (2)$$

where $f(V \geq x)$ is the normalized cumulative frequency of landslide size, obtained from the magnitude-frequency relation and $f(T)$ is the frequency of landslide occurrence for

Table 2: Summary of coefficients (with 95% confidence bounds) for fitted lognormal distributions and power-law tails for fjord deposits, ancient scars and potential instabilities within the Tafjord region (Figure 7). Kolmogorov-Smirnov (KS) test statistics indicate the acceptance of the lognormal distribution at a significance level of 5%. Power-law tails have been fitted for volumes $\geq 0.3 \times 10^6$ m^3.

	Tafjord deposits (80% of volume)	Ancient scars	Tafjord deposits <10,000 years BP (80% of volume)	Potential instabilities (smallest scenarios)	Potential instabilities (largest scenarios)
Lognormal distribution: $f(V \geq x) = 1 - \frac{1}{\sigma\sqrt{2\Pi}} \int_0^x \frac{e^{\frac{-(ln(t)-\mu)^2}{2\sigma^2}}}{t} dt$					
μ	-0.18 (-1.27, 0.91)	0.07 (-0.84, 0.98)	-0.65 (-1.87, 0.56)	-1.35 (-1.94, -0.76)	-1.18 (-1.87, -0.49)
σ	1.89 (1.37, 3.04)	1.94 (1.48, 2.84)	1.81 (1.26, 3.17)	1.15 (0.85, 1.75)	1.38 (1.04, 2.07)
p (KS)	0.70	1.00	0.87	0.93	0.93
Power-law tails for $V \geq 0.3 \times 10^6$ m^3: $f(V \geq x) = ax^{-b}$					
a	0.52 (0.46, 0.58)	0.51 (0.48, 0.55)	0.42 (0.36, 0.48)	0.15 (0.11, 0.20)	0.24 (0.20, 0.29)
b	0.48 (0.34, 0.62)	0.42 (0.34, 0.49)	0.57 (0.39, 0.76)	1.09 (0.61, 1.57)	0.81 (0.49, 1.12)
R^2	0.90	0.95	0.94	0.95	0.91

time period T (in years) obtained from the geological norm. The geological norm reflects the presently expectable frequency and volume distribution of rock slope failures. For the northeastern flank of Tafjord the yearly expectable frequency is 0.0011 ± 0.0002. This results in an annual frequency for an event $\geq 1 \times 10^6$ m^3 from the northeastern flank of Tafjord $f(V \geq 1 \times 10^6, 1) = 3.94 \times 10^{-4}$ based on lognormal distribution and $f(V \geq 1 \times 10^6, 1) = 4.66 \times 10^{-4}$ for a power-law model, corresponding to a recurrence rate of 2,535 and 2,147 years respectively (see Table 3 for 95% confidence bounds). As it can be observed from Table 3 the 95% confidence intervals increase with increasing volumes, reaching very large interval sizes for the largest volumes especially for the calculations based on a lognormal distribution.

It is evident that the resulting hazard estimates are only valid within the Tafjord region. However, the question arises, if the fjord deposit inventory also can be assumed as correct for the entire Storfjord region, since the same technique has been used over the entire fjord system. Assuming that the entire fjord deposit inventory is complete, it is possible to estimate the hazard per time period for a certain volume class based on the frequency of fjord deposits that are younger than 9,000 years BP for the entire Storfjord region (Table 3, Figure 8). The resulting annual frequency for an event $\geq 1 \times 10^6$ m^3 in the entire Storfjord region is 7.92×10^{-4} based on a lognormal distribution and 9.99×10^{-4} for a power-law model, corresponding to a recurrence rate of 1,263 and 1,001 years respectively (see Table 3 for 95% confidence bounds of annual frequency and recurrence rate). As for the Tafjord region, the 95% confidence intervals are very large, especially for large volumes. However, owing to the larger sample size for the calculations covering entire Storfjord, the uncertainties are significantly lower than those for Tafjord. An even larger sample size would be necessarry in order to further decrease the uncertainties in the results. This is, however, not possible for the considered study area, since the inventory is assumed to be already complete. Thus, the obtained results are displaying the best possible hazard estimations for the Storfjord region.

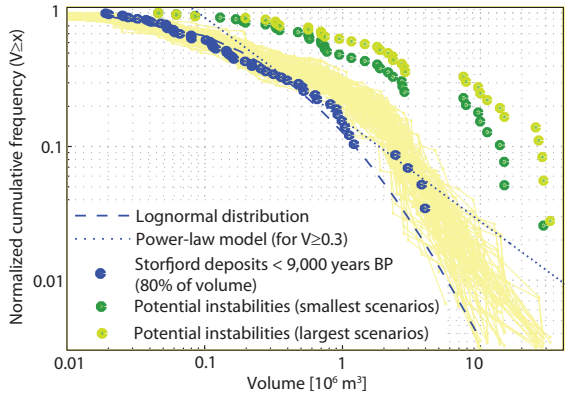

Figure 8: Fitted lognormal distribution and power-law model for Storfjord deposits younger than 9,000 years BP. In addition, the magnitude-frequency distributions of instabilities of the entire Storfjord region are displayed. Those differ significantly from the distribution of the fjord deposits. A segmentation of the registered volumes for the largest scenarios of the potential instabilities randomly into 1 to 15 parts (displayed in yellow) is necessary in order to obtain a distribution that is similar to that of the fjord deposits.

In order to assign hazard values to single potential instabilities further factors have to be considered, since different potential instabilities with the same size do not necessarily pose the same hazard, depending on site specific situations. A detailed study of an inventory of potential instabilities is necessary in order to estimate each landslides susceptibility S. However, quantitative methods to define the susceptibility for large slope failures are lacking in literature. Hantz et al. (2003) propose a method that is based on grouping of instabilities with respect to a more or less subjective geomechanical approach resulting in relative failure probabilities. Those are finally combined with the expected frequency from the magnitude-frequency analysis in order to obtain hazard values. In addition, Hermanns et al. (2013) propose a qualitative hazard classification for Norway.

Table 3: Estimated annual frequencies and recurrence rates (with 95% confidence bounds) for each volume class based on the fitted lognormal distribution and power-law model with $f(T = 1) = 0.0011 \pm 0.0002$ for the northeastern flank of Tafjord (Figure 7, Table 2) and $f(T = 1) = 0.0063 \pm 0.0013$ for the Storfjord region (Figure 8).

		Lognormal distribution			Power-law model		
Volume x	No. of deposits	Frequency $f(V \geq x)$	Annual frequency $f(V \geq x, 1)$	Recurrence rate in years	Frequency $f(V \geq x)$	Annual frequency $f(V \geq x, 1)$	Recurrence rate in years
				Tafjord			
0.01	11	0.986 (0.806, 1.000)	$1.08(0.73, 1.30) \times 10^{-3}$	922 (1,378, 769)	-	-	-
0.1	9	0.819 (0.555, 0.988)	$9.01(4.99, 12.85) \times 10^{-4}$	1,110 (2,004, 778)	-	-	-
0.3	8	0.620 (0.299, 0.919)	$6.82(2.7, 11.94) \times 10^{-4}$	1,467 (3,710, 837)	0.845 (0.583, 1.202)	$9.30(5.25, 15.62) \times 10^{-4}$	1,075 (1,905, 640)
1	5	0.359 (0.069, 0.671)	$3.94(0.63, 8.73) \times 10^{-4}$	2,535 (15,996, 1,146)	0.423 (0.364, 0.483)	$4.66(3.28, 6.28) \times 10^{-4}$	2,147 (3,052, 1,593)
3	3	0.166 (0.009, 0.432)	$1.82(0.08, 5.62) \times 10^{-4}$	5,480 (118,452, 1,779)	0.225 (0.158, 0.314)	$2.48(1.43, 4.08) \times 10^{-4}$	4,035 (7,012, 2,449)
10	0	0.051 (0.000, 0.291)	$5.59(0.04, 37.85) \times 10^{-5}$	17,895 (2,332,962, 2,642)	0.113 (0.064, 0.196)	$1.24(0.57, 2.55) \times 10^{-4}$	8,057 (17,452, 3,923)
				Storfjord			
0.01	57	0.978 (0.924, 0.997)	$6.20(4.65, 7.61) \times 10^{-3}$	161 (215, 131)	-	-	-
0.1	40	0.668 (0.555, 0.797)	$4.23(2.79, 6.08) \times 10^{-3}$	236 (358, 164)	-	-	-
0.3	24	0.374 (0.244, 0.482)	$2.37(1.23, 3.68) \times 10^{-3}$	422 (816, 272)	0.395 (0.328, 0.475)	$2.50(1.65, 3.63) \times 10^{-3}$	399 (606, 276)
1	11	0.125 (0.047, 0.235)	$7.92(2.36, 17.96) \times 10^{-4}$	1,263 (4,245, 557)	0.158 (0.146, 0.170)	$9.99(7.36, 12.94) \times 10^{-4}$	1,001 (1,359, 773)
3	5	0.028 (0.005, 0.090)	$1.79(0.25, 6.90) \times 10^{-4}$	5,584 (39,388, 1,448)	0.068 (0.057, 0.081)	$4.32(2.87, 6.20) \times 10^{-4}$	2,314 (3,479, 1,614)
10	0	0.003 (0.000, 0.022)	$1.96(0.10, 16.80) \times 10^{-5}$	50,751 (1,050,483, 5,951)	0.027 (0.020, 0.036)	$1.72(1.03, 2.76) \times 10^{-4}$	5,798 (9,748, 3,618)

Hazard within this classification, corresponds here to susceptibility. This classification focuses on two types of criteria: 1) unfavorable geological and structural conditions and 2) slope activity and observed deformation. Oppikofer et al. (submitted) implemented this qualitative susceptibility classification for the potential unstable rock slopes in the entire Storfjord region. The obtained rankings r_i have been used to obtain absolute susceptibilities S_i for each potential instability within a certain volume class:

$$S_i = \frac{r_i}{\sum_{i=1}^{n} r_i} \tag{3}$$

where n is the number of potential instabilities within the considered volume class $x_1 \leq V \leq x_2$. Under the assumption that the inventory of instabilities is correct, semi-quantitative annual hazard estimations H_i for each potential instability at the northeastern flank of Tafjord have finally been obtained with the following equation:

$$H_i = f(x_1 \leq V \leq x_2, 1) \times S_i \tag{4}$$

The resulting annual probabilities are very low and range from 1/10,000 to 1/48,000 (Table 4). As expected, the two continously monitored instabilities at Hegguraksla obtain the largest probabilities of 1/10,687 and 1/10,906. However, as for the hazard estimates for the entire Tafjord, the 95% confidence intervals for the annual probabilities are very large (Table 4) and question thus the applicability of these values for hazard assessment. In addition, as presented in Section 4.3 and Figure 7b, instabilities and fjord deposits show slightly different distributions for volumes $> 0.2 \times 10^6$ m^3 and power law exponents for the smallest scenarios of the instabilities are significantly larger than reported values. This may indicate an incorrect inventory of unstable rock slopes and resulting hazard values may be influenced by this. These latter problems, are however only of minor importance considering the large confidence intervals.

The magnitude-frequency distribution of the potential instabilities of the entire Storfjord region differs significantly from the distribution of the fjord deposits (Figure 8). A segmentation of the registered volumes for the largest scenarios of the potential instabilities randomly into 1 to 15 parts is necessary in order to obtain a distribution that is similar to that of the fjord deposits. It can thus be assumed that several of the presently registered instabilities, may fail in more and smaller events, than the currently defined scenarios which are visible on the present topography. A careful re-analysis of the potential instabilities is necessary before individual semi-quantitative hazard values for the potential instabilities of the entire Storfjord region can be defined.

5. Conclusions and perspectives

This study focused on a detailed statistical analysis of the temporal distribution of rock slope failures within a fjord system in western Norway. TCN dating validated the previously obtained relative ages for two fjord deposits. However, a third dated failure surface showed conflicting cosmogenic nuclide and relative ages, indicating a possible incompleteness of the fjord deposit inventory regarding small rock slope failures, even for young ages. Small deposits can probably not be separated when deposited on top of or close to large deposits. The temporal analysis of the fjord deposits revealed that the largest total volumes have failed directly after deglaciation and rock slope failures larger than 5×10^6 m^3 have not been registered within the last 9,000 years. Volumes are not decreasing continuously after deglaciation. The temporal distribution of number of rock slope failures is characterized by a rapid response directly af-

Table 4: Examples of semi-quantitative annual hazard values for the largest scenarios of potential instabilities along the northeastern flank of Tafjord (with 95% confidence bounds). The locations of the instabilities are shown in Figure 2. Ranks are adapted from Oppikofer et al. (submitted). Annual frequencies $f(x_1 \leq V \leq x_2, 1)$ based on a lognormal distribution have been used in order to calculate the resulting semi-quantitative hazard for each volume class $x_1 \leq V \leq x_2$.

Potential instability						
Map	Name	Volume [10^6 m^3]	Volume class [10^6 m^3]	Rank	Relative susceptibility S_i	Semi-quantitative annual hazard H_i
47	Hammaren 1	0.04	0.01-0.1	2.98	0.235	1/23,270 (1/405,930, 1/9,355)
49	Geitsteinen	0.05		4.40	0.346	1/15,771 (1/275,109, 1/6,340)
44c	Grynnvikane 3	0.06		1.46	0.115	1/47,538 (1/829,256, 1/19,112)
43c	Årøldalen 3	0.09		3.85	0.304	1/17,987 (1/313,773, 1/7,231)
H3	Hegguraksla Sør	0.17	0.1-0.3	3.21	0.199	1/22,830 (1/80,158, 1/11,505)
46c	Hegguradalen 3	0.21		3.77	0.234	1/19,425 (1/68,200, 1/9,789)
47b	Hammaren 2	0.22		3.29	0.205	1/22,253 (1/78,128, 1/11,213)
48	Peteigen	0.24		3.44	0.214	1/21,308 (1/74,814, 1/10,738)
46b	Hegguradalen 2	0.28		2.38	0.148	1/30,764 (1/108,012, 1/15,503)
H2	Hegguraksla Nedre	0.47	0.3-1	5.19	0.326	1/10,689 (1/24,490, 1/9,531)
44b	Grynnvikane 2 scenario A	0.56		2.71	0.170	1/20,473 (1/46,908, 1/18,256)
44	Grynnvikane 1	0.66		2.94	0.185	1/18,876 (1/43,249, 1/16,832)
H1	Hegguraksla Øvre	0.74		5.08	0.319	1/10,908 (1/24,992, 1/9,727)
46	Hegguradalen 1	1.79	1-3	3.44	0.224	1/21,046 (1/82,491, 1/10,194)
45	Langhammaren scenario A	2.01		3.98	0.260	1/18,181 (1/71,262, 1/8,806)
43	Årøldalen 1	2.14		4.46	0.291	1/16,227 (1/63,603, 1/7,860)
43b	Årøldalen 2 scenario A	2.33		3.46	0.226	1/20,919 (1/81,994, 1/10,133)

ter deglaciation followed by a constant frequency. The number of rock slope failures and the failed volumes can be assumed as constant since 9,000 years with an annual frequency of 0.0063 ± 0.0013 for the entire Storfjord region and since 10,000 years with an annual frequency of 0.0011 ± 0.0002 for the northeastern flank of Tafjord, reflecting the geological norm within these regions. However, the observed volume-frequency distributions are most likely influenced by undersampling of small deposits for the time periods close to deglaciation due to erosion or overlying younger deposits.

Magnitude-frequency relations of three independent inventories of rock slope failures from the northeastern flank of Tafjord have been evaluated. All three inventories are representing rock slope failures or instabilities within the same lithology, the same topography and consequently underlying the same processes that lead to destabilisation and eventually failure. Even if all three inventories have large uncertainties, they reveal all similar magnitude-frequency relations, which validates the different inventories. Hence the obtained magnitude-frequency relation can be assumed as correct for rock slope processes of the studied magnitudes larger than 0.01×10^6 m^3 for the Tafjord region. Since the same technique has been used to register fjord deposits in the entire fjord system, also the magnitude-frequency relation for the fjord deposits of the entire Storfjord region is assumed to be correct.

The unique combination of three different inventories allowed quantifying the rockslide hazard within the Tafjord and the Storfjord regions. Annual expectable frequencies for certain volume classes have been assessed based on magnitude-frequency analyses of the geological norm. This results in an annual frequency of 1/2,535 based on lognormal distribution and 1/2,147 for a power-law model for failures of $V \geq 1 \times 10^6$ m^3 from the northeastern flank of Tafjord. The resulting annual frequency for failures of $V \geq 1 \times 10^6$ m^3 in the entire Storfjord region is 1/1,263 based on a lognormal distribution and 1/1,001 for a power-law model. Finally, a semi-quantitative hazard estimation can be obtained for all potential instabilities on the northeastern flank above the Tafjord. The annual failure probabilities for the individual instabilities are very low and vary from 1/10,000 to 1/48,000. Failure probabilities for all potential instabilities within the Storfjord region can first be assessed after a re-analysis of the probable scenarios for each instability. However, the uncertainties of the resulting regional as well as local hazard estimates are very high as indicated by large confidence intervals, making the results partly difficult to use for further risk assessments.

This study presents a potential method to quantitatively assess hazard values for large rock slope instabilities in a limited region in western Norway. The assigned semi-quantitative hazard values for each potential instability may form the input for quantitative risk assessments and help on decisions regarding land-use planning or building applications. Future studies need to focus on how to include the uncertainties of the susceptibility into the final hazard values. This is a rather complex step, which can only be solved by including simulations of several combinations of input factors for the susceptibility values. Furthermore, it needs to be investigated in how far the results can be transferred to other regions in Norway, but also worldwide. Re-

gions with a similar geology, a similar glacial history and a similar topography should show similar magnitude-frequency relations. The temporal distribution of rock slope failures following a deglaciation, could be investigated in this study, and the results are valuable for other deglaciated regions in the world, but a larger dataset with absolute dates would be necessary in order to be able to define an exact temporal model.

6. Acknowledgements

We would like to thank Tim Redfield for making it possible to sample places that have and will probably never be visited by other persons again. The authors are also thankful to Martin Panzner for spending his evening hours to fix the apparently uncountable problems with Matlab.

References

Aarseth, I., Austbø, P. K., Risnes, H., 1997. Seismic stratigraphy of Younger Dryas ice-marginal deposits in western Norwegian fjords. Norsk Geologisk Tidsskrift 77, 65–86.

Abele, G., 1974. Bergstürze in den Alpen: ihre Verbreitung, Morphologie und Folgeerscheinungen. Wissenschaftliche Alpenvereinshefte Heft 25, 230.

Balco, G., Stone, J. O., Lifton, N. A., Dunai, T. J., 2008. A complete and easily accessible means of calculating surface exposure ages or erosion rates from ^{10}Be and ^{26}Al measurements. Quaternary Geochronology 3 (3), 174–195.

Ballantyne, C. K., 2002a. A general model of paraglacial landscape response. The Holocene 12 (3), 371–376.

Ballantyne, C. K., 2002b. Paraglacial geomorphology. Quaternary Science Reviews 21 (18-19), 1935–2017.

Ballantyne, C. K., Stone, J. O., 2013. Timing and periodicity of paraglacial rock-slope failures in the Scottish Highlands. Geomorphology 186 (0), 150–161.

Blikra, L. H., 2008. The Åknes rockslide; monitoring, threshold values and early-warning. In: Chen, Z., Zhang, J., Li, Z., Wu, F., Ho, K. (Eds.), Landslides and Engineered Slopes. From the Past to the Future - Proceedings of the 10th International Symposium on Landslides and Engineered Slopes, 30 June - 4 July 2008, Xi'an, China. Vol. 2. Taylor & Francis Group, London, pp. 1089–1094.

Blikra, L. H., Longva, O., Braathen, A., Anda, E., Dehls, J. F., Stalsberg, K., 2006. Rock slope failures in Norwegian fjord areas: Examples, spatial distribution and temporal pattern. In: Evans, S. G., Scarascia Mugnozza, G., Strom, A., Hermanns, R. L. (Eds.), Landslides from Massive Rock Slope Failure; NATO Science Series, IV. Earth and Environmental Sciences, Vol 49. Springer, Dodrecht, Netherlands, pp. 475–496.

Bøe, R., Longva, O., Lepland, A., Blikra, L. H., Sønstegaard, E., Hadlidason, H., Bryn, P., Lien, R., 2004. Postglacial mass movements and their causes in fjords and lakes in western Norway. Norwegian Journal of Geology 84 (1), 35–56.

Brunetti, M. T., Guzzetti, F., Rossi, M., 2009. Probability distributions of landslide volumes. Nonlinear Processes in Geophysics 16, 179–188.

Chaytor, J. D., ten Brink, U. S., Solow, A. R., Andrews, B. D., 2009. Size distribution of submarine landslides along the U.S. Atlantic margin. Marine Geology 264 (1-2), 16.

Crosta, G. B., 2007. Fragmentation in the Val Pola rock avalanche, Italian Alps. Journal of Geophysical Research 112 (F01006), 23.

Cruden, D. M., Hu, X. Q., 1993. Exhaustion and steady state models for predicting landslide hazards in the Canadian Rocky Mountains. Geomorphology 8 (4), 279–285.

Derron, M.-H., Jaboyedoff, M., Blikra, L. H., 2005. Preliminary assessment of rockslide and rockfall hazards using a DEM (Oppstadhornet, Norway). Natural Hazards and Earth System Sciences 5 (2), 285–292.

Dussauge, C., Grasso, J.-R., Helmstetter, A., 2003. Statistical analysis of rockfall volume distributions: Implications for rockfall dynamics. Journal of Geophysical Research-Solid Earth 108 (B6), ETG2.1–ETG2.11.

Dussauge-Peisser, C., Helmstetter, A., Grasso, J.-R., Hantz, D., Desvarreux, P., Jeannin, M., Giraud, A., 2002. Probabilistic approach to rock fall hazard assessment: potential of historical data analysis. Natural Hazards and Earth System Sciences 2 (1/2), 15–26.

Eidsvig, U. M., Medina-Cetina, Z., Kveldsvik, V., Glimsdal, S., Harbitz, C. B., Sandersen, F., 2011. Risk assessment of a tsunamigenic rockslide at Åknes. Natural Hazards 56, 529–545.

Fareth, O. W., 1987. Glacial geology of middle and inner nordfjord, western Norway. Tech. Rep. 408, Geological Survey of Norway.

Fjeldskaar, W., Lindholm, C., Dehls, J. F., Fjeldskaar, I., 10/1 2000. Postglacial uplift, neotectonics and seismicity in Fennoscandia. Quaternary Science Reviews 19 (14-15), 1413–1422.

Frattini, P., Crosta, G. B., 1/1 2013. The role of material properties and landscape morphology on landslide size distributions. Earth and Planetary Science Letters 361, 310–319.

Furseth, A., 2006. Skredulykker i Norge. Tun Forlag, Oslo, Norway.

Ganerød, G. V., Grøneng, G., Rønning, J. S., Dalsegg, E., Elvebakk, H., Tønnesen, J. F., Kveldsvik, V., Eiken, T., Blikra, L. H., Braathen, A., nov 2008. Geological model of the Åknes rockslide, western Norway. Engineering Geology 102 (1-2), 1–18.

Gosse, J. C., Phillips, F. M., 2001. Terrestrial in situ cosmogenic nuclides: theory and application. Quaternary Science Reviews 20 (14), 1475–1560.

Guthrie, R. H., Evans, S. G., 2005. The role of magnitude-frequency relations in regional landslide risk analysis. In: Hungr, O., Fell, R., Couture, R., Eberhardt, E. (Eds.), Landslide Risk Management. Taylor & Francis Group, London, pp. 375–380.

Guzzetti, F., Reichenbach, P., Wieczorek, G. F., 2003. Rockfall hazard and risk assessment in the Yosemite Valley, California, USA. Natural Hazards and Earth System Sciences 3 (6), 491–503.

Haas, F., Heckmann, T., Wichmann, V., Becht, M., 2012. Runout analysis of a large rockfall in the Dolomites/Italian Alps using LIDAR derived particle sizes and shapes. Earth Surface Processes and Landforms 37 (13), 1444–1455.

Hantz, D., Vengeon, J., Dussauge-Peisser, C., 2003. An historical, geomechanical and probabilistic approach to rock-fall hazard assessment. Natural Hazards and Earth System Sciences 3, 693–701.

Henderson, I. H. C., Saintot, A., 2011. Regional spatial variations in rockslide distribution from structural geology ranking: an example from Storfjord, western Norway. In: Jaboyedoff, M. (Ed.), Slope Tectonics. Geological Society, London, Special Publications, 351, pp. 79–95.

Henderson, I. H. C., Saintot, A., Derron, M.-H., 2006. Structural mapping of potential rockslide sites in the Storfjorden area, western Norway: the influence of bedrock geology on hazard analysis. Tech. Rep. 2006.052, Geological Survey of Norway.

Hermanns, R. L., Blikra, L. H., Longva, O., 2009. Relation between rockslide dam and valley morphology and its impact on rockslide dam longevity and control on potential breach development based on examples from Norway and the Andes. In: Bauer, E., Semprich, S., Zenz, G. (Eds.), Proceedings of the 2nd International Conference on Long Term Behavior of Dams, 12th-13th October 2009, Graz, Austria. Gray Universitz of Technology, Graz, Austria, pp. 789–794.

Hermanns, R. L., Blikra, L. H., Naumann, M., Nilsen, B., Panthi, K. K., Stromeyer, D., Longva, O., 2006. Examples of multiple rock-slope collapses from Köfels (Ötz valley, Austria) and western Norway. Engineering Geology 83 (1-3), 94–108.

Hermanns, R. L., Longva, O., 2012. Rapid rock-slope failures. In: Clague, J. J., Stead, D. (Eds.), Landslides: Types, Mechanisms and Modeling. Cambridge University Press, Cambridge, UK, pp. 59–70.

Hermanns, R. L., Niedermann, S., Ivy-Ochs, S., Kubik, P. W., 2004. Rock avalanching into a landslide-dammed lake causing multiple dam failure in Las Conchas valley (NW Argentina) - evidence from surface exposure dating and stratigraphic analyses. Landslides 1 (2), 113–122.

Hermanns, R. L., Oppikofer, T., Anda, E., Blikra, L. H., Böhme, M., Bunkholt, H., Crosta, G. B., Dahle, H., Devoli, G., Fischer, L., Jaboyedoff, M., Loew, S., Sætre, S., Molina, F. Y., 2013. Hazard and risk classification for large unstable rock slopes in Norway. In: Genevais, R., Prestininzi, A. (Eds.), International Conference Vajont 1963-2013. Thoughts and analyses after 50 years since the catastrophic landslide, Padua, Italy - 8-10 October 2013. Sapienza Università Editrice, pp. 245–254.

Hungr, O., Evans, S. G., September 1 2004. Entrainment of debris in rock avalanches: An analysis of a long run-out mechanism. Geological Society

of America Bulletin 116 (9-10), 1240–1252.
Hungr, O., Evans, S. G., Hazzard, J., 1999. Magnitude and frequency of rock falls and rock slides along the main transportation corridors of southwestern British Columbia. Canadian Geotechnical Journal 36, 224–238.
InnovMetric, 2011. PolyWorks: 3D scanner and 3D digitizer software from InnovMetric Software Inc.
Ivy-Ochs, S., von Poschinger, A., Synal, H. A., Maisch, M., 2009. Surface exposure dating of the Flims landslide, Graubünden, Switzerland. Geomorphology 103 (1), 104–112.
Jaboyedoff, M., Derron, M.-H., 2005. A new method to estimate the infilling of alluvial sediment of glacial valleys using a sloping local base level. Geografica Fisica e Dinamika Quaternaria 28, 37–46.
Jaboyedoff, M., Oppikofer, T., Derron, M.-H., Blikra, L. H., Böhme, M., Saintot, A., 2011. Complex landslide behaviour and structural control: a three-dimensional conceptual model of Åknes rockslide, Norway. In: Jaboyedoff, M. (Ed.), Slope tectonics. Geological Society, London, Special Publications, 351, pp. 147–161.
Katz, O., Reichenbach, P., Guzzetti, F., 2011. Rock fall hazard along the railway corridor to Jerusalem, Israel, in the Soreq and Refaim valleys. Natural Hazards 56 (3), 649–665.
Korup, O., Clague, J. J., Hermanns, R. L., Hewitt, K., Strom, A. L., Weidinger, J. T., 2007. Giant landslides, topography, and erosion. Earth and Planetary Science Letters 261 (3), 578–589.
Lacasse, S., 2008. Event tree analysis of Åknes rock slide hazard. In: 4th Canadian Conference on Geohazards : From Causes to Management. Quebec, Canada, pp. 551–558.
Lal, D., 1991. Cosmic ray labeling of erosion surfaces: in situ nuclide production rates and erosion models. Earth and Planetary Science Letters 104 (2-4), 424–439.
Larsen, E., Longva, O., Follestad, B. A., 1991. Formation of De Geer moraines and implications for deglaciation dynamics. Journal of Quaternary Science 6 (4), 263–277.
Laute, K., Beylich, A. A., 2012. Influences of the Little Ice Age glacier advance on hillslope morphometry and development in paraglacial valley systems around the Jostedalsbreen ice cap in Western Norway. Geomorphology 167, 51–69.
Longva, O., Blikra, L. H., Dehls, J., 2009. Rock avalanches - distribution and frequencies in the inner part of Storfjorden, Møre og Romsdal County, Norway. Tech. Rep. 2009.002, Geological Survey of Norway.
Malamud, B. D., 2004. Landslide inventories and their statistical properties. Earth Surface Processes and Landforms 29 (6), 687–711.
McColl, S. T., 2012. Paraglacial rock-slope stability. Geomorphology 153-154, 1–16.
Olesen, O., Blikra, L. H., Braathen, A., Dehls, J. F., Olsen, L., Rise, L., Roberts, D., Riis, F., Faleide, J. I., Anda, E., 2004. Neotectonic deformation in Norway and its implications: a review. Norsk Geologisk Tidsskrift 84 (1), 3–34.
Oppikofer, T., 2009. Detection, analysis and monitoring of slope movements by high-resolution digital elevation models. Ph.D. thesis, University of Lausanne, Switzerland.
Oppikofer, T., Böhme, M., Saintot, A., Hermanns, R. L., Longva, O., submitted. Hazard assessment of unstable and potential unstable rock slopes in Storfjord (Western Norway). In: Proceedings of the IAEG XII Congress, Torino, September 15-19th 2014.
Oppikofer, T., Jaboyedoff, M., Blikra, L. H., Derron, M.-H., 2009. Characterization and monitoring of the Åknes rockslide using terrestrial laser scanning. Natural Hazards and Earth System Sciences 9 (3), 1003–1019.
Oppikofer, T., Jaboyedoff, M., Pedrazzini, A., Derron, M.-H., Blikra, L. H., 2011. Detailed DEM analysis of a rockslide scar to improve the basal failure surface model of active rockslides. Journal of Geophysical Research 116, F02016.
Roberts, D., Gee, D. G., 1985. An introduction to the structure of the Scandinavian Caledonides. In: Gee, D. G., Sturt, B. A. (Eds.), The Caledonide orogen - Scandinavia and related areas. Vol. 1. John Wiley & Sons, pp. 55–68.
Saintot, A., Henderson, I., Derron, M.-H., 2011. Inheritance of ductile and brittle structures in the development of large rock slope instabilities: examples from western Norway. In: Jaboyedoff, M. (Ed.), Slope tectonics. Geological Society, London, Special Publications, 351, pp. 27–78.
Santana, D., Corominas, J., Mavrouli, O., Garcia-Sellés, D., 9/7 2012. Magnitude-frequency relation for rockfall scars using a terrestrial laser scanner. Engineering Geology 145-146, 50–64.
Stark, C. P., Hovius, N., 2001. The characterization of landslide size distributions. Geophysical Research Letters 28 (6), 1091–1094.
Stone, J. O., 2000. Air pressure and cosmogenic isotope production. Journal of Geophysical Research 105 (B10), 23753–23759.
ten Brink, U. S., Barkan, R., Andrews, B. D., Chaytor, J. D., 2009. Size distributions and failure initiation of submarine and subaerial landslides. Earth and Planetary Science Letters 287, 31–42.

Appendix F

List of publications during the PhD studies

F.1 Per-reviewed publications

Böhme, M., Hermanns, R.L., Oppikofer, T., Fischer, L., Bunkholt, H.S.S., Eiken, T., Pedrazzini, A., Derron, M.-H., Jaboyedoff, M., and Blikra, L.H.: Analyzing complex rock slope deformation at Stampa, western Norway, by integrating geomorphology, kinematics and numerical modeling. Engineering Geology, 154, pp.116-130, 2013.

Böhme, M., Hermanns, R.L., Fischer, L., Oppikofer, T., Bunkholt, H.S.S., Derron, M.-H., Carrea, D., Jaboyedoff , M., and Eiken, T.: Detailed assessment of the deep-seated gravitational deformation at Stampa above Flåm, Norway, in: Landslides and Engineered Slopes. Protecting Society through Improved Understanding: Proceedings of the 11th International & 2nd North American Symposium on Landslides, Banff, Canada, 3-8 June 2012, edited by Eberhardt, E., Froese, C., Turner, A.K. and Leroueil, S., CRC Press, pp. 647-652, 2012.

Böhme, M., Saintot, A., Henderson, I., Henriksen, H., and Hermanns, R.L.: Rock-slope instabilities in Sogn & Fjordane County, Norway: a detailed structural and geomorphological analysis, in: Slope Tectonics, edited by Jaboyedoff, M., Geological Society, London, Special Publications, 351, pp. 97-111, 2011.

Dehls, J.F., Fischer, L., **Böhme, M.**, Saintot, A., Hermanns, R.L., Oppikofer, T., Lauknes, T.R., Larsen, Y., and Blikra, L.H.: Landslide monitoring in western Norway using high resolution TerraSAR-X and Radarsat-2 InSAR, in: Landslides and Engineered Slopes. Protecting Society through Improved Understanding:

Proceedings of the 11th International & 2nd North American Symposium on Landslides, Banff, Canada, 3-8 June 2012, edited by Eberhardt, E., Froese, C., Turner, A.K. and Leroueil, S., CRC Press, pp. 1321-1325, 2012.

Hermanns, R.L., Oppikofer, T., Anda, E., Blikra, L.H., **Böhme, M.**, Bunkholt, H., Crosta, G.B., Dahle, H., Devoli, G., Fischer, L., Jaboyedoff , M., Loew, S., Sætre, S., Molina, F.Y.: Hazard and risk classification for large unstable rock slopes in Norway. In: International Conference Vajont 1963-2013. Thoughts and analyses after 50 years since the catastrophic landslide, Padua, Italy - 8-10 October 2013, edited by Genevais, R. and Prestininzi, A., Sapienza Università Editrice, pp. 245-254, 2013.

Hermanns, R.L., Blikra, L.H., Anda, E., Saintot, A., Dahle, H., Oppikofer, T., Fischer, L., Bunkholt, H., **Böhme, M.**, and Dehls, J.F.: Systematic mapping of large unstable rock slopes in Norway, in: Landslide Science and Practice, edited by Margottini, C., Canuti, P. and Sassa, K., Springer, pp. 29-35, 2013.

Hermanns, R.L., Hansen, L., Sletten, K., **Böhme, M.**, Bunkholt, H.S.S., Dehls, J.F., Eilertsen, R.S., Fischer, L., L´Heureux, J.-S., Høgaas, F., Nordahl, B., Oppikofer, T., Rubensdotter, L., Solberg, I.-L., Stalsberg, K., and Yugsi Molina, F.X.: Systematic geological mapping for landslide understanding in the Norwegian context, in: Landslides and Engineered Slopes. Protecting Society through Improved Understanding: Proceedings of the 11th International & 2nd North American Symposium on Landslides, Banff, Canada, 3-8 June 2012, edited by Eberhardt, E., Froese, C., Turner, A.K. and Leroueil, S., CRC Press, pp. 265-271, 2012.

Jaboyedoff, M., Derron, M.-H., Pedrazzini, A., Blikra, L.H., Crosta, G.B., Froese, C.R., Hermanns, R.L., Oppikofer, T., **Böhme, M.**, and Stead, D.: Fast assessment of susceptibility of massive rock instabilities. in: Landslides and Engineered Slopes. Protecting Society through Improved Understanding: Proceedings of the 11th International & 2nd North American Symposium on Landslides, Banff, Canada, 3-8 June 2012, edited by Eberhardt, E., Froese, C., Turner, A.K. and Leroueil, S., CRC Press, pp. 459-465, 2012.

Jaboyedoff, M., Oppikofer, T., Derron, M.-H., Blikra, L.H., **Böhme, M.**, and Saintot, A.: Complex landslide behaviour and structural control: a three-dimensional conceptual model of Åknes rockslide, Norway, in: Slope tectonics, edited by Jaboyedoff, M., Geological Society, London, Special Publications, 351, pp. 147-161, 2011.

F.2 Publications submitted to per-reviewed journals and manuscripts

Böhme, M., Derron, M.-H., and Jaboyedoff, M.: Quantitative spatial analysis of rockfalls from road inventories - a combined statistical and physical susceptibility model, submitted to Natural Hazards and Earth System Sciences.

Böhme, M., Oppikofer, T., Longva, O., Jaboyedoff, M., Hermanns, R.L., and Derron, M.-H.: Analyses of past and present rock slope instabilities in a fjord valley: Implications for hazard estimations, manuscript, submission planned to Earth and Planetary Science Letters.

F.3 Conference abstracts

Böhme, M., Oppikofer, T., Longva, O., Jaboyedoff, M., Hermanns, R.L., Derron, M.-H.: Analyses of past and present rock slope instabilities in a fjord valley: Implications for hazard estimations of large rock slope failures, in: Proceedings of the AGU Fall Meeting, San Francisco, 9-14 December 2013, 2013.

Böhme, M., Hermanns, R.L., Fischer, L., Oppikofer, T., Eiken, T.: Some comments on one of the largest unstable rock slope areas in Norway: The Stampa, Furekamben, Ramanosi unstable area, Flåm, Norway, in: Norsk Geologisk Forening Vinterkonferanse 2011, Stavanger, Norway, 11-13 January 2011. NGF Abstracts and proceedings no. 1, pp. 13-14, 2011.

Böhme, M., Hermanns, R.L., Tukkensæter, Å., Derron, M.-H., Eiken, T., Carrea, D., Jaboyedoff , M.: Structural analysis of the unstable rock slope area at Stampa above Flåm, Norway, in: EGU General Assembly 2010, Geophysical Research Abstracts, 12, p. 13433, 2010.

Böhme, M., Blikra, L.H., Derron, M.-H., Jaboydeoff, M.: Spatial analysis of rock slope instabilities in Western Norway, in: EGU General Assembly 2009, Geophysical Research Abstracts, 11, pp. 7844, 2009.

Böhme, M., Henderson, I.H.C., Saintot, A.. Rockslide investigations in Sogn & Fjordane, Norway, in: Congress Slope-Tectonics 2008, Lausanne, 2008.

Böhme, M., Saintot, A., Henderson, I.H.C.: Rockslide investigations in Sogn & Fjordane, Norway, in: EGU General Assembly 2008, Geophysical Research Abstracts, 10, p. 08637, 2008.

Hermanns, R.L., Hansen, L., Sletten, K., **Böhme, M.**, Bunkholt, H., Dehls, J.F., Eilertsen, R., Fischer, L., L'Heureux, J.-S., Høgaas, F., Nordahl, B., Oppikofer,

T., Rubensdotter, L., Solberg, I.-L., Stalsberg, K., Yugsi Molina, F.X.: Systematic geological mapping for landslide understanding in the Norwegian context, in: 30th Nordic Geological Winter Meeting, Reykjavik, 9-12 January 2012, p. 101, 2012.

Hermanns, R.L., Redfield, T., Fenton, C., Gosse, J., Niedermann, S., Longva, O., **Böhme, M.**: Use of cosmogenic nuclide dating in rockslide hazard assessment in Norway, in: 30th Nordic Geological Winter Meeting, Reykjavik, 9-12 January 2012, p. 103, 2012.

Hermanns, R.L., Oppikofer, T., Anda, E., Blikra, L.H., **Böhme, M.**, Bunkholt, H., Dahle, H., Devoli, G., Eikenæs, O., Fischer, L., Harbitz, C.B., Jaboyedoff, M., Loew, S., Yugsi Molina, F.X.: A hazard and risk classification system for catastrophic rock slope failures in Norway, in: EGU General Assembly 2012, Geophysical Research Abstracts, 14, 2012.

Hermanns, R.L., Oppikofer, T., Anda, E., Berg, H., Blikra, L.H., **Böhme, M.**, Bunkholt, H.S.S., Crosta, G.B., Dahle, H., Fischer, L., Jaboyedoff, M., Loew, S., Yugsi Molina, F.X.: The hazard and risk classification for large unstable rock slopes in Norway, in: Proceedings of the AGU Fall Meeting, San Francisco, 3-7 December 2012, 2012.

Hermanns, R.L., Anda, E., Henderson, I.H.C., Dahle, H., Saintot, A., Blikra, L.H., **Böhme, M.**, Dehls, J.F., Redfield, T.F., Eiken, T.: Towards a hazard classification system for large rock slope failures in Norway, in: EGU General Assembly 2010, Geophysical Research Abstracts, 12, p. 13657, 2010.

Hermanns, R.L., Anda, E., Saintot, A., Henderson, I.H.C., Dahle, H., **Böhme, M.**, Dehls, J.F., Blikra, L.H., Lauknes, T.R., Redfield, T.F., Oppikofer, T., Fischer, L., Bunkholt, H.S.S., Eiken, T.: Systematic mapping of unstable rockslopes with the potential of forming rock avalanches in Norway, in: 2nd Symposium on landslides in the Andes, Geological Congress of Peru, Cuzco, Peru, 28 september-1 oktober, 2010.

Jaboydeoff, M., **Böhme, M.**, Blikra, L.H., Derron, M.-H., Henderson, I.H.C., Oppikofer, T., Saintot, A.: Geological and structural interpretation of Åknes Landslide, in: EGU General Assembly 2008, Geophysical Research Abstracts, 10, p. 08508, 2008.

Jaboyedoff, M., **Böhme, M.**, Blikra, L.H., Derron, M.-H., Henderson, I.H.C., Oppikofer, T., Saintot, A.: Geological and structural interpretation of Åknes Landslide and recent failures, in: Congress Slope-Tectonics 2008, Lausanne, 2008.

Oppikofer, T., **Böhme, M.**, Saintot, A., Hermanns, R.L., Longva, O.: Hazard

assessment of unstable and potential unstable rock slopes in Storfjord (Western Norway), in: Proceedings of the IAEG XII Congress, Torino, September 15-19 2014, 2014.

Oppikofer, T., **Böhme, M.**, Fischer, L., Hermanns, R.L.: Quantification of rotational and toppling movements of unstable rock slopes based on discontinuity orientations, in: EGU General Assembly 2012, Geophysical Research abstracts, 14, 2012.

Oppikofer, T., **Böhme, M.**, Blikra, L.H., Jaboyedoff, M., Saintot, A.: Geological and structural model of Åknes landslide (Norway), in: 33rd International Geological Congress (33IGC), Oslo, Norway - General proceedings. IUGS, Oslo, Norway, 2008.

Saintot, A., Henderson, I., **Böhme, M.**: Slope unstabilities in U-shaped glacial valleys: Sunndalen and Romsdalen (western Norway), in: EGU General Assembly 2008, Geophysical Research Abstracts, 10, p. 10670, 2008.

F.4 Reports

Bunkholt, H., Otterå, S., Yugsi Molina, F.X., Hermanns, R.L., Dehls, J., Osmundsen, P.T., Redfield, T., Eiken, T., **Böhme, M.**: Undersøkelser av ustabile eller potensielle ustabile fjellpartier i Troms - status og planer etter feltarbeid 2011 og 2012. NGU report 2013.021, Geological Survey of Norway, Trondheim, Norway, 2013.

Dahle, H., Anda, E., Sætre, S., Saintot, A., **Böhme, M.**, Hermanns, R.L., Oppikofer, T., Dalsegg, E., Rønning, J.S., Derron, M.-H.: Risiko og sårbarheitsanalyse for fjellskred i Møre og Romsdal. Fylkesmannen i Møre og Romsdal, 2012.

Henderson, I.H.C., Saintot, A., **Böhme, M.**, Henriksen, H.: Kartlegging av mulig ustabile fjellpartier, Sogn og Fjordane. NGU report 2008.026, Geological Survey of Norway, Trondheim, Norway, 2008.

Hermanns, R.L., Bunkholt, H.S.S., **Böhme, M.**, Fischer, L., Oppikofer, T., Rønning, J.S., Eiken, T.: Foreløpig fare- og risikovurdering av ustabile fjellparti ved Joasete-Furekamben-Ramnanosi, Aurland kommune. NGU report 2011.025, Geological Survey of Norway, Trondheim, Norway, 2011.

Hermanns, R.L., Fischer, L., Oppikofer, T., **Böhme, M.**, Dehls, J.F., Henriksen, H., Booth, A., Eilertsen, R., Longva, O., Eiken, T.: Mapping of unstable and potentially unstable slopes in Sogn og Fjordane (work report 2008-2010). NGU

report 2011.055, Geological Survey of Norway, Trondheim, Norway, 2011.

Hermanns, R.L., Oppikofer, T., Anda, E., Blikra, L.H., **Böhme, M.**, Bunkholt, H., Crosta, G.B., Dahle, H., Devoli, G., Fischer, L., Jaboyedoff , M., Loew, S., Sætre, S., Molina, F.Y.: Recommended hazard and risk classification system for large unstable rock slopes in Norway. NGU report 2012.029, Geological Survey of Norway, Trondheim, 2012.

Saintot, A., **Böhme, M.**, Redfield, T.F., Dahle, H.: Field studies of unstable slopes in Sunndalen Valley. NGU report 2008.049,Geological Survey of Norway, Trondheim, Norway, 2008.